UNIVERSITETET
I OSLO

Palladium-based nanoparticles produced by *Escherichia coli:*

Insights into synthesis and physicochemical characterization of microbial nanoparticles.

Ana Lucía Campaña Perilla

Dissertation presented for the degree of
Philosophiae Doctor (PhD)

Supervisor: Pavlo Mikheenko
Co-supervisor: Dirk Linke
Anja Røyne

Department of Physics
Department of Biosciences
Faculty of Mathematics and Natural Sciences
University of Oslo

April 2024

Series of dissertations submitted to the
Faculty of Mathematics and Natural Sciences, University of Oslo
No. 2735

ISSN 1501-7710

Cover: UiO.
Print production: Graphic center, University of Oslo.

Abstract

Microorganisms possess multiple mechanisms to transport, regulate and bind metal ions that can in some cases result in nanoparticle (NPs) biosynthesis. Bacteria can produce a wide variety of metallic NPs including palladium (Pd) NPs. While current industrial practices employ chemical and physical methodologies for NP production, these methods often entail high-energy consumption, the use of toxic chemicals, and the production of waste. Biologically mediated nanoparticle (NP) synthesis offers an eco-friendly and sustainable alternative route for metal NP production.

Pd-based NPs are versatile, well-described catalysts with many different industrial applications. Uniform and size-controlled synthesis of NPs has become a significant area of research due to its influence on their properties. At the nanoscale, small Pd NPs exhibit weak ferromagnetic properties, which can be enhanced by incorporating iron (Fe). The combination of Pd with Fe leads to synergistic effects that enhance the catalytic performance of Pd and modify the magnetic behavior. Surprisingly little is known about the production of Pd-Fe bimetallic nanoparticles by microorganisms, despite their potential applications.

In this thesis, various advanced techniques were used for the systematic characterization of biogenic Pd and Pd-Fe NPs produced by *Escherichia coli* K-12. Using high-angle annular dark field - scanning electron microscope (HAADF-STEM) combined with energy-dispersive x-ray spectroscopy (EDX spectroscopy), the composition, size distribution, and localization of the biosynthesized NPs were analyzed. In addition, atomic force microscopy (AFM) and magnetic force microscopy (MFM) were used as novel methodologies for the direct study of the low magnetic moment of intracellular and extracellular Pd-based NPs within well-preserved cells. Despite the low magnetization, the use of embedded samples enables the direct detection of the magnetic behavior of particles within bacterial cells, providing valuable insights into their biophysical characteristics. This study emphasizes the potential of biogenic Pd-Fe NPs as efficient and sustainable catalyst for hydrogenation reactions, offering environmentally friendly alternatives for various applications, including wastewater treatment and synthesis of fine chemicals.

Sammendrag

Mikroorganismer tar i bruk flere mekanismer for transport, regulering og binding av metallioner som resulterer i biosyntese av nanopartikler. Det har tidligere blitt vist at bakterier kan produsere et bredt utvalg av metalliske nanopartikler, blant annet av palladium (Pd). I dag foregår industriell produksjon av nanopartikler ved hjelp av kjemiske og fysiske metoder som er kjennetegnet ved høyt energiforbruk, toksiske forløpermolekyler og miljøskadelige avfallsstoffer.

Pd-baserte nanopartikler er allsidige og godt beskrevne katalysatorer med flere industrielle anvendelsesområder. Siden nanopartiklenes størrelse har mye å si for deres egenskaper, har størrelseskontroll i syntese av nanopartikler blitt et betydelig forskningsområde. Pd-nanopartikler har svake ferromagnetiske egenskaper, som kan forsterkes ved å inkorporere jern (Fe). Kombinasjonen av Pd og Fe kan gi en synergisk effekt som både kan øke de katalytiske ytelsene til Pd, og modifisere nanopartiklenes magnetiske egenskaper. På tross av de mange og viktige bruksområdene av Pd er imidlertid mekanismene for produksjon av Pd-Fe-bimetalliske nanopartikler ved hjelp av mikroorganismer hittil lite kjent.

I denne avhandlingen er flere avanserte metoder tatt i bruk for å systematisk karakterisere biogeniske nanopartikler av Pd og Pd-Fe, produsert av *Escherichia coli* K-12. Høyvinkel sirkulært mørkefelt - skanning transmisjonselektronmikroskopi (HAADF-STEM) i kombinasjon med energidispersiv røntgenspektroskopi (EDX-spektroskopi) er brukt til å analysere sammensetningen, størrelsesfordelingen og lokaliseringen av biosyntetiserte nanopartikler. For første gang er atomær kraftmikroskopi (AFM) og Magnetisk kraftmikroskopi (MFM) blitt benyttet for å undersøke det lave magnetiske momentet til intra- og ekstracellulære Pd-baserte nanopartikler i godt preserverte celler. På tross av lav magnetisering viser det seg at prøver innstøpt i epoksyharpiks muliggjør direkte detektering av de magnetiske egenskapene til partikler inne i bakterieceller, noe som gir verdifull informasjon om partiklenes biofysiske egenskaper. Dette arbeidet vektlegger potensialet av biogenisk Pd-Fe nanopartikler som effektive og bærekraftige katalysatorer av hydreringsreaksjoner samt muligheten for å utvikle alternative miljøvennlige løsninger med brede anvendelsesområder, som for eksempel behandling av avløpsvann og syntese av fin- og spesialkjemikalier.

Preface

This dissertation is submitted in fulfillment of the requirements for the degree of *Philosophiae Doctor* at the University of Oslo. The thesis structure consists of five chapters and a collection of four papers. Chapter 1 starts with an introduction to the synthesis of palladium nanoparticles by bacteria. Chapter 2 states the main aims of this research, followed by the methods used throughout this work described in Chapter 3. The paper summaries are in Chapter 4 and are accompanied by a general discussion in Chapter 5. Finally, at the end of this thesis are the full versions of the papers with their supplementary material.

The research presented here was conducted at the University of Oslo under the supervision of Prof. Pavlo Mikheenko and Prof. Dirk Linke. Part of the experimental work was carried out at the University of Granada under the supervision of Dr. Mohamed Merroun. The Research Council of Norway through BIOTEK 2021 grant RCN294605 supported this work.

Acknowledgments

This journey began with a wish: to see beyond my limited personal experience and gain a better understanding of the world. A few years ago, in a letter, I wrote, *I would like to become a researcher of the highest educational level*. Now, with the culmination of this Ph.D. thesis, my first expression of gratitude goes to my main supervisor, Pavlo Mikheenko, for providing me with this opportunity. Thank you for reading those words from the other side of the world in the middle of a pandemic and still believing I had the potential to achieve it. I am also infinitely grateful to my supervisor, Dirk Linke, for his support and guidance. Thank you for the invaluable feedback and space to grow. Much appreciation to Anja Røyne for the valuable input and direction provided. At the same time, I would like to thank Athanasios Saragliadis for his generosity in sharing his knowledge and experience, which enriched my journey as a researcher. I must also express my gratitude to Mohamed Merroun for his enthusiasm to collaborate during this work. Thank you for opening the doors to your laboratory, providing invaluable experience, and offering your support. I am grateful to the members of the Microbial Metal Interactions research group for making me feel welcome. Special thanks to Jaime Gómez Bolívar for his incredible help with HAADF-STEM characterization. My appreciation to Johann Osma and Juan Carlos Cruz, who inspired me to pursue research and instilled in me a thirst for knowledge. They motivated me to work in the exciting field of bionanotechnology.

My gratitude also extends to a multitude of individuals who supported me along this arduous journey. In the next lines, I would like to express my thanks:

To my peers and colleagues—Nadeem Joudeh, Masih Mojarrad, Hege Hovland, Daniel Hatlem, Annika Lehmann, and Marta Sanz Gaitero—thank you for the friendship and the time we shared. I am also eternally grateful to Ina Meuskens, Hawzeen Salah Khalil, and Maria Chiara Di Luca. They transformed the rocky paths of my Ph.D. journey into easier and more memorable experiences.

To my work family—Anna Lislerud, Jan-Ole Reese, Sophanit Mekasha, and Patricija Petrikonyte—I am more grateful to you than you will ever know. Thank you for the encouragement, the laughter, and the endless travels. A thousand thanks for teaching me and learning with me. I only wish you the best and look forward to following your progress.

To those who have been or continue to be my roommates in Norway—Deheng Kong, Emma Radler, Xintong Yu, Rike Steenberg, Jaidev Sanketi, Ziyue Wang, Cara Baader, Sofie Mina Stålesen, Martin Lønhøiden, Ellen Hellebust, Eirik Garnås, Marcelo Cajas, and Sivert Kristiansen Hjortung—thank you for sharing yourselves with me. You became the friends and home I needed when I moved so far from my original home. I cherished the spontaneous meals and other random adventures. In particular, Deheng, I cannot thank you enough.

Just like in the quote, “Nothing of me is original. I am the combined effort of everyone I have ever known” - Chuck Palahniuk, the person I am now and the person I want to become is a reflection of those who shaped me.

I would like to express my deepest gratitude to my family. My parents, Oscar and Esmeralda, you are the reason why this journey began. Thank you for your encouragement and patience. For believing in me more than anyone in the world. This work is yours as much as it is mine. Also, to my sister, Laura, for her inconsistent answers and unexpected manifestations in the middle of the night. Thank you for bringing to my life the words I need to hear. As I always say, you were born to make me laugh. Unfortunately, these pages cannot fit the many people of my extensive family I need to thank, my grandmother, my aunts, my uncles, and my cousins. Your love and support mean the world to me.

Finally, a special appreciation goes to my eternal friends, the ones that neither time nor distance can pull apart, Laura Daza, Juliana Noguera, Sergio Flórez, Jessica Pérez, Carlos Ramírez, and Silvana Castillo. You people are an invaluable part of me.

Contents

Abstract **i**

Sammendrag **iii**

Preface **v**

Acknowledgments **vii**

Contents **ix**

List of publications **xi**

Additional publications xii

List of figures **xiii**

List of tables **xiv**

List of abbreviations **xv**

Chapter 1. Introduction **1**

1. Synthesis of metal nanoparticles 1

2. Bacterial synthesis of nanoparticles 3

2.1. Bacteria-metal interactions 4

2.1.1. Metal sequestration *4*
2.1.2. Metal uptake *6*
2.1.3. Metal detoxification *7*
2.1.4. Metal transformation *7*

2.2. Bacterial metal nanoparticles in nature 10

2.3. Biosynthetic nanoparticles 13

2.3.1. Gold and silver nanoparticles *16*
2.3.1. Iron-, cobalt- and nickel-based nanoparticles *16*
2.3.2. Platinum group metals nanoparticles *17*
2.3.3. Other elements, alloys, and bimetallic nanoparticles *17*

3. Palladium-based nanoparticles 19

3.1. Biosynthetic palladium nanoparticles 21

3.2. Applications of palladium-based nanoparticles 22

Chapter 2. Aims of the thesis **23**

Chapter 3. Theory and experimental procedures **24**

1. *E. coli*-mediated synthesis of Pd and Pd-Fe NPs 24

2. The characterization of biogenic nanoparticles 26

2.1. Size, shape and size distribution 26

2.1.1. Transmission Electron Microscopy *26*
2.1.2. Atomic Force Microscopy *28*
2.1.3. Other morphology characterization techniques *30*

2.2. Magnetic properties 31

2.2.1. Principles of magnetism and magnetic materials 31
2.2.2. Magnetic characterization techniques 32
2.2.3. Magnetic force microscopy 33

2.3. Elemental composition, concentration, and chemical state 34

2.3.1. HAADF-STEM images and EDX 35
2.3.2. Further composition characterization techniques 36

2.4. Catalytic activity 37

2.4.1. Biogenic nanoparticles in chemical catalysis 37

2.5. Additional properties 38

Chapter 4. Summary of papers 39

Chapter 5. Discussion 42

1. *E. coli*-mediated synthesis of bimetallic Pd-Fe nanoparticles 42

2. Characterization of microbially synthesized nanoparticles 43

3. Scanning probe microscopy advanced applications for characterization of nanoparticles within cellular structures 46

4. Future work 49

References 51

List of publications

The thesis is based on the following publications that will be referred to with their roman numerals:

Paper I

Campaña, A.L.; Gomez-Bolivar, J.; Merrun, M.L.; Linke, D.; & Mikheenko, P. **Microbial synthesis and characterization of bimetallic Pd-Fe nanoparticles produced by *Escherichia coli*.** *(Manuscript)*

Paper II

Campaña, A. L.; Claxton, J.; Joudeh, N.; Linke, D.; & Mikheenko, P. **Detection of microbial nanoparticles within biological structures by AFM and MFM.** (*Manuscript*)

Paper III

Campaña, A. L.; Joudeh, N.; Høyer, H.; Røyne, A.; Linke, D.; & Mikheenko, P. (**2020**). **Probing van der Waals and magnetic forces in bacteria with magnetic nanoparticles.** In *2020 IEEE 10th International Conference Nanomaterials: Applications & Properties (NAP)* (pp. 01NSSA03-1). IEEE. doi: 10.1109/nap51477.2020.9309722

Paper IV

Campaña, A. L.; Joudeh, N.; Mikheenko, P.; & Linke, D. (**2021**). **Magnetic decoration of *Escherichia coli* loaded with Palladium nanoparticles.** In *2021 IEEE 11th International Conference Nanomaterials: Applications & Properties (NAP)* (pp. 1-5). IEEE. doi: 10.1109/nap51885.2021.9568523

Review I (encompassing pages 1-19 of thesis with minor alterations)

Campaña, A.L.; Saragliadis, A.; Mikheenko, P.; & Linke, D. **Insights into the bacterial synthesis of metal nanoparticles.** *Frontiers in Nanotechnology* **2023**, 5, doi:10.3389/fnano.2023.1216921.

Additional publications

Other publications written in the course of the Ph.D. studies, which are related but not fully associated with the thesis:

1. Florez, S.L.; Campaña, A.L.; Noguera, M.J.; Quezada, V.; Fuentes, O.P.; Cruz, J.C.; Osma, J.F. CFD **Analysis and Life Cycle Assessment of Continuous Synthesis of Magnetite Nanoparticles Using 2D and 3D Micromixers**. *Micromachines* **2022**, 13, 970. doi: 10.3390/mi13060970

2. Guillén, A.; Ardila, Y.; Noguera, M.J.; Campaña, A.L.; Bejarano, M.; Akle, V.; Osma, J.F. **Toxicity of Modified Magnetite-Based Nanocomposites Used for Wastewater Treatment and Evaluated on Zebrafish (Danio rerio) Model**. *Nanomaterials* **2022**, 12, 489. doi: 10.3390/nano12030489

3. Campaña, A.L.; Guillén, A.; Rivas, R.; Akle, V.; Cruz, J.C.; Osma, J.F. **Functionalization and evaluation of inorganic adsorbents for the removal of cadmium in wastewater**. *Molecules* **2021**, 26, 4150, doi:10.3390/molecules26144150.

4. Mojarrad, M.; Hamid, J.; Campana, A. L.; Dang, V. -S.; Crisan, A.; Mikheenko, P. (**2021**). **Using Magnetic Nanoparticles to Improve Flux Pinning in $YBa_2Cu_3O_x$ Films.** In *2021 IEEE 11th International Conference Nanomaterials: Applications & Properties (NAP)*, Odessa, Ukraine, **2021**, pp. 1-5, doi: 10.1109/nap51885.2021.9568543.

List of figures

Figure 1. Illustration of the top-down and bottom-up approaches for the synthesis of metal nanoparticles [29]. 2

Figure 2. Schematics of bacteria interaction with heavy metals and mechanisms of nanoparticle formation [29]. 5

Figure 3. Illustration of bacterial magnetotaxis. Bacteria cells are aligned with the geomagnetic field of the earth due to a magnetic torque created by the intracellular chains of magnetosomes. The cells move along the field lines to the oxic-anoxic transition zone of the aquatic habitat. 11

Figure 4. Consumption of palladium by industry reported in Nornickel Annual report 2021 [223]. 20

Figure 5. Standardization curve for CFU/mL versus OD_{600} for *E. coli* K-12 BW25113 in LB media at 37°C. 24

Figure 6. General protocol for Pd NPs biosynthesis by *E. coli* K12 cells in MOPS buffer at 37°C with agitation. (a) Pd uptake, (b) addition of sodium formate as electron donor and (c) Pd reduction. Created in BioRender 25

Figure 7. Ray paths in conventional TEM, bright field and dark field image mode. Modified from [259]. 27

Figure 8. (a) Parameters of cantilever oscillation and schematic of probe scanning on a sample with embedded nanoparticles by (b) AFM and (c) MFM 29

Figure 9. Images of the scanning probe microscope JPK NanoWizard 4.0 used for AFM and MFM study. 30

Figure 10. Schematic of magnetization curves of magnetic materials. 32

Figure 11. Interatomic forces vs tip lift height from the sample surface. AFM and MFM modes of operation, contact mode, tapping mode and non-contact mode Modified from [295]. 33

Figure 12. HAADF-STEM images of *E. coli* K-12 bacteria and magnified view of cell surface loaded with Pd and Fe molar ratio (a) 1:2 and (b) 1:1 (Pd:Fe). 35

Figure 13. Schematic of AAS study of Pd-based nanoparticles synthesized by *E. coli*. Created in BioRender 36

Figure 14. High-angle annular dark field scanning electron microscope (HAADF-STEM) micrographs of (a) *E.coli*-Pd/$Fe_{0.5}$, (b) *E.coli*-Pd, and (c) *E.coli*-Pd/Fe_1 samples. Inset show bacteria membrane at higher magnification. 44

Figure 15. (a) HAADF-STEM micrograph of biosynthetic NPs in an *E.coli*-Pd/Fe_1 sample showing the co-localization of (b) Pd (pink) and (c) Fe (blue). (d) EDX of a NPs cluster cross-section. 45

Figure 16. High-resolution TEM bright field images showing lattice spacing of Pd-Fe NPs in *E.coli*-Pd/Fe_1 sample. 46

Figure 17. Example of phase shift images of Pd-Fe NPs synthetized by *E. coli* embedded in resin recorded with a magnetic tip at lift heights of a) 12, b) 20, c) 22, d) 50, and e) 200 nm and with a non-magnetic tip at lift heights of f) 5, g) 8, h) 9, i) 12, and j) 22 nm.....48

List of tables

Table 1. List of relevant standard reduction potentials (E0) in respect to the standard hydrogen electrode at 298.15 K (25 °C) and 101.325 kPa (1 atm). The list is in alphabetical order, according to the symbol of metal element. Taken from [92]. Published in [29]. 8

Table 2. Bacteria-mediated metal-based nanoparticles reported in the literature [29]. 13

Table 3. Bacteria-mediated bimetallic metal-based nanoparticles reported in the literature [29]. 18

List of abbreviations

4-NP	4-nitrophenol
4-AP	4-aminophenol
AAS	Atomic absorption spectroscopy
AC	Alternate current
ADF	Annular dark field
AFM	Atomic force microscopy
ATP	Adenosine triphosphate
DC	Direct current
DLS	Dynamic light scattering
EDX	Energy-dispersive x-ray spectroscopy
EELS	Electron Energy Loss Spectroscopy
EPS	Exopolysaccharide
FCC	Face-centered cubic
FTIR	Fourier transform infrared spectrometry
HAADF	High-angle annular dark-field
HR-TEM	High-resolution TEM
ICP-MS	Inductively coupled plasma mass spectrometry
LB	Lysogeny Broth
MAI	Magnetosome island
MFM	Magnetic force microscopy
MNPs	Metal nanoparticles
MRI	Magnetic resonance imaging
NADH	Nicotinamide adenine dinucleotide
NIR	Near infrared radiation
NPs	Nanoparticles
OD	Optical Density
SAED	Selected area diffraction
SQUID	Superconducting quantum interference device
STEM	Scanning transmission electron microscopy
TEM	Transmission electron microscopy
TGA	Thermal gravimetric analysis
VSM	Vibrating sample magnetometry
XPS	X-ray photoelectron spectroscopy
XRD	X-ray diffractometry

Chapter 1. Introduction

Nanoparticles (NPs) are defined as small structures with dimensions of 1 - 100 nm that can be comprised of a variety of materials such as carbon, metal, or organic substances. At the limits of this dimensions (<10 nm), some literature may also refer to them as nanoclusters which are typically composed of up to 100 atoms and possess relevant to nanoparticles physicochemical properties [1]. Metal-based nanoparticles (MNPs) contain at least one metallic element and display diverse shapes. Most of them have different properties compared to bulk metals due to their large surface-to-volume ratio, unique electromagnetic behavior, and high catalytic activity [2]. In literature a variety of MNPs is described, which not only comprise pure metals nanoparticles (e.g., Au, Ag, Pd, Pt, Fe), but also minerals or metal oxides NPs (e.g., Fe_2O_3, Co_3O_4, TiO_2), metal sulfides (e.g., Fe_3S_4, CdS), doped metal/metal compounds, and metal-organic complexes [3].

The unique behavior of nanoparticles and other nanostructured materials is strictly size-dependent and can provide improved functional performance in a variety of technical applications. Examples of industrial applications of MNPs include their use in chemical catalysis, cosmetics, detergents, water remediation, and even medical applications. The particular electromagnetic properties of Fe-based nanoparticles have secured their place as one of the most frequently used contrast agents in medical imaging [4,5] while the antibacterial properties of Ag have been effectively enhanced when it is used in the nanoparticle form [6–9]. The large active surface of MNPs makes them highly reactive, and therefore, nanoparticles based on Ag, Ni, Pt, Pd, and other elements, are distinctly effective in heterogeneous catalysis [10–13]. Pd nanoparticles are an example of an efficient catalyst of Suzuki-Miyaura reactions, in which carbon-carbon single bonds are formed to produce a complex variety of molecules that are especially important for the pharmaceutical industry [14]. Other useful potential applications include the degradation of a variety of toxic Azo dyes present in the wastewater produced by the textile industries [10,11,15], and their use in anticancer treatments [16].

1. Synthesis of metal nanoparticles

The targeted production of nanoparticles with specific properties such as defined shapes or size distributions requires strict control of the experimental conditions. The choice of synthesis method profoundly influences the characteristics of the resulting metal nanoparticles, including size, crystallinity, porosity, roughness, and shape [17,18]. Tailoring these parameters is crucial, as they dictate the nanoparticles' physicochemical attributes and, consequently, their performance in various applications. Current methods for MNP synthesis are based on different chemical, physical, or biological methods, which can be classified into two major categories: (a) top-down and (b) bottom-up approaches (Figure 1). The preferred approach is dependent on the desired particles characteristics, the size of production, cost of operation, and the applications intended for the produced nanoparticles [19].

Top-down methods involve physical or chemical processes that aim to reduce or decompose large substrates or bulk materials. Preparation of MNPs by these methods allows the large-

scale production of the high purity nanoparticles, which is crucial for many applications. One commonly employed top-down approach is mechanical milling, where bulk metal is subjected to intense mechanical forces, resulting in the fragmentation of the material into nanoparticles [20]. Other methods include, sputtering [21], chemical etching [22], laser ablation [23], electroexplosion [24], lithography [25], sonication [26], ultraviolet irradiation [27], and electron beam evaporation [28]. Traditional top-down methods can produce particles with well-controlled shapes and uniform sizes, however, they usually require specialized fabrication facilities, large amounts of energy, produce hazardous waste and entail high production costs [25]. Additionally, most of them are not suitable for the preparation of extremely small-sized nanoparticles (<10nm) [17,25].

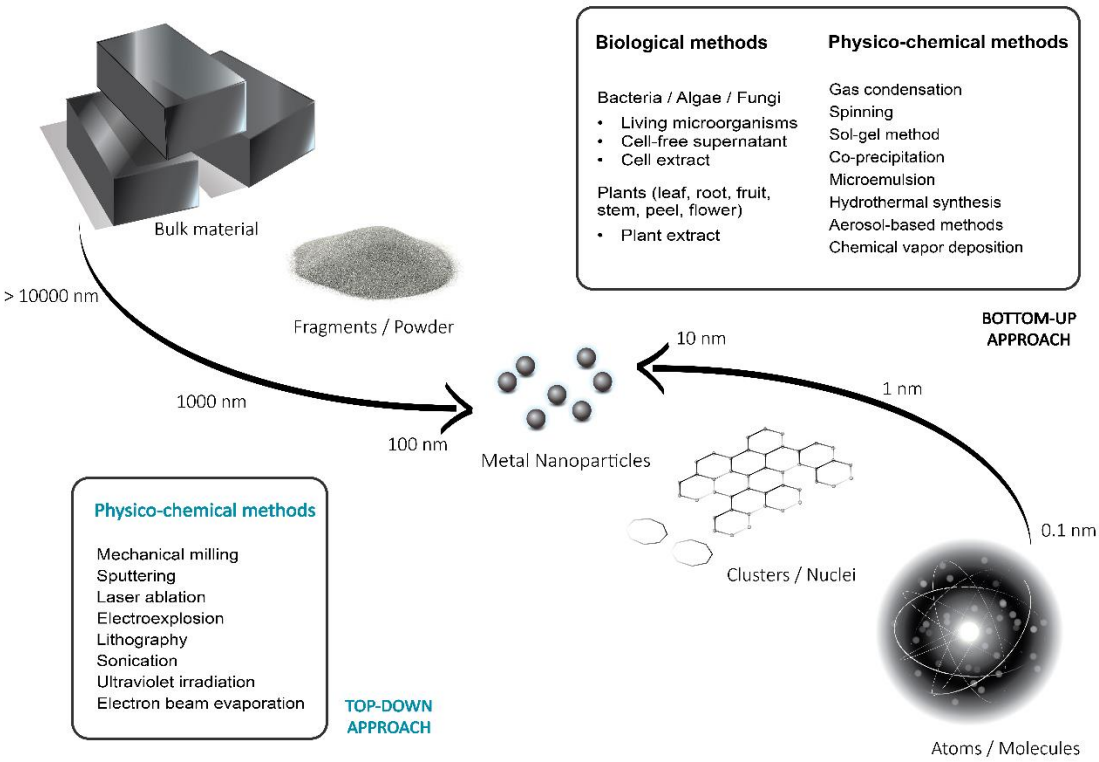

Figure 1. Illustration of the top-down and bottom-up approaches for the synthesis of metal nanoparticles [29].

In the bottom-up approaches, dissolved or evaporated substances are used as the basis for growth and synthesis of the particles. Using a variety of chemical reactions and physical processes, the building blocks are assembled by controlled precipitation, crystallization and condensation with a low energy input to result in the nanoparticles [30]. These bottom-up approaches are widely used, as they tend to be more accessible and cheaper compared to the top-down methods. Among them are gas condensation [31], spinning [32], sol-gel method [33], co-precipitation [34], microemulsion technique [35], hydrothermal synthesis [36], aerosol-based methods [37–39], plasma arcing [40], and chemical vapor deposition [41]. Frequently, they are referred to as wet methods since most of them involve solvents, stabilizers, reducing agents and other chemicals. Nanomaterials produced by these methods often must be capped

to restrict the particle growth and to obtain homogeneous nanoparticle populations. Capping agents are stabilization molecules widely employed to control the material's particle size, agglomeration, and morphology. They attach to the surface of the nanoparticle and reduce the surface energy, which has a direct effect on the dispersion of the NPs in wet media. Examples include gums, cationic surfactants, polymers, and plant extracts [42]. The toxicity of some of the capping agents and other chemicals involved in this process has proven to be an important disadvantage of the techniques, along with the lack of precise control of particle shape, size and dispersity [25]. As an alternative, bio-based methods have received increasing attention, as they promise a more reliable, nontoxic and eco-friendly synthesis of MNPs [43].

2. Bacterial synthesis of nanoparticles

The production of metal nanoparticles using biological methods belongs to the bottom-up approaches. A great variety of organisms such as plants, bacteria, fungi, and algae have been explored for their potential to synthesize, for example, silver, gold, iron, palladium, selenium, zinc, and platinum-based nanoparticles [43–46]. In addition, not only living organisms, but also many chemical substances derived from the metabolism of microbes and plants, such as biopolymers and biological extracts have been proposed as agents for the biological synthesis of MNPs [19,47]. The natural reduction and stabilization agents in these reactions result in a potentially more sustainable synthesis compared to current chemical and physical methods. In general, these biological methods are considered to be more inexpensive, nontoxic, and environmentally benign as most reactions occur at room temperature and with a low energy input [48]. However, it is pertinent to note that these bio-nanoparticles tend to be polydisperse and difficult to purify. Some of the most significant challenges of nanoparticle biosynthesis include the control of size distribution and dispersity. In addition, it is important to understand the pathways of reduction that may lead to efficient nanoparticle production, and to develop suitable purification protocols [49].

During the microbial reduction of metals into MNPs, cations are transformed into ions with a lower valence. A special case is the precious metals, including Pd, Pt, Au, and Ag, that are easily reduced into elementary forms [50]. The challenge of producing nanoparticles using bacteria, is identifying the exact chemical components and mechanisms involved in nanoparticle formation. The pathways may result in nanoparticles formed only extracellularly, intracellularly, or both, and there is a debate about which method is the most efficient for production of NPs in industrial processes. The intracellular nanoparticles formed in living cells are attached to the biological material, making their purification difficult; however, capping of the nanoparticles provides better control of their size, generating more homogeneous populations of biocompatible nanoparticles with interesting novel physical and chemical properties. In contrast, nanoparticles produced externally are preferred in many cases due to their faster production, facile recovery, and simple purification.

Reports on the synthesis of nanoparticles with bacteria can be categorized into three main methodologies, where NP production is mediated by intact living cells, by bacterial cell-free supernatants, or by cell lysate supernatants (cell extracts). Nanoparticles produced by biological methods are usually capped with non-toxic biomolecule coatings. These bio-

coatings can enhance bio-compatibility of the particles e.g. in medical applications, and can also work as stabilizers that promote the formation of homogeneous small-size nanoparticles by preventing their aggregation [44]. An example is the reduced toxicity of iron oxide nanoparticles by the addition of a biocompatible coating of polysaccharides that enables targeted delivery of materials for cancer therapy [51]. The biological synthesis of metal nanoparticles has many potential uses not only in biomedical applications, but also in bioremediation, bioleaching, and biocorrosion [52].

2.1. Bacteria-metal interactions

Bacteria have ubiquitous interactions with metals. They can be classified into the homeostasis of essential metals, and (heavy) metal resistance to harmful metals. Some metals are important as micronutrients whereas other (heavy) metals (such as Al, Pd, Cd, Au, Hg, Ag) are toxic to living organisms and do not have specific biological roles [53]. The essential metals are nutrients and trace elements for key metabolic processes, such as metals in the bacterial respiratory chain. Therefore, microbes have developed a variety of often highly specific mechanisms for metal transport, oxidation/reduction, or detoxification. Nevertheless, the unintentional uptake of high concentrations of metal ions or toxic heavy metals can occur, and microorganisms have developed different strategies to cope with heavy metal stress. Microbial populations can survive in metal-polluted locations by, directly or indirectly, modifying the metal availability through physical or biochemical mechanisms to protect their integrity [43]. The complex mechanisms developed by different species and strains vary and depend both on the native environment and on the heavy metal content. The basic mechanisms of bacteria-metal interactions can be divided into the following four categories:

2.1.1. Metal sequestration

Many essential biological processes involve metal ions, and in particular, redox active transition metals like manganese, iron, cobalt, copper and magnesium. For instance, divalent ions such as Mn^{2+} and Fe^{2+}, are indispensable for oxidative stress resistance or as cofactors for the respiratory chain in bacterial core metabolism [54]. Hence, microorganisms have evolved pathways of metal sequestration to transport ions and to regulate ion availability. In the simplest case, the sequestration of metal ions occurs by adsorption. In Figure 2, metal ions are depicted as positively charged entities interacting with the bacterial membrane and other biomolecules. During adsorption, deprotonated functional groups (carboxyl, phosphonate, amine, and hydroxyl groups) on the cell surface result in a net negative charge which attracts metal cations and leads to non-specific binding of the metal to the cell surface [55]. This process is independent of the cell metabolism, and it is mainly influenced by factors such as temperature, pH, ionic strength, concentration and by the complex composition of the microorganism's surface. As an example, Gram-positive bacteria expose a large amounts of carboxyl groups in their peptidoglycan-rich cell walls, making them efficient metal chelators [56]. As a consequence of this sequestration, these metals are enriched on the cell surface and can be taken up by specific transport processes (discussed below).

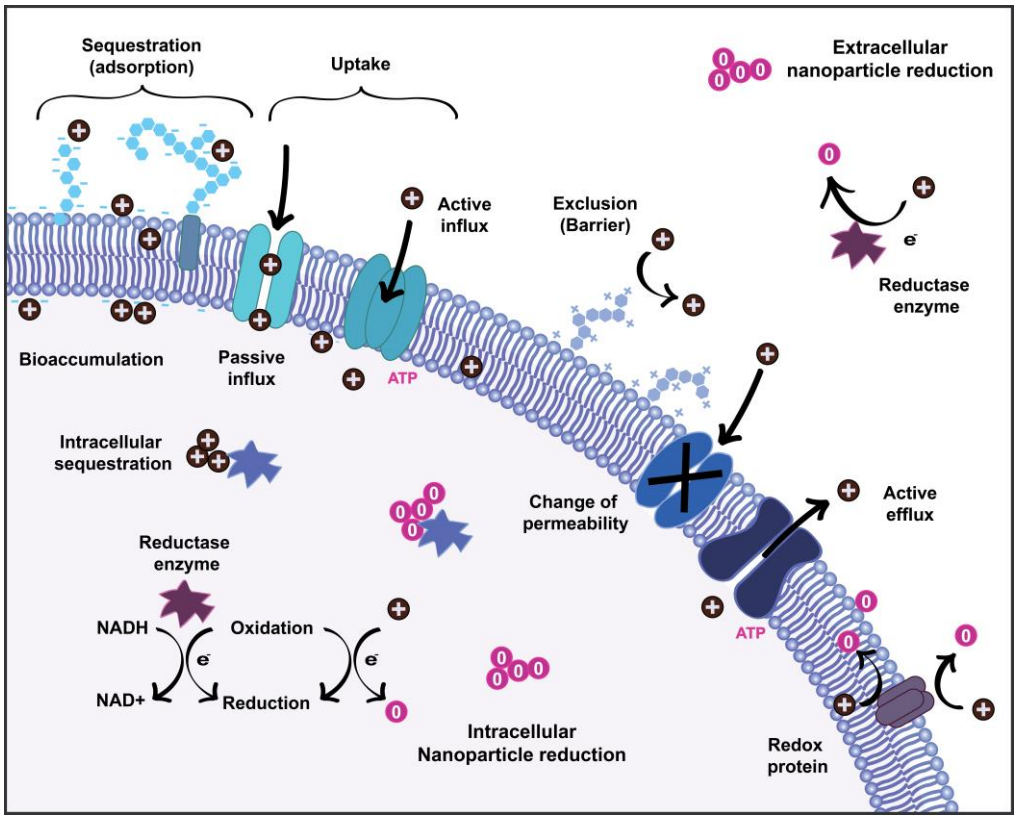

Figure 2. Schematics of bacteria interaction with heavy metals and mechanisms of nanoparticle formation [29].

Overall, the extracellular sequestration of heavy metals not only allows to accumulate relevant metabolic cofactors, but it is also a defense mechanism against toxic metals, by reducing the availability of unwanted metal ions. Polymers secreted by bacteria such as the exopolysaccharide (EPS) coatings of some species, have the ability to adsorb and bind metals extracellularly, thus acting as a protective layer that prevents the uptake of toxic metals [57]. Bacteria are likely to sequester non-essential metal ions, such as Au and Pd, by adsorption mechanisms. Compared to other microorganisms, Gram-negative bacteria such as *Acinetobacter calcoaceticus*, *Erwinia herbicola*, *Pseudomonas maltophilia* and *Pseudomonas aeruginosa* have the highest ability to accumulate metals such as gold [58]. This is a result of the surface charge present on the Gram-negative bacterial membrane, which promotes the gold adsorption from aqueous solutions. In the same way, the biosorption of Pd is presumably a result of the chemical affinity of metal complexes such as $[PdCl_4]^{2-}$ for protonated groups on the cell surface at an acidic pH [59].

Free metal ions passively or actively transported from outside of the membrane into the cytoplasm can pose a danger to the cell and must be immobilized or transformed. Bacteria can produce metabolites, like metallothioneins, phytochelatins and glutathione with high affinity for metals for the intracellular sequestration of metal ions. Metallothioneins are small, cysteine-rich proteins that are directly involved in the homeostasis of different metal ions, including Cu^{+} and Zn^{2+}. These proteins have been reported in bacteria such as *Bacillus altitudinis* MT422188 and *Mycobacterium tuberculosis* where they are expressed under Zn^{2+} and Cu^{+} induced stress,

respectively [60,61]. The immobilization of the ions decreases the toxicity; however, the metal sequestration mechanisms are limited by the saturation of the binding sites in the extracellular and intracellular matrix [57].

2.1.2. Metal uptake

The metal ions in proximity to the extracellular layers can be imported by passive or active influx through the different layers of the cell wall, using non-specific transporters, metal-specific channels or passive diffusion (Figure 2) [57]. The indispensable uptake of essential metals is highly regulated and typically mediated by specific, energy-dependent uptake systems. In *E. coli, Alcaligenes eutrophus* and many other enterobacteria, essential trace elements such as Ni^{2+}, Co^{2+}, and Zn^{2+} ions are transported into the cell by constitutive Mg^{2+} transport systems [62,63]. These relatively unspecific uptake systems allow the 'cost-effective' accumulation of macronutrients such as Mg and of trace metal ions in environments with habitual metal concentrations. In extreme conditions, with deficits in trace metals, bacteria can upregulate genes related to specific, ATP-dependent uptake systems for these elements in order to transport the ions against the concentration gradient. The TonB-dependent transporter, OprC, is repressed in *P. aeruginosa* by high exogenous Cu ion concentrations and expressed in anaerobic conditions to bind and transport $Cu^{+/2+}$ [64]. In environments with low availability of essential metals, many bacteria also secrete metal-sequestering proteins or other chelators to bind the biologically relevant ions and to specifically import them [54]. An example of this mechanism are iron siderophores, which are low molecular weight compounds known for their high affinity for Fe ions. Siderophores are frequently used by pathogenic bacteria to chelate Fe^{2+} and Fe^{3+} in host environments that are otherwise deprived of free Fe ions [61]. The siderophores with bound ions are then recognized by specific outer membrane receptors that guide the chelated ions through energy-dependent ATP-binding cassette (ABC) transporters [65,66]. Because of the different chemical properties of Fe^{3+} and Fe^{2+}, bacteria utilize different specific transport systems (and siderophores) for each ion [67,68]. Examples of different transport systems involved in bacterial Fe uptake, include MntH, ZupT, YfeABCD, FutABC, EfeUOB and Feo [67].

The uptake of precious metals like Au, Ag, Pt, and Pd ions into bacteria is not well understood, as cells do not possess inherent active, specific transport mechanisms to regulate non-essential ion uptake. The absorption of toxic heavy metals is presumably a process carried out by passive mechanisms such as diffusion. Therefore, at elevated concentrations, non-essential metals can interact with the cell, cross into the cytoplasm and accumulate there [69]. However, some authors suggest that heavy metals like Pd may also accidentally be absorbed and imported into living cells through systems specific for essential metallic metabolites, such as Fe, Ni, Cu or Zn [70]. Metal ions with comparable properties and ion radius, due to their similar conformations, can out-compete essential ions in binding to proteins. As an example, the high affinity of Hg and Cd ions to cysteine-rich sites in Zn-binding proteins results in translocation of these toxic metals. A similar effect is found in Cu-binding proteins with Au and Ag as competing metal ions [71]. A special case of non-essential metal uptake is the homeostasis mechanism of specialized metal-resistant bacterial strains for some toxic heavy metal ions. In the case of *Cupriavidus metallidurans*, genes in the *gig* (gold-induced genes) operon are

strongly upregulated after sequestration of Au ions in the membrane. The proteins encoded by this operon are suggested to be directly involved in the import of Au ions into the cytoplasm to prevent the harmful action of Au^{3+} in the periplasm. The reduced complexes there are later removed from the cytoplasm [72,73].

2.1.3. Metal detoxification

If not regulated, high concentrations of metals would have adverse effects in the metabolic processes of the cell. In metals such as Cu, their redox activity favors the formation of active oxygen species, which explains their toxicity. Excess of essential metals or toxic, non-essential heavy metals also leads to mismetallation of proteins which results in their inactivation [74]. The exposure to high concentrations of heavy metals activates a mechanism of defense called metal exclusion, in which the permeability of the cell membrane, the envelope, or the surface layer is modified to prevent or reduce the further influx of metal ions (Figure 2). Bacteria can alter the composition of the cell wall in an attempt to form a barrier for ions. A well-known example of this mechanism is the reduction of the expression of Porin channels in heavy-metal resistant mutants of *E. coli*. In this case, pore proteins such as OmpF are expressed at a reduced rate, leading to increased Cu and Ag resistance [75–77]. In a complementary mechanism, the active efflux of metal ions involves the use of highly specific membrane transport systems. This process to decrease the concentration of harmful metal ions inside the cell is widely spread among bacteria. The transport of cations and anions from the cytoplasm against a concentration gradient requires energy. The involved efflux pumps can be broadly classified by their energy source into ATP-dependent and proton-gradient-based systems. Further classifications are based on sequence similarity, transport function and substrate specificity [78–80].
Some examples of well-studied heavy metal efflux pumps are the P-type ATPase transport protein CopA, known to be involved in copper resistance [81] and the resistance-nodulation-cell division (RND) family proteins, CzcA and CusA, which bind and export Cu^{+} and Ag^{+} in *E. coli* [82]. In partly silver-resistant *E. coli* bacteria, the detoxification mechanism for silver is based on the expression of the CusCFBA copper/silver efflux systems that actively export the silver ions from the cytoplasm and bind it in the periplasm [83]. In some bacteria, metal ions transported by efflux pumps may be retained in the periplasm even after the efflux process, along with the metal ions sequestered by EPSs and by other metal-binding proteins [84]. The ions bioaccumulated in the cytoplasm, periplasm and in the extracellular matrix can later become sites for nucleation and formation of nanoparticles (Figure 2).

2.1.4. Metal transformation

Some microorganisms have a remarkable ability to transform heavy metal ions in their environment and to produce MNPs. Even when sequestered, the high reactivity of transition metal ions could disrupt metabolic processes or damage DNA molecules. Various metal ions have a high binding affinity for biological macromolecules such as nucleic acids, or thiol-containing proteins [79,85], and, therefore, they need to be transformed into inert or less toxic substances. This is mediated by redox-active metabolic pathways in order to change solubility and toxicity, and often leads to complexation or precipitation of metals extracellularly

[57,86,87]. Alternatively, biomethylation is a metabolic process in which methyl groups are transferred to the toxic metal ions or metalloids to create less toxic, sometimes volatile compounds. Hg, Sn, As, Se, Te, Au, Tl and Pb have been reported as methyl group acceptors in primary and secondary metabolic processes [88]. The resulting products are more toxic than the inorganic compounds, in many cases, so it is debatable whether methylation is, in fact, a detoxification mechanism. However, it is important to note that the volatility has an important effect on reducing the concentration of the metals in the surrounding environment. Extended descriptions of the general pathways for biomethylation can be found elsewhere [89–91].

Table 1. List of relevant standard reduction potentials (E0) in respect to the standard hydrogen electrode at 298.15 K (25 °C) and 101.325 kPa (1 atm). The list is in alphabetical order, according to the symbol of metal element. Taken from [92]. Published in [29].

Reaction	*E_0 (Volts)*
$Ag^{+} + e \rightleftharpoons Ag$	0.7996
$AuCl_4^{-} + 3\,e \rightleftharpoons Au + 4\,Cl^{-}$	1.0020
$Cd^{2+} + 2\,e \rightleftharpoons Cd$	-0.4030
$Co^{2+} + 2\,e \rightleftharpoons Co$	-0.2800
$Co^{3+} + e \rightleftharpoons Co^{2+}$	1.9200
$Cr^{2+} + 2\,e \rightleftharpoons Cr$	-0.9130
$Cr^{3+} + e \rightleftharpoons Cr^{2+}$	-0.4070
$Cr^{3+} + 3\,e \rightleftharpoons Cr$	-0.7440
$Cr_2O_7^{2-} + 14\,H^{+} + 6\,e \rightleftharpoons 2\,Cr^{3+} + 7\,H_2O$	1.3600
$Fe^{2+} + 2\,e \rightleftharpoons Fe$	-0.4470
$Fe^{3+} + 3\,e \rightleftharpoons Fe$	-0.0370
$Fe^{3+} + e \rightleftharpoons Fe^{2+}$	0.7710
$2\,HFeO_4^{-} + 8\,H^{+} + 6\,e \rightleftharpoons Fe_2O_3 + 5\,H_2O$	2.0900
$Mn^{2+} + 2\,e \rightleftharpoons Mn$	-1.1850
$Mn^{3+} + e \rightleftharpoons Mn^{2+}$	1.5415
$MnO_2 + 4H^{+} + 2\,e \rightleftharpoons Mn^{2+} + 2\,H_2O$	1.224
$Ni^{2+} + 2\,e \rightleftharpoons Ni$	-0.2570
$[PdCl_4]^{2-} + 2\,e \rightleftharpoons Pd + 4\,Cl^{-}$	0.5910
$[PdCl_6]^{2-} + 2\,e \rightleftharpoons [PdCl_4]^{2-} + 2\,Cl^{-}$	1.2880
$[PtCl_4]^{2-} + 2\,e \rightleftharpoons Pt + 4\,Cl^{-}$	0.7550
$[PtCl_6]^{2-} + 2\,e \rightleftharpoons [PtCl_4]^{2-} + 2\,Cl^{-}$	0.6800
$TcO_4^{-} + 8\,H^{+} + 7\,e \rightleftharpoons Tc + 4\,H_2O$	0.4720
$Ti^{2+} + 2\,e \rightleftharpoons Ti$	-1.6280
$UO_2^{2+} + 4\,H^{+} + 6\,e \rightleftharpoons U + 2\,H_2O$	-1.4440
$Zn^{2+} + 2\,e \rightleftharpoons Zn$	-0.7618

Some bacteria can decrease the mobility of metal ions through enzymatically promoted redox reactions that reduce the metals irreversibly, leading to the assembly into metal clusters. An illustration of the general process of reduction of the metal ions to neutral ions by redox proteins intra- and extracellularly can be found in Figure 2. The electron-accepting potential of different

metal ions known to be reduced by bacteria are shown in Table 1. The reduction potential is expressed as the E_0 value, ranging from very negative E_0 values for compounds that are easily oxidized, to large positive E_0 values for compounds that readily accept electrons (are easily reduced). "Precious" metals such as Au, Pd or Ag have cations species with very high positive potentials and are frequently reduced into nanoparticles by bacteria.

The cornerstone of every living organism is energy conservation where chemical or light energy is ultimately converted into adenosine triphosphate (ATP). ATP production is facilitated by substrate-level phosphorylation, oxidative phosphorylation, or photophosphorylation. In order to achieve this, electrons need to be transferred in an oxidation-reduction coupled reaction. This electron movement within the cell is facilitated by electron carriers, such as nicotinamide adenine dinucleotide (NAD^+/NADH), which promotes a diversity of reduction-oxidation reactions as they allow a variety of electron partners to interact with each other [93–95]. It is these metabolic reactions and electron carriers that are diverted and used for metal ion reduction.

On an extracellular level, bacterial growth is heavily influenced by the oxidation-reduction (redox) potential of the environment, and in turn, bacteria can modify the redox potential of their environment. Surprisingly, this ability is highly species-specific and can be exploited to identify different species by using redox electrodes [96]. A change in redox potential indicates the availability of electron acceptors and donors. Since bacteria can inhabit every niche that can support life, their diversity is also manifested in the type of electron acceptors that they can utilize intracellularly. Under aerobic respiration conditions, oxygen is the final electron acceptor while under anaerobic respiration conditions, a variety of electron acceptors can be utilized, such as nitrate (NO^{3-}), trimethylamine oxide/dimethyl sulfoxide (TMAO/DMSO), carbon dioxide (CO_2) or organic electron acceptors such as fumarate, depending on the bacterial species studied [97,98]. Metal-based respiration is characterized by the utilization of manganic manganese (Mn^{4+}) or ferric iron (Fe^{3+}) as electron acceptors. Bacteria can reduce these metal compounds through mechanisms that involve redox-active proteins like reductases, cytochromes, and metallothioneins [99].

Sulfate- and metal-reducing bacteria are frequently employed for the synthesis of metal nanoparticles, as these organisms are rich in membrane redox-active proteins and therefore easily enzymatically reduce different metal ions. These 'reducing' microorganisms can use the metal cations as terminal electron acceptors while performing anaerobic respiration, reducing Fe^{3+} to Fe^{2+} and Mn^{4+} to Mn^{2+} for energy conservation [100]. These proteins however, are not necessarily highly specific and multiple enzymes are capable of reducing several redox-active metals ions [101]. The interaction of some bacteria with non-essential, toxic metal ions such as Au^{3+}, Ag^+, Pd^{2+} and Pt^{2+} also upregulates the expression of multiple redox-active enzymes located on the cell walls, in periplasmic space and intracellular contents, such as hydrogenases and NADH reductases, which can reduce ions to insoluble complexes that are subsequently transformed into MNPs [70,102]. One example is nitrate reductase known to be involved in the bioreduction of the bound Ag^+ to Ag^0 in *Bacillus licheniformis* as defense from heavy metals exposure [103,104]. As suggested by their negative reduction potential (Table 1), the NAD(P)H-dependent reduction of ions such as Cd^{2+}, Zn^{2+}, Co^{2+} or Ni^{2+} to metallic form may not be energetically favored, so the reduction of these ions is uncommon in bacteria and the particular cases of reduction must involve different mechanisms [62]. In *Shewanella* strains,

EPS-induced reduction and indirect electron transfer using electron shuttles such as flavins, L-cysteine, and quinones are possible alternative pathways that have been thoroughly described elsewhere [105]. Metal NPs reduced and precipitated in the extracellular and intracellular space may possess different characteristics than their chemically produced counterparts. The biomolecules associated with them create a biological cap that stops nanoparticle growth, minimizes cytotoxicity, and may affect their chemical and physical properties [106]. The reduced metal particles accumulate without much effect on the cell population. Therefore, the formation of MNPs can be regarded as a by-product of microbial defense mechanisms, bacterial metabolism, or as a biomineralization process intended to control, immobilize, or decrease the heavy metal bioavailability.

2.2. Bacterial metal nanoparticles in nature

Even though naturally occurring nanoparticles are widely found in living organisms, the intracellular accumulation of solid metals is usually not a favorable condition for the cells and can lead to cell death. A complete metal particle detoxification would require energy and elaborated mechanisms of particle excretion [107]. This is probably the reason why only few bacterial species produce metal-based nanoparticles as part of their normal metabolic processes. The most remarkable example are magnetotactic bacteria, an extraordinary group of Gram-negative organisms that rely on biosynthetic iron-based crystals to orient and migrate along the geomagnetic field lines in a behavior known as “magnetotaxis” (Figure 3) [108]. The highly specialized organelles made of nanometer-sized metal crystals wrapped in a membrane are called magnetosomes. They are composed of magnetic iron oxide magnetite (Fe_3O_4) or iron sulfide greigite (Fe_3S_4) of different shapes and sizes depending on the exact bacterial species. The magnetosomes are frequently aligned in chains across the motility axis of the cell. This imparts the bacteria with a permanent magnetic dipole moment, causing them to align passively in a parallel orientation with external magnetic fields [109]. The cells swim along the geomagnetic field lines of the earth to the oxic-anoxic interface of the aquatic habitat where there are the most favorable conditions for their growth [110].

Despite the abundance of magnetotactic bacteria in the environment, only a few strains have been isolated into pure culture due to their particular growth requirements. Strains from the proteobacterial genus *Magnetospirillum* are the most common isolates. However, recent publications report up to 16 different lineages that include *Proteobacteria*, *Nitrospirota*, and *Omnitrophota* [111,112]. The strains *Magnetospirillum gryphiswaldense* MSR-1 (first isolated in 1991 by Schleifer *et al.* [113]), *Magnetospirillum magnetotacticum* strain MS-1 and *Magnetospirillum magneticum* AMB-1, are currently the most studied bacteria for the understanding of magnetosome formation and its complex genetic regulation [114]. In *M. gryphiswaldense* MSR-1, the magnetosome island (MAI) comprises most of the genes that control the magnetosome synthesis. These genes encode all the essential processes in the majors steps of the organelle formation and determine the morphology and chemical composition of the particles [115,116]. In the past, different models of magnetosome biomineralization have been proposed [108,114,117]. Currently, four major steps are considered necessary to achieve the biomineralization. The first step is (i) the cytoplasmic

membrane invagination into vesicles, followed by (ii) the arrangement of specific magnetosome proteins into the organelle membrane. Then, (iii) the internalization and accumulation of iron into the vesicles by energy-dependent transport proteins takes place. Here, the cell rapidly chemically transforms the Fe ions and combines them into metal crystals. Specific proteins guide this process in order to avoid the toxic effect of intracellular Fe. Finally, (iv) the magnetosomes are assembled into a linear chain along cytoskeletal filaments [115].

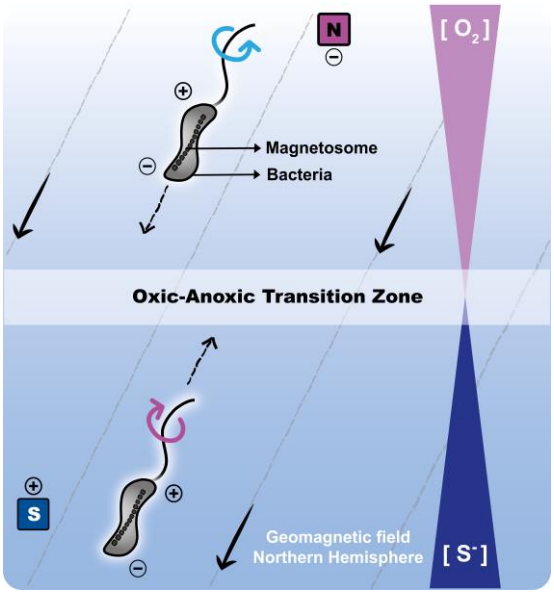

Figure 3. Illustration of bacterial magnetotaxis. Bacteria cells are aligned with the geomagnetic field of the earth due to a magnetic torque created by the intracellular chains of magnetosomes. The cells move along the field lines to the oxic-anoxic transition zone of the aquatic habitat.

The bacteria tightly control the size and morphology of the magnetosomes. Magnetosome crystals typically fall in a size range of about 30-120 nm. However, some species can form particles up to 250 nm in length [108]. The spirillum-shaped bacterium *M. magneticum* AMB-1, originally collected from fresh water sediments of a natural spring in Tokyo, presents magnetite magnetosomes with an average diameter of 50 nm, aligned in chains of around 15 particles per cell [118]. In contrast, the *M. gryphiswaldense* MSR-1 bacteria were found to produce chains of up to 60 homogeneous magnetosomes with particle sizes of about 42 nm [117]. Both strains, like other bacteria from the *Magnetospirillum genus*, produce cubo-octahedral crystalline magnetosomes. In general, three different morphologies of magnetosomes can be found in nature: (i) cubic or cubo-octahedral, (ii) elongated hexa- or octahedral and (iii) even more elongated crystals with large, anisotropic faces, showing tooth, arrowhead, or bullet shapes [119]. These crystal structures are consistently replicated in the magnetosomes of bacteria of the same strain and have a direct influence on the final magnetic behavior of the particles.

The magnetosomes, due to their narrow size distribution, low aggregation, and strong ferromagnetism, have many potential technical applications. The low toxicity of bacterial

magnetosomes in comparison with synthetic magnetic nanoparticles makes them especially attractive for biomedical applications. Cytotoxicity of bacterial magnetosomes varies depending on various factors, including cell type, incubation time, and concentration. While many types of magnetite nanoparticles (such as Superparamagnetic iron oxide nanoparticles (SPION)) are considered cytotoxic at exposure levels above 70-100 µg/mL [120–122], a study by Alphandéry *et al.* in MDA-MB-231 cells suggested low cytotoxicity due to magnetosome exposure at concentrations below 1000 µg/mL, which can be further improved by removing bacterial endotoxins and using biocoatings [112,123]. In a recent study, Gwisai *et al.* evaluated the use of the ferromagnetic properties of AMB-1 bacterial magnetosomes for targeted cancer therapy. Thanks to their susceptibility to external magnetic fields, magnetotactic bacterial cells were magnetically manipulated and studied as a vehicle for tumor infiltration and drug delivery [124]. In a similar approach, Xing *et al*. successfully demonstrated the colonization and ablation of tumors in mice by means of *in vivo* magnetically manipulated *M. magneticum* AMB-1 bacteria, showing their enormous potential for an efficient cancer treatment [125]. Other potential application of magnetosomes include their use as magnetic resonance contrast agents. *In vivo* experiments were conducted on mice to examine how magnetosomes were distributed and eliminated after injection as a contrast agent in magnetic resonance imaging (MRI). The researchers concluded that their use in MRI was adequate in terms of spatial resolution and sensitivity [126].

Microorganisms play an important role in the process of biomineralization and metal geochemistry. The metals transformation into nanoparticles is also a natural process observed in some astounding microorganisms known as dissimilatory metal-reducing bacteria. In anoxic environments with abundant metal species such as Fe^{3+}, $Mn^{3+/4+}$, U^{6+}, Cr^{6+}, Co^{3+} and Tc^{7+}, these metal cations are reduced into nanoparticles by the bacteria [127,128]. All these elements have in common that they are good electron acceptors due to their high reduction potential. Then, during anaerobic respiration, the bacteria can replace oxygen as the terminal electron acceptor with the available cations. Fe^{3+} is the most abundant possible electron acceptor in anoxic environments. Due to its comparatively high reactivity with oxygen, elemental Fe is not frequently found in nature, but instead, is commonly found in the form of iron oxides. In metal- and sulfur-reducing microorganisms like, *Geobacter sulfurreducens*, *Geobacter metallireducens* GS15 and *Shewanella oneidensis* MR-1 (*S. oneidensis* MR-1), specialized membrane proteins are suggested to be involved in the Fe^{3+} reduction. Their outer membranes are rich in c-type cytochromes that transfer electrons coupled to the oxidation of lactate and other carbon sources to soluble Fe^{3+} oxides resulting in iron oxide NPs [129–131]. Many Fe-based NPs naturally synthesized by bacteria consist of diverse compositions of iron oxides. The metal-based anaerobic mechanism of respiration is considered part of the natural cycle of precipitation of many heavy metals into anoxic sediments [128]. Multiple processes of bioremediation of heavy metals from the environment and contaminated water streams have been engineered based on the reducing ability of these bacteria [132]. Other transition metals such as gold, silver, and copper have high positive reduction potentials and are exchanged with iron. Bacteria readily precipitate them during remediation, which can then be applied to the biogenic production of these metal nanoparticles.

2.3. Biosynthetic nanoparticles

Bio-inspired NPs of different metals have been successfully synthesized using a large variety of bacterial strains. Under optimal conditions in temperature, pH, and redox state, some bacterial species can reduce metal ions and form nanoparticles. Among the metals successfully recovered by bacteria in form of nanoparticles are iron, manganese, chromium, cobalt, palladium, gold, silver, arsenic, selenium, uranium, and polonium [85]. Their resulting size-distribution, morphology and functional properties are highly dependent on the protocols used for the biosynthesis as well as on the type of bacteria and metal involved. In Table 2, details from recent, published protocols for metal nanoparticles fabrication using different bacterial strains are listed.

Table 2. Bacteria-mediated metal-based nanoparticles reported in the literature [29].

Metal	Name of organism	NP	Size	Morphology	Localization	Reference
Au	*Bifidobacterium lactis*	Au	5–40 nm	Hexagonal	Intracellular	[133]
	Bacillus cereus	Au	20–50 nm	Spherical / Hexagonal / Octagonal	Extracellular	[134]
	Bacillus Licheniformis	Au	60–146 nm	Spherical	Intracellular	[135]
	Caldicellulosiruptor changbaiensis CBS-Z	Au	1–20 nm	----	Membrane	[136]
	Escherichia coli	Au	6–60 nm	Spherical	Extracellular	[133]
	Lactobacillus casei	Au	7–56 nm	----	Membrane	[137]
	Marinobacter pelagius RS11	Au	2–10 nm	Spherical / Triangular	----	[138]
	Paracoccus haeundaensis BC74171	Au	15–35 nm	Spherical	Extracellular	[139]
	Pseudomonas stutzeri KDP_M2	Au	10–20 nm	Spherical	----	[140]
	Sporosarcina koreensis DC4	Au	92 nm	Spherical	Extracellular	[141]
	Vibrio alginolyticus	Au	100–150 nm	Anisotropic	----	[142]
Ag	*Aeromonas* THG-FG1.2	Ag	8–16 nm	Spherical	Supernatant	[143]
	Bacillus brevis	Ag	22–60 nm	Spherical	Supernatant	[144]
	Bacillus cereus	Ag	5–7 nm	Spherical	----	[145]
	Bacillus clausii	Ag	30–80 nm	Spherical	Supernatant	[146]
	Bacillus Pumilus ROM6	Ag	20–70 nm	Spherical	Supernatant	[147]
	Escherichia coli 116AR	Ag	5–70 nm	----	Membrane	[83]
	Escherichia coli Top 10	Ag	2–40 nm	----	Supernatant	[148]
	Lactobacillus Acidophilus	Ag	10–20 nm	Spherical	Supernatant	[149]
	Lactobacillus brevis	Ag	30–100 nm	Spherical / Triangular / Hexagonal	Supernatant	[150]

	Paenarthrobacter nicotinovorans MAHUQ-43	Ag	13–27 nm	Spherical	Supernatant	[151]
	Pseudomonas aeruginosa	Ag	25 nm	Spherical	Supernatant	[152]
	Pseudomonas putida MVP2	Ag	6–16 nm	Spherical	Membrane / Supernatant	[153]
	Pseudomonas stutzeri	Ag	22–46 nm	Spherical	Extracellular	[154]
	Pseudomonas stutzeri	Ag	10–50 nm	Anisotropic	----	[155]
	Sporosarcina koreensis DC4	Ag	102 nm	Spherical	Extracellular	[141]
	Stenotrophomonas maltophilia	Ag	93 nm	Cuboidal	Supernatant	[156]
Pt	*Escherichia coli* MC4100	Pt	2.3–4.5 nm	Spherical	----	[157]
	Pseudomonas kunmingensis ADR19	Pt	3.95 nm	Spherical	Supernatant	[158]
	Psychrobacter faecalis FZC6	Pt	2.49 nm	Spherical	Supernatant	[158]
	Vibrio fischeri NRRL B-11177	Pt	3.84 nm	Spherical	Supernatant	[158]
	Jeotgalicoccus coquinae ZC15	Pt	5.74 nm	Spherical	Supernatant	[158]
	Sporosarcina psychrophila KC19	Pt	4.24 nm	Spherical	Supernatant	[158]
	Kocuria rosea MN23	Pt	5.85 nm	Spherical	Supernatant	[158]
	Pseudomonas putida KT244	Pt	8.06 nm	Spherical	Supernatant	[158]
	Acinetobacter calcoaceticus	Pt	2-3.5 nm	Cuboidal	Intracellular / Membrane	[159]
Pd	*Bacillus benzeovorans*	Pd	1.7–5.8 nm	Anisotropic	Intracellular	[70]
	Bacillus megaterium Y-4	Pd	10–40 nm	Spherical	Intra / Extracellular	[102]
	Bacillus wiedmannii MSM	Pd	10–36 nm	----	Membrane	[160]
	Citrobacter sp.	Pd	11.3-15.6 nm	----	Membrane	[161]
	Citrobacter sp.	Pd	17.6–25.8 nm	Anisotropic	Membrane	[162]
	Cupriavidus metallidurans	Pd	20–40 nm	Dendrite-Shaped	Intracellular	[163]
	Desulfovibrio desulfuricans	Pd	3–13 nm	----	Intra / Extracellular	[164]
	Desulfovibrio desulfuricans	Pd	1.1–6.9 nm	Cubo-octahedron	Intracellular	[70]
	Escherichia coli BL21	Pd	2–3 nm	Spherical	Intracellular	[165]
	Escherichia coli MC4100	Pd	1–30 nm	Anisotropic	Intracellular / Membrane	[166]
	Shewanella loihica PV-4	Pd	4–10 nm	Spherical	Intra / Extracellular	[167]
	Shewanella oneidensis MR-1	Pd	2–12 nm	Spherical	Extracellular	[168]
	Shewanella oneidensis MR-1	Pd	2–25 nm	----	Supernatant	[169]
Fe	*Bacillus cereus*	Fe_3O_4	18–29 nm	Spherical	Supernatant	[170]
	Bacillus subtilis	Fe_3O_4	60–80 nm	Spherical	Supernatant	[171]

	Escherichia coli	Fe_3O_4 / Fe_2O_3	18 nm	Spherical	Intra / Extracellular	[68]
	Proteus vulgaris	----	20–30 nm	Spherical	Supernatant	[172]
	Pseudomonas aeruginosa	Fe_3O_4 / Fe_2O_3	----	----	Extracellular	[68]
	Pseudomonas putida	Fe	1–4 nm	Spherical	Intra / Extracellular	[173]
Co	*Bacillus pasteurii*	Co_3O_4	10–31 nm	Anisotropic	----	[174]
	Bacillus subtilis	Co_3O_4	31.2 nm	Anisotropic	----	[175]
	Bacillus subtilis	Co_3O_4	2–5 nm	----	Membrane	[176]
	Bacillus thuringiensis	Co	84.81 nm	Spherical	----	[177]
	Marinobacter hydrocarbonoclasticus	Co	8–22 nm	Spherical	Intracellular	[173]
	Microbacterium sp. MRS-1	Co_3O_4	10–100 nm	Spherical / pentagonal	Intra / Extracellular	[178]
	Micrococcus lylae	Co_3O_4	2–10 nm	----	Membrane	[179]
	Proteus mirabilis 10B	Co_3O_4	22.1 nm	Quasi-spherical	Intracellular	[180]
Ni	*Bacillus subtilis*	$Ni_3(PO_4)_2$	40–90 nm	Anisotropic	----	[181]
	Microbacterium sp. MRS-1	NiO	100–500 nm	Quasi-spherical	Extracellular	[182]
	Pseudomonas alcaliphila	Ni	----	Anisotropic	Intra / Extracellular	[50]
Zn	*Alkalibacillus sp.* W7	ZnO	1–30 nm	Hexagonal / Quasi-spherical	Supernatant	[183]
	Cyanobacterium Nostoc sp. EA03	ZnO	50–80 nm	Star shape	Supernatant	[184]
	Bacillus sp PTCC 1538	ZnO	99 nm	Nano-rods	----	[185]
	Halomonas elongata IBRC-M 10214	ZnO	18.11 nm	Anisotropic	Supernatant	[186]
	Lactococcus lactis NCDO1281	ZnO	55 nm	Spherical	----	[185]
	Pseudomonas geniculata	Zn	4–13 nm	Spherical	Intracellular / Membrane	[173]
	Shewanella oneidensis MR-1	ZnS	5.1 nm	Spherical	Extracellular / Membrane	[187]
Cu	*Enterococcus thailandicus*	Cu	1–4 nm	Spherical	Intracellular	[173]
	Escherichia sp. SINT7	Cu	22.33–39.00 nm	Spherical	Extracellular	[188]
	Pseudomonas fluorescens MAL2	Cu	20–80 nm	Spherical / hexagonal	----	[189]
Ti	*Halomonas elongata* IBRC-M 10214	TiO_2	104.63 nm	Spherical	Supernatant	[186]

Cr	*Alishewanella sp.* WH16-1	Cr_2O_3	100-200 nm	Spherical	Intracellular	[190]
	Bacillus cereus	Cr_2O_3	8-60 nm	Anisotropic / Spherical	Extracellular / Membrane	[191]
	Bacillus subtilis	Cr_2O_3	4-50 nm	Spherical	----	[192]
Cd	*Bacillus badius*	CdS	20- 80 nm	----	Supernatant	[193]
	Pedobacter sp. UYP1	CdS	2.8-4.9 nm	Anisotropic	Extracellular	[194]
	Raoultella sp. X13	CdS	5-8 nm	----	----	[195]

2.3.1. Gold and silver nanoparticles

Metallic gold (Au) and silver (Ag) can be used in a wide range of applications due to their high stability, oxidation resistance, and biocompatibility. In nanoparticle form, gold displays an improved potential for chemical catalysis and has antimicrobial effects, while Ag NPs are of special interest for their uses in the biotechnology industry. Drug delivery, diagnostics, cancer treatment and antibacterial agents are some of their most known applications for the NPs [196] Despite these antibacterial properties, some microorganisms have been successfully used to synthesize Au and Ag NPs. One of the first bacterial species studied for the reduction of Au was *Bacillus subtilis*. In their work, Beveridge and Murray exposed bacterial cells to solutions of Au^{3+} chloride at room temperature and observed the formation of Au NPs of octahedral morphology with sizes of approximately 5 – 25 nm [43,197]. Since then, many other species and strains have been examined for their capacity to synthesize Au and Ag NPs of diverse morphologies and dimensions. Extracellular and intracellular Ag NPs have been produced by several bacterial species, including *Pseudomonas* [103,152], *Lactobacillus* [149,150] and *Bacillus* [144–147] genus. *Pseudomonas stutzeri* cells produce Au NPs in the size range of 10 – 20 nm when incubated in a medium with chloroauric acid ($HAuCl_4$) as the precursor [140] and Ag crystalline nanoparticles when cultured in presence of high concentrations of silver salt ($AgNO_3$) [198]. Thus far, however, the complex mechanisms of Au and Ag NPs formation by bacteria are still not completely understood. For *Lactobacillus casei* bacteria, it was found that high cell numbers and high concentrations of Au salt solutions inhibit the particle formation. The same study suggested a direct participation of unsaturated fatty acids from di- and tri-glycosyldiacylglycerol glycolipids in the membrane in the formation of Au NPs [137].

2.3.1. Iron-, cobalt- and nickel-based nanoparticles

Iron, cobalt and nickel are indispensable elements for bacteria. They are known mainly as co-factors in important processes, such as biological redox reactions. In microorganisms, there are highly specific and efficient systems for the transport and regulation of these elements in the cell to avoid their accumulation and toxicity in the cytoplasm [199]. Taking into account that at high concentrations Fe, Ni and Co are extremely toxic to bacteria, the interaction between the metals and the cells has to be carefully controlled. Organisms, such as bacteria, can utilize various sources to fulfill their nutritional requirements and have elaborate mechanisms to regulate the uptake of metal ions. Some bacteria, including metal-reducing and magnetotactic bacteria (see above), also have the ability to reduce Fe ions and form crystals naturally.

Bio-production of metal nanoparticles is frequently described as a clean, simple, and economic way to obtain magnetic NPs. It should be noted that not just the reduced metal, but also some iron, nickel and cobalt oxides possess remarkable magnetic properties that are attractive in countless applications, making the development of new methods for the synthesis of ferromagnetic nanoparticles an attractive field of research. Fe and Co are highly reactive in zero-valent state, and when in contact with aqueous solutions, they rapidly oxidize. Therefore, the NPs produced by bacteria are typically composed of more stable, oxidized forms of cobalt and iron such as Co_3O_4 and Fe_3O_4 [200]. Due to its low redox potential, the reduction of Ni ions by bacteria is not energetically favorable for NP formation under standard growth conditions [50]. However, a recent study with metal-reducing bacteria *Pseudomonas alcaliphila* described the successful reduction of Ni^{2+} by incubation at 28°C under aerobic conditions in a solution with 2 mM $NiCl_2$ and sodium citrate as an electron donor. The formed Ni NPs were found intracellularly and in the bacterial periplasm, with irregular shapes [50].
Iron-based NPs produced by *E. coli* living cells can be found intracellularly and extracellularly, depending on the iron precursor used, the pH, and the metal concentration [68]. *E. coli* and *P. aeruginosa* cell extracts facilitate the synthesis of spherical magnetic Fe_3O_4 NPs when incubated in 1 mM $FeSO_4$ at pH 6.5 for 48 h and 37°C [68]. In *G. sulfurreducens,* the upregulation of c-cytocrome OmcC in Co-rich environments is an indication of Co competition with Fe for binding to the cytochromes, which ultimately promotes the reduction of Co^{2+} to Co^0 and its precipitation on the cell surface [200]. In other methods, Co_3O_4 NPs of 10 - 31 nm size are produced by chemical alteration in the media when the urealytic *Bacillus pasteurii* hydrolyzes urea in the presence of high concentrations of $Co(NO_3)_2$ [174].

2.3.2. Platinum group metals nanoparticles

Metals from the Platinum group of elements are notorious for their outstanding catalytic properties, especially when used in nanoparticle form. The synthesis of Pd and Pt NPs by bacteria has progressed rapidly, and a wide range of bacterial species and strains have been studied for the efficient production of nanoparticles. A recent study by Mikheenko *et al.* describes the formation of Pd NPs by sulfate-reducing bacteria, *Desulfovibrio desulfuricans*, and their application for the Heck reaction and hydrogenation. The examination of the samples showed Pd NPs on the cell surface and in the different membrane layers with sizes in the range of 3 – 13 nm [164]. *Pseudomonas kunmingensis* ADR19, *Psychrobacter faecalis* FZC6 and *Pseudomonas putida* KT244 synthesize spherical Pt NPs of the average particle sizes of 3.95, 2.49 and 8.06 nm [158]. Other species, such as *Acinetobacter calcoaceticus,* synthesize small cuboidal Pt NPs of 2 - 3.5 nm in size [159].
The potential applications of Pt NPs include their use in diagnostics [201], anticancer treatments [202], and as antibacterial agents [203]. For the case of Pd in nanoparticle form, it is utilized for hydrogenation and as a carbon-carbon bond forming catalyst in Heck reactions and in Suzuki-Miyaura coupling. A further description of palladium-based nanoparticles synthesis and applications can be found in the following sections.

2.3.3. Other elements, alloys, and bimetallic nanoparticles

Many other types of metal-based nanoparticles have been produced successfully using bacteria. These include nanoparticles composed of elements such as Zn, Cr, Cd, Ti, Cu and different mixtures of metals. For example, antibacterial nanoparticles made of TiO_2 and ZnO can be bio-synthesized with bacteria. The Gram-negative bacterium *Halomonas elongata* can be used to produce spherical TiO_2 NPs and anisotropic ZnO NPs by incubating the cells with various concentrations of $TiO(OH)_2$ and $ZnCl_2$ solutions at different temperatures. The synthesized TiO_2 and ZnO NPs were on average of 104.63 ± 27.75 and 18.11 ± 8.93 nm in size, respectively [186]. Other examples are the nanoparticles produced by the metal-reducing bacterium *S. oneidensis* MR-1, known for its ability to live in heavy-metals polluted environments and studied for the synthesis of NPs of a wide range of metal ions, including ZnS [186], Pd [168,169], Cr [204] and U [205]. Synthesis of Te NPs has also been reported using a methanogenic microbial consortium in 270 mL continuous reactors as an alternative of Te recovery in wastewater treatments [206].

Table 3. Bacteria-mediated bimetallic metal-based nanoparticles reported in the literature [29].

Name of organism	NPs	Size	Morphology	Localization	Reference
Bacillus benzeovorans	Pd-Ru	1–8 nm	Core-shell	Membrane	[207]
Cupriavidus necator	Pd-Au	10–50 nm	Spherical	Membrane	[208]
Deinococcus radiodurans	Au-Ag	60–400 nm	Spherical	Supernatant	[209]
	Au-Ag	----	Spherical	Supernatant	[210]
Escherichia coli	Au-Pd	16 nm	Spherical	Intracellular/ Membrane	[211]
	Pd-Ru	1–3 nm	Core-shell	Intracellular/ Membrane	[212]
Lactobacillus	Au-Ag	100–500 nm	Irregular	Membrane	[213]
Paenibacillus polymyxa	FeO-MnO	11–54 nm	Spherical	Supernatant	[214]
Shewanella oneidensis	Pd-Fe_3O_4	5.5 nm	----	----	[215]
	Au-Fe_3O_4	15.4 nm	----	----	[215]
	PdAu-Fe_3O_4	8.3 nm	----	----	[215]
	Pd-Pt	3–40 nm	Spherical	Intracellular/ Extracellular	[216]
	Pd-Au	1–50 nm		Intracellular/ Extracellular	[217]
	Pd-Ag	5–60 nm	Core-shell	Membrane	[218]
	Pd-Au	4–15 nm	Core-shell	Extracellular	[218]
Shewanella putrefaciens	Pd-Pt	4–60 nm	Flower-shaped	Membrane	[219]
Spirulina platensis	Au-Ag	17–25 nm	Core-Shell	Supernatant	[220]

Although microbial-mediated monometallic nanoparticles have been extensively studied, there is limited research on the production of bimetallic nanoparticles by bacteria. The synergistic

effect of metal combinations can result in superior or novel catalytic, electronic, and optical properties. Therefore, bimetallic nanoparticles often exhibit improved performance that could be interesting for different applications [216]. Exposing bacteria to high concentrations of various mixes of heavy metal ions can result in the formation of nanoparticles made of combinations of these elements. Bimetallic nanoparticles can have structures such as core-shell, alloys, crown jewel, cluster-in-cluster, hollow, and porous NPs [221] and it is not surprising that the synthesis methodology has a direct effect on the final architecture of the formed bimetallic NP. An example is the synthesis of spherical bimetallic Pd-Pt NPs by S. *oneidensis* MR-1 prepared by incubation of the cell's biomass in a Pd^{2+} and Pt^{4+} mixed solution. Research showed that the synthesized polycrystalline Pd-Pt NPs possessed an improved catalytic performance in comparison with pure Pd or Pt NPs [216]. Extracellular biosynthesis of bimetallic FeO-MnO NPs can be performed using *Paenibacillus polymyxa*. In this case, cell-free extracts were incubated with solutions of $FeCl_3$ and $MnSO_4$ at 45°C in the dark for 5 h and the formed spherical nanoparticles had sizes in the range from 11.28 to 543 nm. These particles are useful as micronutrient additives to fertilizers for crop production [214]. For core-shell Pd-Ru bimetallic NP production, Gomez-Bolivar *et al.* incubated *E. coli* bacteria in a Pd^{2+} solution for an initial reduction of Pd under H_2 on the cell surface. The biomass with Pd^0 was then resuspended in Ru^{3+} solution for Pd-Ru NPs formation. Pd-Ru NPs were synthesized mainly at the cell surface, although small MNPs were also present intracellularly [212]. Table 3 summarize examples of bimetallic nanoparticles produced by different bacteria.

3. Palladium-based nanoparticles

Palladium is a precious metal with outstanding catalytic, mechanical, and electronic properties. It is extensively used in catalytic converters to help reduce harmful emissions from vehicles and, it is crucial in a large variety of industrial-scale chemical reactions. In particular, it is an indispensable tool for modern organic synthesis [222]. According to reports from 2021, automobiles accounted for the largest amount of palladium consumption, followed by electronics, chemical catalysis, dental alloys, and jewelry (Figure 4) [223]. The outermost configuration of the electron shell of palladium is atypical when compared with other elements from the same group in the periodic table [224]. Pd possesses an empty fifth shell (Pd $4d^{10}5s^0$) and a density of states just below the Fermi level, nearly satisfying the Stoner criterion for ferromagnetism. [225]. Bulk or atomic Pd are then paramagnetic, however, there are a few special cases in which palladium can be forced to behave magnetically, including close to surfaces, material boundaries, in modified lattices, or low dimensions [226]. Therefore, Pd local structure, shape, and size are highly correlated with material activity and general properties [227]. When produced in sizes between 1 and 100 nm, palladium presents unique features useful in various applications. For example, ferromagnetic moment has been reported in small cluster of Pd of less than 7 nm in size [225,228]. Pd NPs of 2.1 nm biosynthesized by bacteria have also been shown to display ferromagnetic behavior [229]. The generation of small Pd nanoparticles results in a higher degree of interfacial interaction between the metal and the medium, making them more efficient and reactive than the bulk material [227]. In nanoparticle

form, palladium is frequently utilized for selective hydrogenation [230] and as a carbon-carbon bond-forming catalyst in Heck reactions [164] and Suzuki-Miyaura couplings [218].

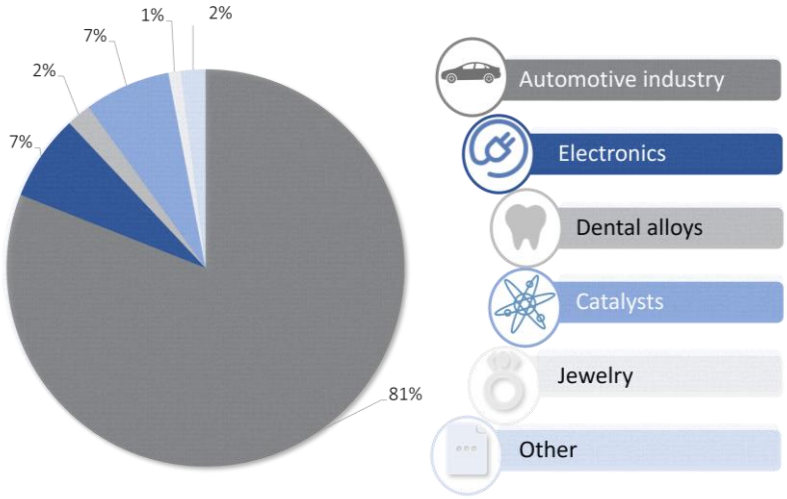

Figure 4. Consumption of palladium by industry reported in Nornickel Annual report 2021 [223].

Several chemical and physical methods can be used to synthesize palladium nanomaterials in various shapes and sizes. For instance, the top-down approach described by Salman *et al.* uses pulsed laser ablation in liquid resulting in Pd NPs with spherical morphology and fcc crystalline structures [231]. Another example is the hydrothermal method from the bottom-up approach which produces tetrahedral Pd nanocrystals as indicated by Fu *et al.* in their research [232]. The three primary components used in the chemical synthesis of Pd NPs include a metal precursor, a capping or stabilizing agent, and a reducing agent [233]. Synthesis protocols first require a Pd source such as a Pd salt. Na_2PdCl_4 (Sodium tetrachloropalladate (II)) is among the most common Pd NP precursors. Then, production involves reduction agents like hydrogen, citrate, or sodium borohydride that facilitate electron movement to Pd ions. The capping agents ensure stability and prevent aggregation of the resulting nanoparticles. Stabilizers like different kinds of polymers, polyelectrolytes, and ligands are frequently employed. Some examples include hexadecyltrimethylammonium bromide (CTAB) [234], polyvinylpyrrolidone (PVP)[235], polyvinyl alcohol (PVA)[235], and sodium dodecyl sulphate (SDS)[236]. In any case, these additives are in general complex molecules not found easily in nature. Hence, capping agent toxicity is one of the principal disadvantages of Pd NPs synthesis by chemical methods.

Due to Pd scarcity, limited production, and high cost; innovative methods to synthesize, reuse, and recycle it are in high demand [237]. Methods for palladium recovery after being discarded (e.g. in catalytic assays) include pyrometallurgical methods, chemical reduction, electrochemical, and biological methods [238–241]. Pyrometallurgical methods consume huge amounts of energy and contribute to pollution while wet chemical methods require large leaching time and result in low metal recovery rates leading to a significant waste of Pd resources [240]. Bio recovery strategies are cleaner and more attractive from an economical

point of view and are particularly suitable for metals recovery at low concentrations [239]. Environmentally friendly microbial-based recovery uses mild reaction conditions and simple protocols. Yet, little is known about the processes, bacteria strains and microbial communities optimal for recovery, or the efficiency of the methods [238].

3.1. Biosynthetic palladium nanoparticles

Recent studies on palladium-based nanoparticles highlight the potential of biological methods for small NP synthesis. It is easy to find plant-mediated, bacteria-mediated, algae-mediated, or fungi-mediated processes for MNP production [233]. Plant-mediated methods are widely applied due to their simplicity and straightforward purification. In particular, plant extracts carry components that serve as a reducing agent as well as a stabilizer [233,242]. Among the bioactive compounds are water-soluble plant metabolites and antioxidant constituents, for instance, terpenoids, vitamins, alkaloids, glycosides, flavonoids, and phenolic compounds [237,242]. These compounds are usually found in extracts derived from diverse plant components, such as leaves, seeds, fruits, and roots. For example, researchers have utilized *Persea americana* bark extract to produce 16 nm Pd NPs [243]. Palladium NPs synthesis using algal extracts has also attracted great attention for various applications as antibacterial, antibiofilm, and anticancer agents [244]. An example is use of the green alga *Botryococcus braunii* which produces cubical, spherical, and truncated triangular shape Pd NPs of 4.89 nm in size with antimicrobial activity against Gram-positive and Gram-negative bacterial strains [245]. Fungi-mediated synthesis can also biosynthesize Pd NPs. Extracts of *Agaricus bisporus,* an edible mushroom have been shown to produce 13-nm Pd NPs [246].

The synthesis of Pd NPs using microorganisms, as mentioned above, could be done using intact living cells, by cell-free supernatants, or by cell lysate supernatants (cell extracts). Using living cells can result in intracellular and extracellular nanoparticles. Typical synthesis of intracellular Pd NPs by bacteria is performed under anaerobic conditions and starts with incubating the microorganisms in aqueous solutions of Pd precursors, such as Na_2PdCl_4. The cells are then loaded with metal ions, and a reducing agent, sodium pyruvate, formate, or H_2 gas, is added as an external electron donor to accelerate the metal reduction [237]. For the *in vitro* biosynthesis of nanoparticles, the cells are ultrasonicated and centrifuged. Then only the cells lysate supernatant is incubated with the Pd precursor solution. Some examples of Pd NPs biosynthesis include the metal-reducing bacterium S. *oneidensis* MR-1, which can synthesize *in vitro* 2–12 nm Pd NPs [168], metal-resistant species *Cupriavidus metallidurans* [163], and sulfate-reducing bacterium *Desulfovibrio fructosivorans* [247]. Other strains studied for their capacity for Pd NP synthesis, which are not specialized in metal reduction for detoxification include, *E. coli* [165], *Bacillus megaterium* [102], and *Bacillus benzeovorans* [70].

As shown in the section 2.3.3, a large portion of the microbial bimetallic nanoparticles currently produced are Pd-based nanoparticles. Pd synergy with different metals and elements frequently results in novel or enhanced properties [208,215,219]. Various examples of bimetallic Pd-based nanoparticles are found in Table 3. Bimetallic nanoparticles based on Pd and Fe produced by bacteria were not previously reported. However, they have been produced by other biological methods. Examples of plant-mediated synthesis include the use of bark extract of

Ulmus davidiana var. *japonica,* root extract of *Euphorbia condylocarpa* M. bieb., and grape leaf extract [248–250].

3.2. Applications of palladium-based nanoparticles

The study of microbial Pd NPs synthesis has increased in recent years, but few works have evaluated their use for specific applications. Nevertheless, some research has been conducted on biosynthesized Pd-based nanoparticles for catalysis, biomedical applications, and nano-electronics. As mentioned above, catalysis is one of the main uses for Palladium, which includes various hydrogenation and C-C bond-forming reactions. For instance, Pd NPs produced by a thermophilic protein SP1 isolated from aspen plants (*Populus tremula*) and expressed in *E. coli* cells were described to be effective for converting acetylene feedstock into ethylene and ethane [165]. An additional example is the sulfate-reducing bacterium *Desulfovibrio alaskensis* G20 which can synthesize Pd NPs with high catalytic activity. Research by Era *et al.* [251] suggests these NPs to be effective for the ligand-free Suzuki Miyaura reaction of aryl bromides and phenylboronic acids.

It is well known that metal nanoparticles have several applications in biomedicine, including biocompatible materials, antibacterial nanoparticles, drug delivery, imaging, and therapeutic agents. In the case of Pd, one example is the antibacterial activity of Pd NPs produced by *Bacillus megaterium* Y-4, expressed under near infrared radiation (NIR) irradiation [252]. The evaluation of their performance demonstrated a good photothermal killing efficiency with potential uses in photothermal therapy for theranostic applications. In the area of nano-electronics, studies also revealed potential uses of biogenic Pd. The work of Matsena *et al.* [161] showed that the addition of Pd NPs synthesized by *Citrobacter sp.* to the anode of bio-electrochemical systems, such as microbial fuel cells can improve their performance for the generation of energy. Hence, the Pd NPs synthesized by bacteria have potential to be as good as other chemically and physically produced MNPs in diverse applications. It is therefore imperative to continue research of their synthesis pathways and industrial utilization. Further development in this field holds promise for a more sustainable and economically viable industrial use of Pd NPs.

Chapter 2. Aims of the thesis

The present work is part of the Bioengineered Palladium Nanoparticles (BEDPAN) project funded by the Research Council of Norway, RCN294605, as part of the Center for Digital Life Norway. The project's general goal is to generate and use engineered bacterial strains for the production of Pd NPs with tailored properties suitable for diverse applications in catalysis, electronics, and biomedicine. This thesis encompasses the systematic study of Pd-based nanoparticle biosynthesis by *E. coli* strains to elucidate their novel physicochemical characteristics and evaluate the enhancement of useful properties such as catalytic activity and magnetism. Advanced characterization methods are required to understand the properties and synthesis of nanoparticles. However, current methods have some limitations since there are no techniques for the simple characterization of weak magnetic single NPs within cellular structures, so the development of suitable innovative techniques is essential. The magnetic characterization of Pd-based NPs is of particular interest in this work as the improvement of the NPs ferromagnetic properties would have a positive impact in applications such as catalysis. It facilitates the reuse and recovery of Pd NPs after they are exploited in catalytic reactions. Through these studies, feedback is provided for improving synthesis protocols and generating engineered bacteria that would produce nanoparticles with enhanced properties.
In order to achieve this, the aims of the thesis are to:

a) Demonstrate *Escherichia coli* proficiency in tailored nanoparticle synthesis using Pd and Fe as model metals for bimetallic microbial nanoparticle production.

b) Characterize the physical and chemical properties of microbial Pd and Pd-Fe NPs to provide feedback for engineered nanoparticle development.

c) Develop and optimize a simple characterization technique for the assessment of the magnetic properties of nanoparticles produced by bacterial cells.

d) Elucidate the influence of nanoparticle size, structure, and composition on the catalytic activity and magnetic properties of microbial Pd-based nanoparticles.

Chapter 3. Theory and experimental procedures

Biosynthesis of Pd-based nanoparticles, as described above in Chapter 1 can be done using various biological materials and different production protocols. The final features of the nanoparticles change according to the applied methods; therefore, a thoughtful characterization of the samples is necessary before they were used or tested for different applications. In this section, the general methodology employed during the biosynthesis of Pd-based nanoparticles by *E. coli* bacterial cells is described. A more detailed description of the specific samples preparation, characterization, and testing can be found in Paper I and Paper II. The theory behind the most relevant techniques for biogenic nanoparticle characterization is also explained in this section.

1. *E. coli*-mediated synthesis of Pd and Pd-Fe NPs

Escherichia coli K-12 strain BW25113 was selected as a model organism to produce Pd-based nanoparticles. The particular use of *E. coli* bacteria in this work offers several additional advantages. Due to rapid bacterial growth, the cultivation of *E. coli* can be easily scaled up for large-scale NPs production if needed for industrial applications [253]. Also, the use of exhaustively researched *E. coli* bacteria strains has the potential to be genetically modified to express specific proteins or peptides related to the reduction of metal ions that may lead to the formation of improved metal NPs.

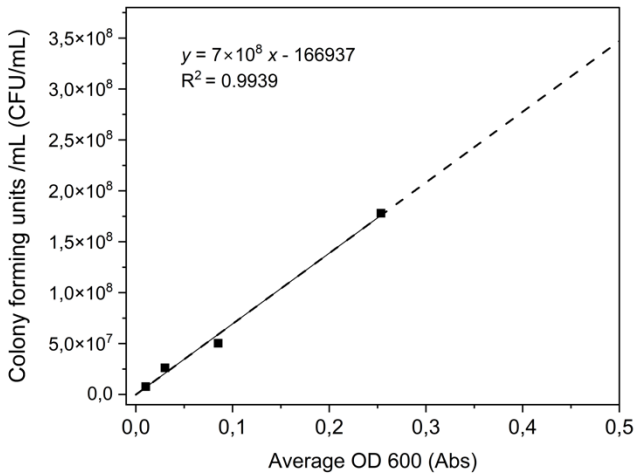

Figure 5. Standardization curve for CFU/mL versus OD_{600} for E. coli K-12 BW25113 in LB media at 37°C.

Previous studies demonstrated the successful biosynthesis of Pd nanoparticles using various *E. coli* strains [59,212]. Here, a modified version of these protocols was used to synthesize monometallic Pd and bimetallic Pd-Fe NPs (**Paper I**). The production of Pd nanoparticles by

bacteria is typically performed in the absence of O_2; therefore, the bacteria used during this work were grown in Lysogeny Broth (LB) overnight (16 h) at 37 °C under anaerobic conditions. Anaerobic conditions were approximated in this work by packing the falcon tubes with the media to the top and tightly sealing them.

The bacterial cell number was normalized using the Optical Density (OD) recorded at 600 nm with the help of a spectrophotometer. The OD_{600} can be correlated to colony forming units per mL (CFU/mL) of plated bacterial suspension at different dilutions [254]. The samples were normalized to ensure that in all the experiments a similar number of bacterial cells was used for nanoparticle synthesis. Each dilution of cells was measured in a spectrophotometer. Then, the plates with the dilutions were incubated overnight at 37 ^{o}C, and colonies were enumerated. A standard curve was established to relate the optical density to an approximated bacterial CFU/mL (see Figure 5). All the bacteria solutions were normalized to an OD_{600} of 3.5 which is equal to 2.5×10^9 CFU/mL.

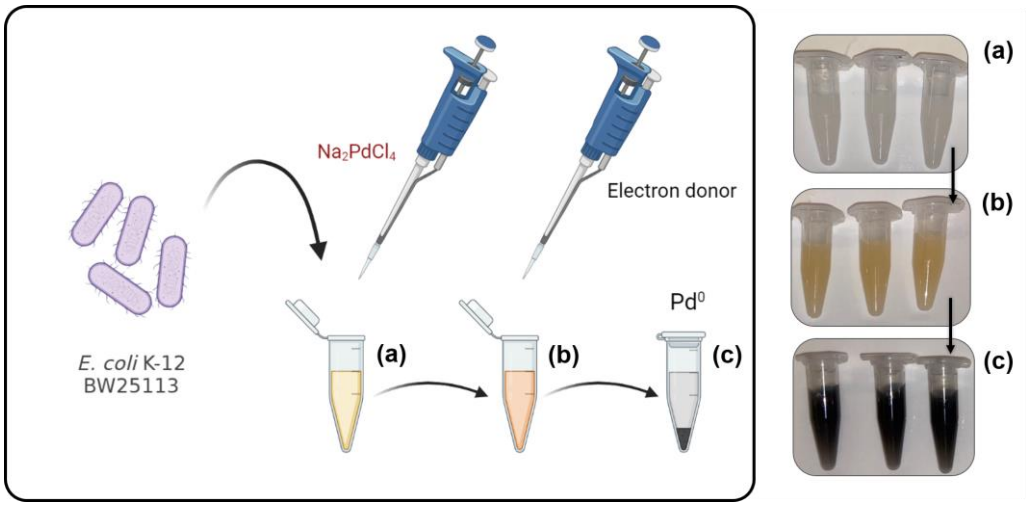

Figure 6. General protocol for Pd NPs biosynthesis by E. coli K12 cells in MOPS buffer at 37°C with agitation. (a) Pd uptake, (b) addition of sodium formate as electron donor and (c) Pd reduction. Created in BioRender

The bacterial cells were incubated in solutions of Pd(II) or Pd(II) + Fe(III) at 37°C with 200 rpm agitation (Figure 6). Sodium tetrachloropalladate (II) (Na_2PdCl_4) dissolved in 0.01M HNO_3 at 1mM concentration was used as a palladium precursor, while for Fe, Iron (III) chloride ($FeCl_3$) in distilled H_2O was selected. This thesis investigated different Pd and Fe ratios. Specific details about the Pd and Fe concentrations in the samples are described in the methods section of **Paper I**, **Paper II**, **Paper III**, and **Paper IV**. Metal ions are absorbed by bacteria during incubation in metal-rich solutions (Figure 6). Pd loading can be monitored by spectrophotometry using a tin (II) chloride ($SnCl_2$) assay [59,255]. The reaction between $SnCl_2$ and metals from the Platinum group of elements is an easy colorimetric method to quantify small amounts of the metal in solution [256]. Red-brown complexes are formed when $PdCl_4$ and $SnCl_2$ interact in HCl, and their color is proportional to Pd concentration. Thus, comparing absorbance at 463 nm with a calibration curve allows quantitative determination of Pd from media. This reaction was first used to establish the minimum incubation time to achieve Pd

uptake close to 100% from the solution by the cells. Cells were incubated for two hours under agitation before the addition of a reducing agent. Sodium formate was selected as an electron donor to promote the reduction of the Pd and Fe in the cells into nanoparticles. A black precipitate is the indication of nanoparticle formation (Figure 6 (c)).

2. The characterization of biogenic nanoparticles

Nanoparticles characteristics can be classified in physical and chemical properties. Among the most important physical features are the particle's morphology (size, shape, size distribution), magnetic moment, as well as the optical, mechanical, and thermal properties. In the case of chemical properties, elemental composition, chemical state, concentration, and catalytic activity are the main features [257]. In this section, the most relevant characterization techniques are described, with special emphasis on the methodologies used during this research.

2.1. Size, shape and size distribution

The size, size distribution, and shape of the particles are important characteristics that dictate the final catalytic activity and influence on the magnetic behavior of Pd-based nanoparticles. Multiple techniques are available for the evaluation of these properties of nanomaterials. The most common methods used to measure NP size distribution and shape include dynamic light scattering (DLS), UV/Vis spectrometry, x-ray diffractometry (XRD), atomic force microscopy (AFM), and transmission electron microscopy (TEM) [257], among others. In this work, TEM, and scanning probe techniques such as AFM were used to the study of Pd and Pd-Fe NP properties. An extended description of how these techniques work and why they are important for the characterization of our samples is described in the following subsections.

2.1.1. Transmission Electron Microscopy

Transmission Electron Microscopy (TEM) is a powerful imaging technique that employs a beam of electrons to visualize structures up to atomic resolution (<0.1 nm) [258,259]. In conventional TEM (Figure 7(a)), part of the parallel beam will pass through an ultra-thin specimen without interacting with the material atoms. At the same time, other electrons are diffracted or absorbed by the specimen, leading to variations in the intensity. The resulting electron pattern is then magnified and focused on a fluorescent screen or digital detector. This generates highly detailed images of the specimen or diffraction patterns [260]. By modifying the focus of the intermediate lens to the back-focal plane of the objective lens, it is possible to move from image mode to diffraction mode (Figure 7)[261].
The image and diffraction modes can provide different information on the specimen as morphology, size, shape, particle aggregation, and crystal lattice [262]. Therefore, TEM is useful for the study of a variety of samples, among them, nanomaterials and biological samples. The integration of techniques such as Energy Dispersive x-ray Spectroscopy (EDX) and

Electron Energy Loss Spectroscopy (EELS) also permits the study of chemical composition within different regions of the sample. EDX will be further discussed in Chapter 3 Section 2.3.

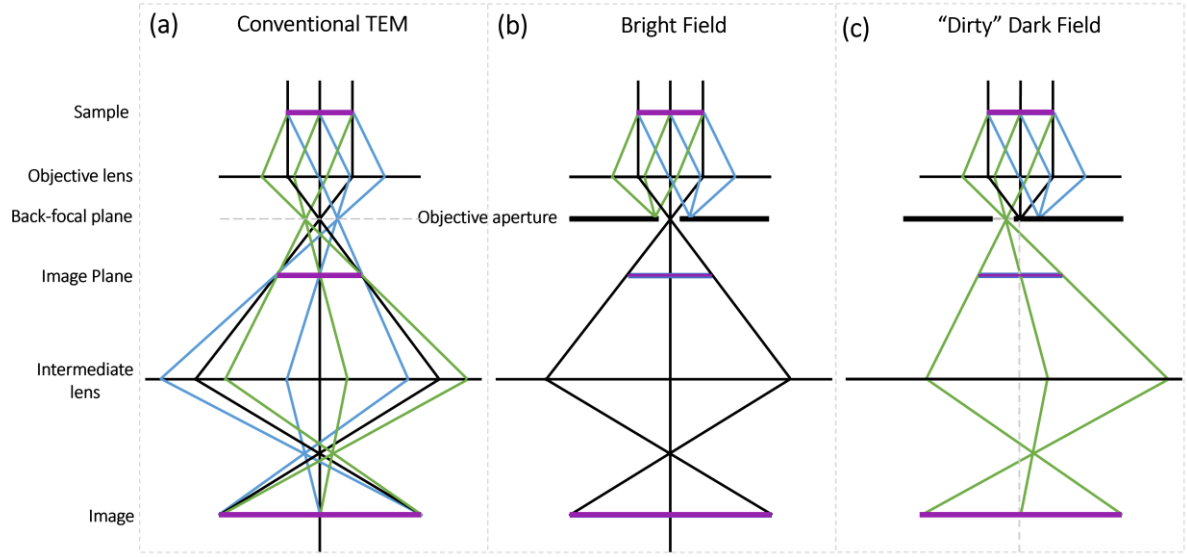

Figure 7. Ray paths in conventional TEM, bright field and dark field image mode. Modified from [261].

In TEM, a beam of electrons is emitted from an electron gun and accelerated by an electromagnetic field. The operation happens under a high vacuum to facilitate the transmission of electrons. Elements with higher atomic numbers, characterized by greater electron densities, diffract the electron beam more hence they exhibit more pronounced contrast in TEM images. An example is metal nanoparticles within cellular structures that normally have higher contrast than biological materials. To enhance the contrast of specimens with low atomic number elements, such as biological samples, it is possible to use staining reagents e.g. osmium tetroxide [263]. In general, the contrast in TEM originates from the thickness and composition of the sample [260].
There is also a complementary loss of intensity when the diffracted and transmitted electrons passing through the sample are not separated. Hence, the use of an objective aperture improves strongly the contrast of the images [261]. In bright field mode, the aperture is placed so that only transmitted electrons can pass (Figure 7(b)) [260]. On the other hand, dark field images are formed when only diffracted electrons are selected. This can be achieved by moving the aperture (dirty dark field, Figure 7(c)) or by tilting the incident illumination on the specimen [260]. In practice, the second method is commonly used since it is less affected by lens aberrations [261].

High-resolution TEM (HR-TEM) is an imaging mode that allows the direct imaging of the crystallographic structure of a sample at the atomic level [263]. Here, the phase contrast of the smallest features in the samples is used for imaging. HR-TEM images are sensitive to sample thickness and orientation, lattice spacings, atomic species, and their interaction with electrons. It is frequently used to determine particle sizes and shapes too [264]. For instance, the study of ZnO NPs biosynthesized by *Lactobacillus plantarum* TA4 with HR-TEM revealed spherical,

hexagonal, and oval-shaped particles, with sizes ranging from 49.2 to 369.5 nm and an average size of 191.8 ± 69.1 nm [265]. Another example is the study of the crystal lattice of biosynthesized Ag NPs that revealed interplanar spacings of 0.25 nm and allowed the determination of face-centered cubic (fcc) crystal structure [266].

Sample thickness is an important factor that influences image quality in TEM studies. Materials need to have dimensions small enough to be electron transparent and therefore good sample preparation is crucial in TEM studies [260]. Sample preparation for TEM depends on the type of material. Nanoparticles and powders are frequently diluted and deposited on top of supported grids while biological samples, such as bacterial cells can be embedded into resin and cut into thin films with a diamond knife before being deposited onto a grid [263]. A suitable sample preparation method needs to balance the choices of contrast, resolution, and sample preservation [267].

In this work, TEM was used to determine the nanoparticle location with respect to the cellular structures. HR-TEM was employed for the determination of crystal structure and particle size. The samples were prepared by embedding the cells with Pd and Pd-Fe NPs in an epoxy resin. Cells were previously fixed to preserve their features. The samples were then cut with a diamond knife into thin slices of 70 nm, which were deposited on 100 µm copper grids.

2.1.2. Atomic Force Microscopy

AFM is a scanning probe technique that enables the visualization, manipulation, and analysis of surfaces on the nanoscale [268]. Customarily, AFM employs a sharp probe that scans the surface of a sample, measuring and mapping its properties with high resolution. As the cantilever tip approaches the sample surface, intermolecular forces such as van der Waals forces, electrostatic forces, and chemical bonding forces come into play. The study of the different interactions makes AFM a multiparametric technique capable of evaluating various physicochemical properties of samples [269].

AFM offers several operational modes. In static mode (contact mode), the tip maintains constant contact with the sample, providing high-resolution topographical information. The deflection of the cantilever in response to interactions with the sample surface is monitored using a laser beam reflected off the back of the cantilever onto a position-sensitive detector. As the tip moves across the sample, the cantilever deflection is continuously adjusted to maintain a constant force between the tip and the surface [270]. The resulting topographical information is used to construct a detailed three-dimensional map of the sample surface with nanoscale resolution. In this mode, three images can be acquired simultaneously: height, deflection, and friction.

In dynamic mode, known originally as tapping mode, the tip oscillates near its resonance frequency above the surface, detecting the forces between the tip and the sample. In contrast to contact mode, the probe only touches the surface at the end of its downward oscillation movements, reducing the possibility of damage due to friction between the tip and the sample [271,272]. Dynamic mode also prevents dragging weakly adsorbed materials along the sample surface [273]. The tip experiences different attractive and repulsive forces coming from intermolecular interactions with the surface in each oscillation cycle. This can be recorded simultaneously as oscillation parameters such as amplitude, frequency, phase shift, and

cantilever deflection [[271] (Figure 8 (a)). Amplitude modulation is a simple feedback method used to adjust the tip height to keep the amplitude constant when measuring rough topographies. Compared to frequency modulation, it requires fewer feedback loops [272].

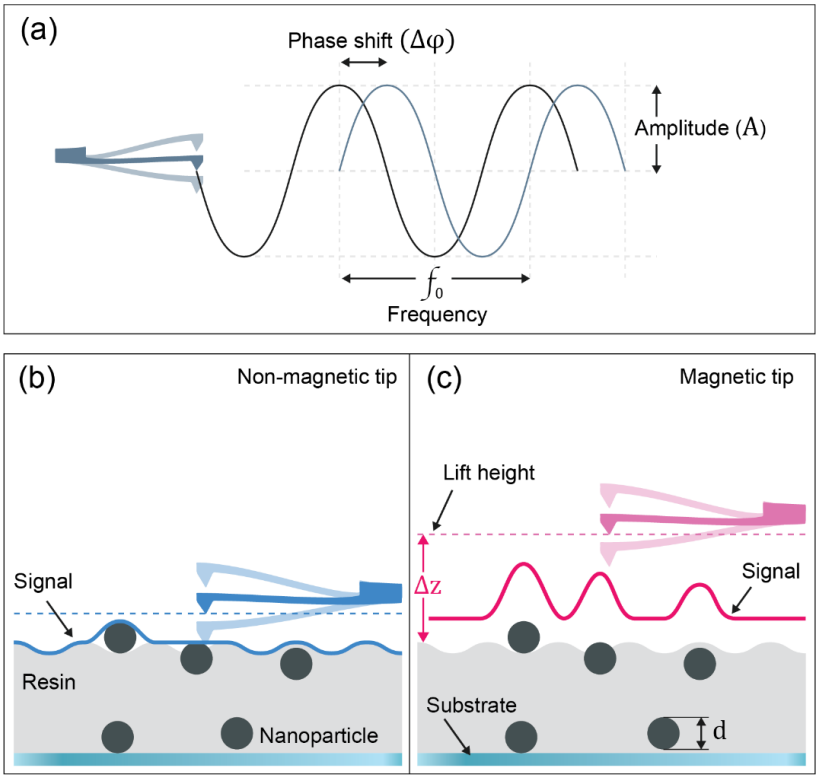

Figure 8. (a) Parameters of cantilever oscillation and schematic of probe scanning on a sample with embedded nanoparticles by (b) AFM and (c) MFM

AFM has been exploited beyond topography imaging of material surfaces. Various kinds of physical and chemical interactions, such as current, voltage, and force quantification have been acquired for a wide range of materials that include biological molecules, living cells, nanomaterials, polymers, and semiconductors [274,275]. Different materials require different sample preparations. For instance, the study of biosynthetic Se NPs produced by *Bacillus* sp. E5 in AFM requires the deposition of cell suspension on coverslips which allows the visualization of bacteria along with extracellular nanoparticles [276]. A similar protocol was used for the study of ZnO NPs synthesized by *Aeromonas hydrophila* bacteria in AFM [277]. Other sample preparation methods involve the purification of nanoparticles, lyophilization, and drying of the powder dilution on top of smooth surfaces [278,279]. Some suitable substrates for AFM studies of nanomaterials and biological samples include freshly cleaved mica, glass, and silicon oxide. In addition to their natural flat surface, these surfaces are easy to clean or modify [274]. The straightforward sample preparation and the possibility to study the samples in different mediums such as air, vacuum, and even liquid solutions make AFM an attractive technique for the study of biosynthesized nanoparticles. However, the current protocols still fail to provide a simple pathway to study intracellular nanoparticles at their place of formation. In AFM scans, contrast arises from the interaction between the scanning tip at distinct regions of the sample. During this work, dynamic mode was used to study the surface of our sample.

The well-known specimen preparation of ultrathin slices of resin-embedded samples typically used in TEM studies was employed in this work as a new pathway for the AFM examination of bacteria with Pd and Pd-Fe NPs.
The resin slices were analyzed by AFM using a scanning probe microscope JPK NanoWizard 4.0 shown in Figure 9. For AFM imaging, the instrument was equipped with commercial pyramid-tipped silicon cantilevers PPP-FM (Nanosensors, Switzerland) with a tip radius of approximately 7 nm.

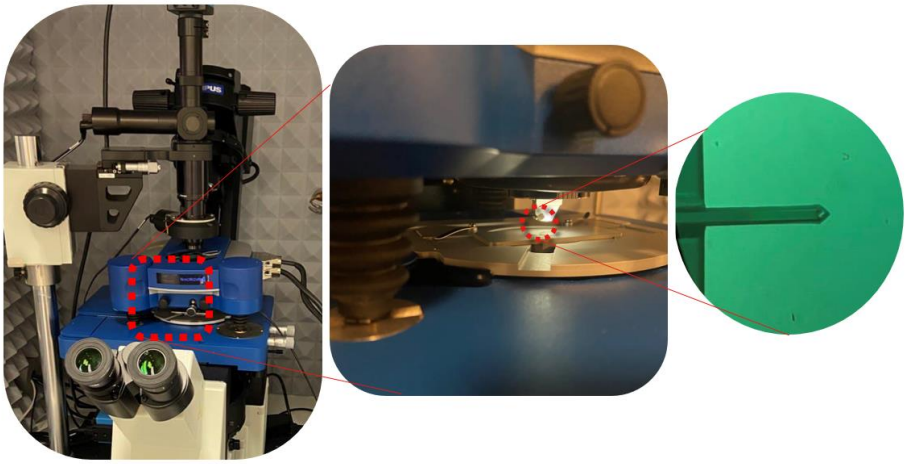

Figure 9. Images of the scanning probe microscope JPK NanoWizard 4.0 used for AFM and MFM study.

2.1.3. Other morphology characterization techniques

In DLS studies, a laser beam is directed at a sample containing nanoparticles in suspension. Random Brownian motion of the nanoparticles causes variations in the scattered light intensity over time [280]. The speed of a particle depends upon its size; large particles have low speeds and small particles have high speeds [281]. In collisions with particles, light wavelengths change according to their motion. In this way, the measurement of the intensity fluctuations provides information about particle size and size distribution [280].
UV/Vis spectrometry is also often used to characterize particle size. The surface plasmon resonance of metal nanoparticles such as Au NPs generates an extinction spectrum that varies with size, shape, and particle aggregation [282]. The UV/Vis spectra of the nanoparticles are recorded and analyzed using Mie theory, which solves the Maxwell equations and relates extinction and scattering efficiencies to the diameters of metal particles [283].
XRD is a powerful technique used to investigate the crystal structure of materials among them nanoparticles. When incident x-rays strike the sample, they interact with the electrons in the atoms. The x-rays cause the electrons to oscillate, re-radiating x-rays in various directions and interfering with each other constructively or destructively. This interference results in a diffraction pattern when the conditions satisfy Bragg's law [281]. The diffraction pattern is a series of peaks corresponding to specific crystallographic planes within the sample. The diffraction peaks can give information about the crystal structure, including the lattice

parameters and crystal symmetry. In the case of crystalline nanoparticles, it is also possible to measure the average particle size through the Scherrer equation ($D = K\lambda/\beta \cos\theta$) [284]. This equation relates the width of the peak at half of its height (β) at a particular diffraction angle (θ), with the crystalline size (D) when studied with x-rays of wavelength λ. K is the Scherrer constant.

2.2. Magnetic properties

2.2.1. Principles of magnetism and magnetic materials

Magnetism is a property of materials that can arise from two principal sources, the movement of charged particles or the orbital and spin moments of elementary particles [285]. In the first case, the movement of charged particles such as electrons or ions creates a magnetic field around them. This effect is known as electromagnetic induction and is described by Ampere's law. The second source of magnetism comes from the interaction of elementary particles. The orbital motion of electrons around the nucleus and their spin generates angular momentum and therefore magnetic moment. In the same way, an electric current through a circular loop creates a magnetic field [286]. The magnetic moment of electrons can be added up and the atomic magnetic moment depends in principle on the electronic configuration of the atoms.

Magnetization of a specimen can be classified following its response to an external field into paramagnetic, diamagnetic, and ferromagnetic. Paramagnetic materials tend to align their magnetic moments under an external magnetic field. It's a weak form of magnetism and its strength is directly proportional to the applied field [287]. Opposite to this, the diamagnetic materials present weak negative magnetization when subjected to a magnetic field.

Ferromagnetism is a property of materials caused by spontaneous alignment of electron spin and orbital magnetic moments. Ferromagnetic materials possess permanent magnetism. Under an external field, the magnetic domains will start to align in a favorable direction sustaining a growing magnetization. The magnetization value when all the domains are aligned parallel under an external magnetic field is called saturation magnetization (M_s). The relationship between the magnetization of a material and the external magnetic field can be described by magnetization curves (Figure 10). A ferromagnetic material curve exhibits hysteresis loops as a result of residual magnetization when exposed to a magnetic field of a specific orientation. Some other important parameters include the remanence (M_r), which is the remaining magnetization in the ferromagnetic material after removal of an external magnetic field, and the coercivity (H_c), which is the magnetic field necessary to demagnetize a fully magnetized material [287,288]. Traditional magnetic materials include alloys of ferromagnetic metals: Fe, Co, and Ni.

Superparamagnetism is a particular case of ferromagnetism present in single-domain magnetic materials with negligible remanence and coercivity [287]. Magnetic materials that reach a small dimension (e.g., nanoparticles) at a critical diameter will demagnetize spontaneously as a result of thermal effects. Their behavior is then similar to a paramagnetic material. However, their magnetic moment align under external fields with a much higher magnetization [288].

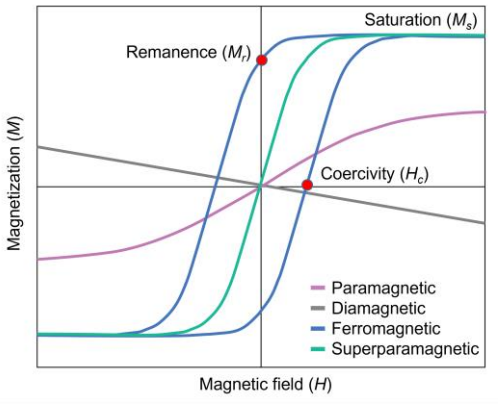

Figure 10. Schematic of magnetization curves of magnetic materials.

2.2.2. Magnetic characterization techniques

At the nanoscale, the study of magnetic behavior requires the use of highly sensitive techniques capable of measuring the weak signals coming from magnetic interactions in small-volume samples [281]. Magnetic properties characterization is typically done by techniques such as vibrating sample magnetometry (VSM), superconducting quantum interference device (SQUID) magnetometry, and magnetic force microscopy (MFM).

The magnetic study of samples by VSM describes the magnetic behavior of a material using direct current (DC) or alternate current (AC). Typical magnetometry techniques record the magnetization of the sample under a variable external magnetic field to find the hysteresis loop. A sample is placed in a suitable non-magnetic sample holder which is attached to the end of the VSM sample rod and then vibrated within a copper coil that generates a uniform magnetic field [281,289]. Typically, a magnetic field is swept from zero to maximum, then maximum to minimum, and then back to zero at constant temperature [263]. It is a simple and inexpensive way to provide information about the magnetic moment of material. However, it is not as sensitive as other methods like SQUID magnetometry [290]. Although, similar to VSM, SQUID magnetometry is the standard for the characterization of magnetic materials [291]. The main difference from VSM is that SQUID consists of a coil made with superconducting wire and Josephson junctions that typically require cryogenic temperatures to operate. SQUID magnetometry measures the changes in the critical current of a superconducting loop as a function of the magnetic flux threaded through the loop making it an extremely sensitive technique that can detect very weak magnetic fields [291,292].

In this work, we are interested in the evaluation of the magnetic properties of nanoparticles biosynthesized by bacteria cells. As mentioned above, nanoparticles accumulate close to their place of formation. Usually, NPs are distributed in the sample in the extracellular space, the bacterial membrane, and in the cytosol. Biogenic Pd and Pd-Fe NPs in our study are not the exception (Paper I). Particles formed at different locations on the sample have different morphologies, so the question arises if their magnetic properties differ based on where they are formed. The study of the magnetic behavior of single nanoparticles is then desirable. However, methods like VSM and SQUID magnetometry evaluate total magnetic moment of the bulk material. The development of a method that can relate the magnetic behavior to the particle

location in the cells is required. Single nanoparticle studies have been performed before with the use of MFM [293–295]. The following section describes MFM basic principles and their application to the study of nanoparticles.

2.2.3. Magnetic force microscopy

MFM comes from the same family as AFM techniques. Standard cantilevers are coated with magnetic layers containing elements such as cobalt or iron [291]. Sharp magnetic tips are used to scan the surface of the samples. The cantilever then responds to the interactions of intermolecular forces in addition to the magnetic fields generated by the specimen. The intermolecular interactions are composed of repulsive and attractive forces. Most repulsive forces decay rapidly with distance (within fractions of nm) as described by Pauli-exclusion principles and electron–electron Coulomb interactions (Figure 11). The attractive forces including van der Waals interactions and electrostatic forces, can be measured over long distances from the surface, in some cases up to 100 nm [296]. Magnetism makes part of the long-range interactions; it is prevalent at distances at which van der Waals forces are typically not detected anymore.

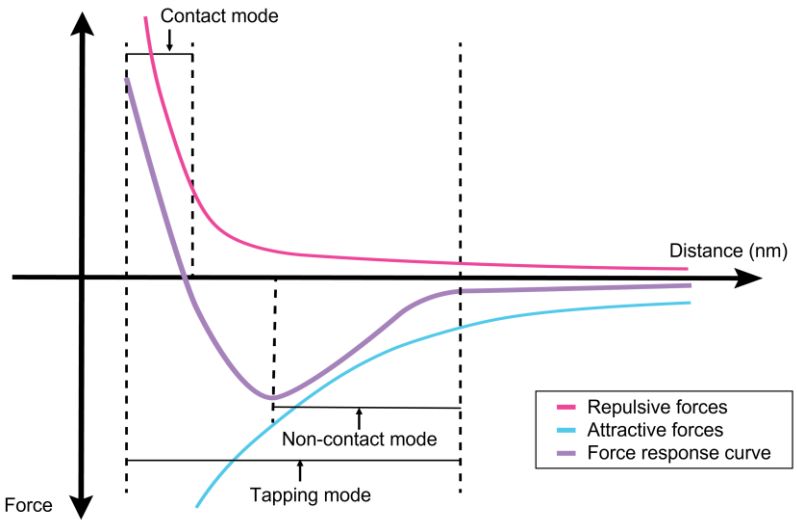

Figure 11. Interatomic forces vs tip lift height from the sample surface. AFM and MFM modes of operation, contact mode, tapping mode and non-contact mode Modified from [297].

MFM operates in a similar way to AFM. In non-contact mode, the surface repulsive forces are prevalent and not optimal for studying magnetic interactions (Figure 11). Hence, the imaging of the specimen by MFM is mainly done in dynamic mode. The most common MFM method is the two-pass scanning technique. Here, images are obtained by scanning each line twice. In the first scan, the topographic information from the surface is recorded just like in the tapping mode of AFM but then a second scan is produced by lifting the tip from the surface at a lift height (Δz) that allows the separation of the magnetic signals from all the other intermolecular forces [298,299] (Figure 8 (c)). Non-contact scanning is used for this second scan.
The interaction of the tip with the forces normal to the surface (F_z) produces variations in the oscillation parameters. The force gradient normal to the surface will result in a shift in the

resonance frequency (Δf_0), the amplitude (ΔA), and the phase ($\Delta\varphi$) of the cantilever oscillations, which can be expressed in the forms [300]:

$$\Delta f_0 = -\frac{f_0}{2k}\frac{\partial F_z}{\partial z} \quad (1)$$

$$\Delta A = \frac{A_0 Q}{2k^2}\left(\frac{\partial F_z}{\partial z}\right)^2 \quad (2)$$

$$\Delta\varphi = -\frac{Q}{k}\frac{\partial F_z}{\partial z} \quad (3)$$

where k and Q are the cantilever spring constant and the quality factor of the cantilever, respectively. The value Q reflects the intrinsic properties of the cantilever, at the resonant frequency and the specific medium (air, liquid, or vacuum). f_0 and A_0 are the resonance frequency and amplitude in the medium without external forces, respectively. The most common parameter used to study magnetic samples in MFM is the phase shift of oscillation. Then various works also model the magnetic interactions between the tip and the sample as dipole-dipole interactions [281]. This allows us to derive an expression that describes the gradient of the force normal to the sample surface as [301]:

$$\frac{\partial F_z}{\partial z} = \frac{6\mu_0 m_t m_{NP}}{\pi\,(s + z_0)^5}, \quad (4)$$

where m_t and m_{NP} are the magnetic moments of the tip and the NPs, respectively, and μ_0 is the vacuum magnetic permeability. s is the height from the surface, and z_0 is the additional distance expressed as $z_0 = d_m/2 + d_t/2$, where d_m and d_t are the diameters of the NP and the tip, respectively. Some examples include the study by Schreiber *et al.* [293] that evaluated the magnetic response of superparamagnetic nanoparticles by measuring the phase shift values on top of the nanoparticles at different lift heights. Another study estimated the remanent magnetization of Co-based NPs deposited on an Al substrate by analysis of the phase shift of the magnetic cantilever above the particles [295].

During this research, both AFM and MFM studies were done in the two-pass dynamic mode. The phase shift, height, and amplitude parameters were used to represent the sample. The phase shift on top of Pd and Pd-Fe nanoparticles at different locations of the samples were evaluated.

2.3. Elemental composition, concentration, and chemical state

The elemental composition is among the most relevant features of the samples. For the determination of the composition, concentration and chemical state, there exist a wide range of methodologies. The most used techniques are fourier transform infrared spectrometry (FTIR), energy-dispersive x-ray spectroscopy (EDX), atomic absorption spectroscopy (AAS), x-ray

photoelectron spectroscopy (XPS), UV/Vis spectrometry, inductively coupled plasma mass spectrometry (ICP-MS), and XRD.

2.3.1. HAADF-STEM images and EDX

The scanning transmission electron microscopy (STEM) has the similar functions as TEM but is equipped with more beam deflection coils used to focus the electron beam. This makes it possible to scan the specimen with an electron beam as a probe. Electron scattering by a sample emits a variety of signals that can be detected by detectors at different angles and positions. Bright field, annular dark field (ADF), or High-angle annular dark-field images (HAADF) can be formed. HAADF images use high-angle incoherent elastically scattered electrons, which carry information about the sample elemental composition. The intensity of high angle scattering, also known as Rutherford scattering, increases with the atomic number. Therefore, HAADF imaging is also called Z-contrast imaging [260,262,302].
Elemental maps of the sample can also be recorded using x-rays emitted by the sample. EDX uses an x-ray detector placed at an optimal angle above the sample to collect x-rays emitted after electron interaction with the specimen to produce elemental maps of the sample. When a sample is bombarded with high-energy electrons it emits characteristic X-rays due to the interactions between the incident radiation and the atoms in the sample. These emitted X-rays have energies specific to each element, allowing for their identification [303]. The x-ray emission increases with the atomic number too, so it is optimal for heavy element characterization due to a better contrast [262]. HAADF-STEM can be acquired simultaneously with EDX spectroscopy enabling the mapping of elemental composition and structural details. During this study, the distribution of Pd and Fe in the bacteria sample after nanoparticle formation was studied with HAADF-STEM and EDX (Figure 12). The resulting elemental distribution maps were also employed to confirm the nanoparticles elemental composition.

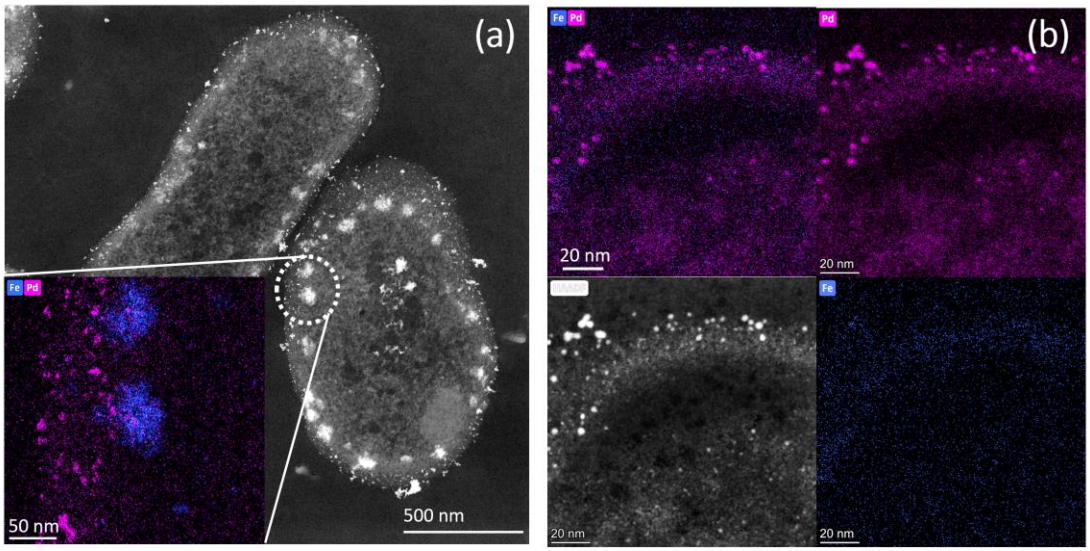

Figure 12. HAADF-STEM images of E. coli K-12 bacteria and magnified view of cell surface loaded with Pd and Fe molar ratio (a) 1:2 and (b) 1:1 (Pd:Fe).

2.3.2. Further composition characterization techniques

One of the best methods for determining the amount of metal in nanomaterials is AAS [304]. This technique is used to quantitatively analyze the concentration of various elements in a sample based on their absorption of light at specific wavelengths. The absorption is specific to each element, and the amount of absorbed light is proportional to the concentration of that element in the sample. The sample after a process of preconcentration and dissolution in acids is introduced into a flame and vaporized. Light at a specific wavelength passes through this gaseous sample and absorption is analyzed [305]. In this work, the amount of Pd and Fe in the biosynthesized NPs was quantified by AAS. The samples were digested using aqua regia before their study (Figure 13) and light sources specific to Pd and Fe were used.

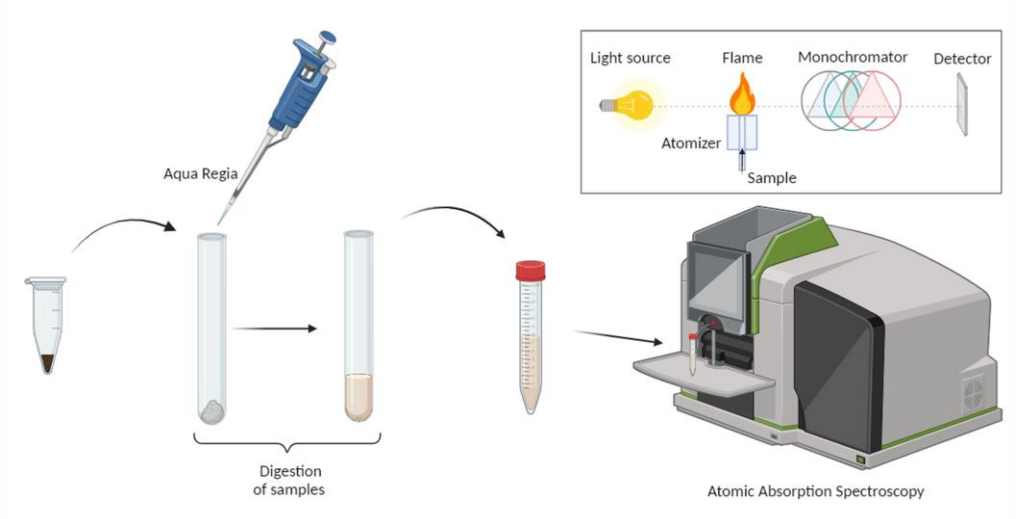

Figure 13. Schematic of AAS study of Pd-based nanoparticles synthesized by E. coli. Created in BioRender

ICP-MS is another technique frequently employed for element concentration analysis. Similar to AAS, it first atomizes the sample, however, it is then ionized in an inductively coupled plasma, and the resulting ions are detected and quantified by mass spectrometry [306]. This makes it a highly sensitive method that allows simultaneous detection of multiple elements.

Techniques such as FTIR can also be used to study elemental composition. Here the absorption of infrared light by molecular vibrations is measured. Different functional groups absorb at characteristic frequencies, allowing the identification of compounds. The vibrations of molecules are directly related to their symmetry, which can be used to determine the formation of bonds on surfaces [307]

Another example is XPS which provides information about elemental composition along with chemical states on the sample surface. It analyzes the photoelectrons emitted when x-rays interact with a sample. The binding energies of these electrons reveal the elemental composition, and their intensity provides quantitative information [308]. XPS is particularly relevant for the study of surface chemistry and identifying oxidation states. It can provide vital information about the presence of a chemical functional group and the composition of surface-bound molecules [309].

For composition identification, the XRD technique mentioned above (Section 2.1.3) is also useful. It can be employed for the identification of crystal structures of unknown materials in the sample. The diffraction patterns found with XRD of the biogenic NPs powders in this work were compared with the crystal structure reported for different crystalline Pd and Fe standards in a database.

2.4. Catalytic activity

Catalysis is defined as the acceleration or facilitation of a chemical reaction by a substance (catalyst). The catalyst lowers the activation energy, making the reaction proceed more rapidly. The most commonly encountered catalyst types are materials containing metals, oxides, or sulfides [310]. Metal nanoparticles with a high surface area and more active sites than in bulk, promote faster reactions and increase product yield [311]. Transition metals are especially effective as catalysts due to their unfilled *d*-bands. Noble metals such as Au, Pt, Pd, and Ag, along with other metals like Fe, Cu, Ni, and Co have been studied in nanoparticle form mainly in heterogeneous catalysis [311].
An important model reaction used normally to test metal nanoparticle catalytic activity in an aqueous solution is the reduction of p-nitrophenol by sodium borohydride. Sodium borohydride serves as the source of ions (H^-), which are responsible for reducing the nitro group ($-NO_2$) of 4-nitrophenol (4-NP) to an amino group ($-NH_2$), resulting in the formation of 4-aminophenol (4-AP). This movement of ions (H^-) cannot proceed on its own and must be promoted by a catalyst (metal), like Pd [219]. The reaction occurs under ambient conditions, and it can easily be monitored. UV/Vis spectroscopy is used to observe the decrease in the absorption of 4-nitrophenol at wavelength of 400 nm [312]. The efficiency of the reaction serves as an indication of nanoparticle catalytic activity.

2.4.1. Biogenic nanoparticles in chemical catalysis

Biosynthetic nanoparticles produced by bacteria have been studied for different catalytic applications. The most studied reactions are related to the degradation of dyes, removal of heavy metal ions, catalytic dehalogenation, and 4-nitrophenol reduction, among others [313]. Examples are given in this section.
Matsena *et al.* [162] tested the catalytic activity of Pd NPs biosynthesized by *Citrobacter* sp. bacteria for the reduction of Cr(VI) to Cr(III) against chemically produced NPs. In their work, a UV/Vis spectrophotometer was used to monitor the reaction and it was found that biogenic Pd NPs performed better than their chemically produced counterparts. However, the study of the same reaction with Pd NPs synthesized by *Cupriavidus metallidurans* CH34 using formic acid (HCOOH) as a reductant showed that chemically produced Pd NPs were more efficient for the removal of Cr(VI). Tan *et al.* [163] indicated a removal efficiency of 96% after 20 min for chemical Pd NPs while biogenic Pd NPs only had 85% after 50 min. Other Pd NPs produced by *Desulfovibrio desulfuricans* have been evaluated for the Heck coupling reaction between iodobenzene and ethyl acrylate. The study results show that biogenic Pd outperformed a commercial Pd-based catalyst by 10 – 25 % [164].

The degradation of Azo dyes by microbially synthesized Cu NPs was studied by Noman *et al*. [188]. In their work, Cu NPs were produced from a native *Escherichia* sp., and tested for the degradation of different azo dyes. The degradation assays indicated that Cu NPs decolorized congo red, malachite green, direct blue-1, and reactive black-5 at a dye concentration of 25 mg L^{-1} after 5 h of sunlight exposure with efficiencies of 97.07%, 90.55%, 88.42%, and 83.61%, respectively.

2.5. Additional properties

Other important characteristics of nanoparticles include the optical and thermal properties. Due to their small size, some nanoparticles exhibit effects like surface plasmon resonance, where their electrons collectively oscillate in response to incident light [314]. This property has important uses in the size determination of some metal nanoparticles by methods such as UV/Vis mentioned above. Other applications based on specific properties include photothermal therapy and photothermal imaging due to localized resonance. Certain nanoparticles can also emit light upon excitation, displaying fluorescence or photoluminescence. Absorption, transmission, reflection, and light emission are some of the most important optical properties [315]. Techniques such as UV/Vis, fluorescence spectroscopy, and thermal gravimetric analysis (TGA) are typically used to study these effects. The latter technique measures changes in mass as a function of temperature, helping to understand thermal stability and decomposition processes in nanoparticles [281].

Chapter 4. Summary of papers

In this section, the summary of the four main papers that comprise this thesis is included:

Paper I

Microbial synthesis and characterization of bimetallic Pd-Fe nanoparticles produced by *Escherichia coli*.

The manuscript delves into a bacteria-mediated approach to synthesize bimetallic NPs utilizing *Escherichia coli* (*E. coli*). In addition to its rapid growth rate, this organism is easy and inexpensive to culture, making it ideal for industrial applications. Aligned with the BEDPAN project objectives, the protocols for biogenic Pd NP production by bacteria cells were modified by the addition of other metals such as Fe to enhance the catalytic and magnetic properties of the nanomaterial. The strategy developed resulted in the synthesis of bimetallic Pd-Fe nanoparticles not previously reported using *E. coli*. Extensive characterization of these nanoparticles revealed a predominant composition of Pd with trace amounts of Fe. Biosynthesized Pd and Pd-Fe NPs demonstrated excellent catalytic activity in the 4-NP reduction reaction, yet the catalytic activity was notably enhanced with the addition of Fe. *E. coli* was found to generate distinct populations of Pd-Fe NPs, each exhibiting unique features such as size and clustering. It is noteworthy that the mean size of the nanoparticles varied based on the site of formation: outside bacterial cells it was 2.2 nm of diameter, while inside was 1.3 nm. Given the sensitivity of Pd NP magnetic properties to size variations, it is anticipated that these NP populations will display distinct magnetic responses. However, the purification and characterization of these as individual populations pose significant challenges. The work described in Paper II, Paper III, and Paper IV attempts to provide novel methods to characterize these samples.

A drawback of our microbial NP synthesis protocol is the tendency of both metals to agglomerate, resulting in disordered bimetallic particles lacking a defined structure and exhibiting slightly unpredictable properties. However, Pd-Fe NPs, when compared to pure Pd NPs, exhibit significantly improved catalytic activity than their monometallic counterparts. By using Pd-Fe NPs instead of pure Pd NPs, the necessary amount of precious metal for catalytic reactions is decreased, reducing costs and increasing economic viability.

Paper II

Detection of microbial nanoparticles within biological structures by AFM and MFM.

Advanced methods for characterizing the properties of NPs necessitate the samples to be processed in different ways. Frequently, the study of multiple properties, such as size, localization and magnetic behavior cannot be done simultaneously. In the case of the study of magnetism with Vibrating Sample Magnetometry (VSM), the NPs are usually in dry powder

form, preventing the assessment of specific particle populations within a sample. Building up from the work presented in Paper I, this paper introduces a characterization approach for evaluating NPs within biological samples using Atomic Force microscopy (AFM) and Magnetic Force Microscopy (MFM). This approach involves AFM and MFM scanning of thin slices of resin-embedded bacteria with NPs, a sample preparation technique previously employed in EM studies, but never for the direct study of biosynthetic nanoparticles within cellular structures. Our findings reveal a notable agreement between AFM and TEM in delineating bacteria topography and providing information on Pd and Pd-Fe nanoparticle size and localization. Nevertheless, achieving resolution for distinguishing between single nanoparticles and clusters remains challenging.

The introduction of MFM not only validates topographical findings, but also offers valuable insights into the magnetic properties of both intracellular and extracellular nanoparticles. Our sample preparation protocol facilitates direct interaction between the magnetic tip and the magnetic material within the cells, enabling the assessment of biogenic NPs magnetic properties without the need for intricate purification procedures, even while studying weakly magnetic nanoparticles. The comparison with a two-dipole model of interaction between the magnetic tip and the nanoparticles indicates a good approximation of our data to pure magnetic signal of the sample. The assessment of weakly magnetic nanoparticles produced by bacteria serves as a model for comprehending broader implications of nanoparticle interactions within biological systems.

Paper III

Probing van der Waals and magnetic forces in bacterial samples containing magnetic nanoparticles.

In this work, the study of the magnetic properties of biosynthesized Pd-Fe NPs by AFM and MFM described in the Paper II is extended further. The sample protocol based on the well-established TEM methods for embedding biological samples in epoxy resin was used for both AFM and MFM. Normal methodologies consist in the purification of the nanoparticles or the deposition of the bacteria with nanoparticles on top of smooth surfaces. This prevents the study of bacteria structures interaction with the nanoparticles, their localization and the relation between NP size and magnetic properties. Here, using MFM, a magnetic tip scans above the sample surface, registering its interaction with magnetic nanoparticles, as well as providing information about the sample topography and particle distribution. However, Pd-based materials have low magnetic moment, hence this demands the tip to be in close proximity to the sample surface, within a distance of a few nanometers. Working at such small distances introduces complications, as van der Waals forces also act on the tip, preventing the isolation of the magnetic force.

To address this challenge, first a simulation of the magnetic field of a nanoparticle and a tip was conducted. This model was later compared with the AFM and MFM characterization of the sample for low to high lift heights from the surface. This protocol allowed us to identify that for the measured sample, the study with MFM at 22 nm above the surface is optimal for detecting magnetic forces without significant interference from van der Waals interactions. At

this distance, pure magnetic maps were generated, clearly visualizing Pd-Fe nanoparticles. This suggests that the MFM technique is a convenient tool for resolving the magnetic properties of nanoparticles within biological samples.

Paper IV

Magnetic decoration of *Escherichia coli* loaded with Palladium nanoparticles.

A new method was developed for the optimization of biosynthesized Pd nanoparticles studied with MFM. Based on the results from Paper II and Paper III, the MFM characterization of the samples allowed the study of the nanoparticles distributed at different locations in the cells and in the extracellular space. However, nanoparticles within the cellular structures are smaller in size than extracellular ones, as reported in Paper I, and therefore difficult to resolve. The MFM study of the sample demonstrated the possibility of collecting magnetic signals from extracellular nanoparticles while studying the sample at lift heights above 22 nm. However, the intracellular nanoparticles, due to their weak magnetic fields are presented as dark regions within the bacterial cells. The divergence of magnetic field lines from individual dipoles and the merging of field lines from different NPs are suggested as the causes of this effect. This paper explores the enhancement of the magnetic signal of Pd-Fe NPs through the deposition (additional doping) of 10 nm commercial Fe_2O_3 NPs into the sample, coupled with a strong external perpendicular magnetic field. Due to their magnetic nature, the added NPs accumulate in an ordered pattern in the extracellular regions without a magnetic signal and are evenly distributed on weak magnetic nanoparticles. This strategy aims to facilitate the visualization of intracellular NPs. As a result of this approach, the magnetic signal of Pd-Fe NPs was increased in bacteria by 15-fold. Bacterial cells displayed a more pronounced black contrast as a result of this signal enhancement. Moreover, the bacterial cells exhibited a well-defined line profile around them, in contrast to the diffuse appearance observed without the enhancement. These advancements, however, were not yet sufficient for the individual resolution of intracellular Pd-Fe NPs.

Chapter 5. Discussion

1. *E. coli*-mediated synthesis of bimetallic Pd-Fe nanoparticles

The synthesis of MNPs by bacteria cells has been described before for a variety of strains (Table 2, [29]). The complex mechanisms of defense that bacteria originally developed against heavy metal toxicity (Chapter 1 Section 2.1) are now studied to generate different MNPs with similar or enhanced activity comparable with their chemical produced counterparts, and produced in an environmentally friendly way [43,44,132]. Currently, the synthesis of MNPs involves the mining of metals and further transformation by a chemical or physical method into nanoparticles (Chapter 1 Section 1). Metal extraction is highly polluting and limited in yield [316]. Therefore, the growing use of precious metals in the industry cannot keep up with the supply. Using bacteria to recover and reuse scarce metals could be of great benefit to reduce pollution and decrease mining activity. Some bacteria have the ability to immobilize and precipitate metal ions found in liquid environments, such as contaminated residual waters. Subsequently, these bacteria convert the sequestered heavy metals from wastewater into valuable nanoparticles that can be use in different applications.

Despite the growing interest in metal NP production in bacteria (Chapter 1 Section 3), it is surprising how little is known about the mechanisms of metal nanoparticle synthesis by bacteria cells. It is still unclear how bacterial metabolic side reactions complete precious MNPs formation, but even more, it is unknown how the microbial synthesis pathways can be exploited and tuned to achieve the desired production of nanoparticles for commercial use. Palladium is an expensive element among these precious but limited metal resources with many important applications in industry. Previously, it has been successfully produced as NPs by various bacteria strains (Chapter 1 Section 3). Pd, which was selected in this work as the base metal of the nanoparticles (**Paper I**), is therefore the perfect candidate as a test case for the elucidation of MNP formation by microorganisms and for the evaluation and fine-tuning of MNPs properties to enhance their activity or tailor them for a specific application.

Among the most interesting properties of Pd-based nanoparticles are their strong catalytic activity and their size-dependent magnetic behavior. Small MNPs with a high surface area and available active sites are more chemically reactive and therefore more effective in catalytic reactions than larger particles. As mentioned in Chapter 1 Section 3, Pd can behave magnetically when reaching low dimensions. In nanoparticle form, it displays ferromagnetism when in sizes between 1-10 nm [228,317–319]. Remarkably, the synthesis mediated by bacteria cells was reported to also be able to produce small sized magnetic Pd NPs [229]. The magnetic properties of Pd are however weak when compared to other ferromagnetic magnetic materials (**Paper II**). Therefore, to overcome this, the addition of small amounts of a ferromagnetic element was used to increase the magnetic moment. Fe was selected as the second metal for Pd-based microbial nanoparticle synthesis. Doping of Pd with Fe is described to generate large magnetic moments due to Pd atoms polarization when in contact with Fe atoms [320]. Hence, the first aim (**Aim (a)**) of this work was to demonstrate the synthesis of bimetallic Pd-Fe NPs mediated by bacteria. In the past, researchers reported the synthesis of Pd-Fe bimetallic

nanoparticles from different biological sources. Plant-mediated synthesis is one of the most studied biological pathways for bimetallic nanoparticle production [248–250]. However, few bacterial strains have been demonstrated to generate them. Pd-Fe NPs produced by *E. coli* cells have not been reported before. In **Paper I**, I report an effective protocol for the synthesis of monometallic Pd and bimetallic Pd-Fe NPs by *E. coli* bacteria. Various ratios of Pd/Fe were tested to find the optimal relation that generates Pd-Fe NPs with enhanced catalytic or magnetic features.

It is known that the reduction of Pd by bacteria is not restricted to metal- and sulfur-reducing microorganisms but a large group of Gram-negative bacteria with no documented capacity for reducing metals are suitable too [321]. Due to rapid bacterial growth, simple, and economical cultivation, *E. coli* was selected as a model organism for nanoparticle biosynthesis [253]. The results of the study described in **Paper I** suggest that the conditions for efficient production of Pd and Pd-Fe NPs require the use of live bacteria cells. Usually, the nanoparticle formation steps using live cells involve exposure of the bacteria to a medium rich in metal, adsorption of metal ions and reduction, which is promoted by metabolically mediated side reaction with the input of a reducing agent (Chapter 1 Section 3.1). As Pd is not an essential element for bacteria, there is no dedicated transporter complex for its import and, thus it presumably enters the cells through other inorganic ion transporter complexes or by passive diffusion (Chapter 1 Section 2.1.2). **Paper I** reported a limited metal uptake by heat-killed bacteria cells when compared to normal cells and a slow reduction of the ions into nanoparticles. The efficiencies of particle production in this case are significantly lower compared to those achieved by living cells, and a large amount of precious metal is lost in the residual medium after adsorption by the biological material. The recovery of Pd and Fe from the media by living *E. coli* measured by AAS is above 90 % in most of the cases reported in this work, demonstrating that active metabolic processes mediate the NP production.

Noteworthy is that the particle size and the reactivity of biosynthetic Pd NPs can be adjusted by the relative amount of biomass to a metal ions, as reported in [322]. Here, the variable material is Fe added to the same biomass while keeping the Pd concentration constant. The question arises then whether the differences in particle morphology will affect the magnetic and catalytic properties of nanoparticles. In the following section, I discuss these features from the characterization biosynthetic Pd-Fe nanoparticles.

2. Characterization of microbially synthesized nanoparticles

The second aim (**Aim (b)**) of this work was to perform detailed characterization of Pd and Pd-Fe NPs using various advanced techniques. The changes in the physical and chemical properties of the NPs due to modifications in the synthesis are useful for the development of better protocols. In **Paper I**, STEM visualization demonstrated intracellular and extracellular Pd and Pd-Fe nanoparticle formation in cells (Figure 14). Cell membrane-bound NPs had an average size of 1.3 ± 0.4 nm, while extracellular NPs were as big as 2.2 ± 0.6 nm. This is an indication of the influence of nucleation site localization on the size distribution. It has been suggested by others that bacteria-metal interaction within the cells leads to capping of the NPs with biological macromolecules, preventing aggregation and promoting smaller intracellular

NP formation [323]. Interestingly, the mean particle size for both extracellular and intracellular nanoparticles seem to increase with the concentration of Fe used. The study of elemental composition by HAADF-STEM with EDX analysis revealed the bimetallic nature of the NPs (Figure 15 (a-c)).

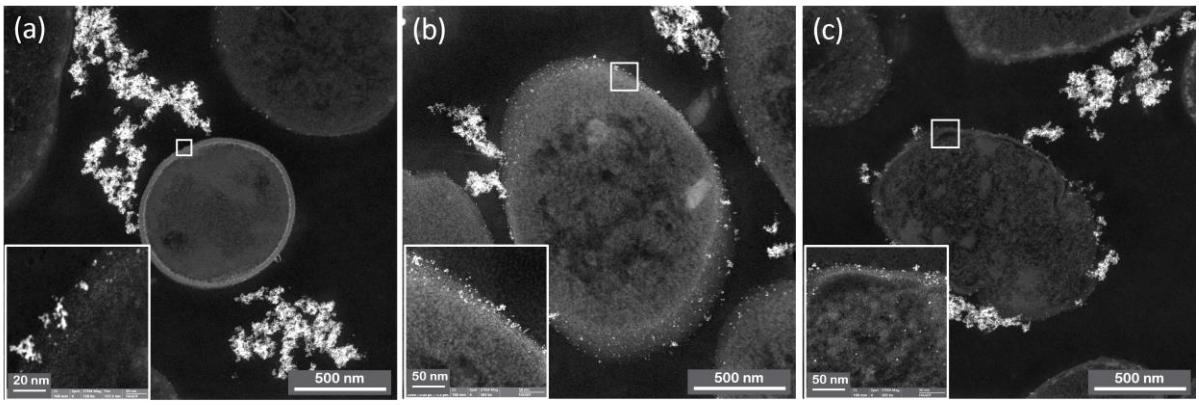

Figure 14. High-angle annular dark field scanning electron microscope (HAADF-STEM) micrographs of (a) E.coli-Pd/Fe$_{0.5}$, (b) E.coli-Pd, and (c) E.coli-Pd/Fe$_1$ samples. Inset show bacteria membrane at higher magnification.

The maps of Pd and Fe co-localization showed nanoparticles richer in Pd than in Fe at the extracellular and membrane levels (Figure 15(d)). In the *E. coli* intracellular space, smaller NPs containing pure Pd were found, but less frequently. This could be explained by the fast sequestration and further reduction of Fe ions once they reach the intracellular space before they can be integrated into the Pd NPs, which is consistent with the large deposits of intracellular Fe found in STEM images. One disadvantage of our synthesis protocol for microbial NPs is that both metals tend to agglomerate forming heterogeneous bimetallic particles, lacking a defined structure, and making their properties slightly unpredictable. Methods outlined in [212] for synthesizing Pd-Ru bimetallic nanoparticles, employing sequential metal reduction, have successfully generated core-shell structures. Applying a similar protocol to current Pd-Fe NPs production may enhance metal distribution, leading to more homogeneous populations.

The crystal structure of the NPs, assessed via HR-TEM, selected area diffraction (SAED) rings, and XRD, revealed fcc Pd formation (Figure 16). The increase in Fe concentration induced a slight decrease in *d*-spacing, characteristic of "contracted" Pd-Fe alloys [60]. Compressive strain in Pd-based alloys can enhance orbital overlap, produce expansion of the *d*-bandwidth, and weaken the adsorption strength of the material [61]. XRD also showed disruption of bacterial organic molecules upon exposure to Pd and Fe. A limitation found for the evaluation of the biosynthetic nanoparticles in XRD is the background signal attributed to bacterial biomass and other amorphous structures in the samples that obstruct the calculation of the average crystal size of the nanoparticles. Methods to clean or purify the nanoparticles would be useful before the study of the sample to reduce the noise in the measurements in the obtained diffraction curves by removing most of the amorphous structure effects. However, harsh cleaning methods could also have a disrupting effects on the original material properties [324].

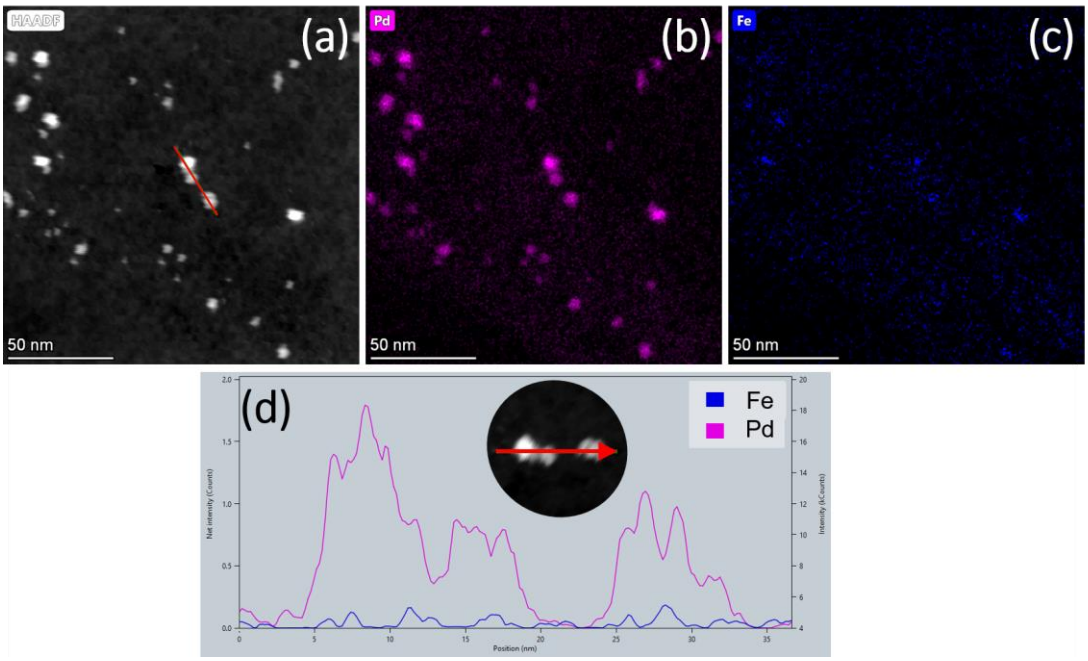

Figure 15. (a) HAADF-STEM micrograph of biosynthetic NPs in an E.coli-Pd/Fe$_1$ sample showing the co-localization of (b) Pd (pink) and (c) Fe (blue). (d) EDX of a NPs cluster cross-section.

FTIR analysis revealed changes in bands characteristic for bacterial biomass, including frequency shifts, intensity variations, and appearance of new peaks. Our measurements suggest an interaction of Pd and Fe primarily with P=O, -CH_2, and -CH_3 functional groups. These groups are likely to play a significant role in bacterial metal uptake, sequestration, and subsequent nanoparticle growth [325]. TGA curves revealed variable mass losses in regions linked to simple organic molecules, suggesting their reduced concentration in the Pd-Fe samples. This agrees with our FTIR findings, indicating that cells loaded with Pd and Fe exhibit lower lipid or fatty acid chain amounts, due to ion sequestration and metal toxicity. The remaining weight in the last phase of TGA curves, following the sample pyrolysis, typically consists of inorganic material, oxides, and carbon black [326]. Samples with high mineral content show less mass loss because the evaporation temperatures of inorganic elements are much higher than those used in the experiment. TGA measurements indicated that the final weight of the samples did not correlate with the amount of loaded metal in the bacteria. For instance, the control sample without Pd showed a similar final weight to heat-killed cells with traces of Pd. Despite expectations of higher final weight in heat-killed samples due to the heavy metal presence, both samples exhibited nearly identical weights. We suggest that this similarity indicates a faster decomposition of organic molecules in the presence of the metal, with the metal acting as a catalyst, accelerating the volatilization and degradation of biomolecules.

As mentioned in Chapter 3 Section 2.4, the model reaction of 4-nitrophenol (4-NP) reduction to 4-aminophenol (4-AP) with $NaBH_4$ is a common test for the catalytic properties of MNPs. Normally, this reduction is challenging without a catalyst, but Pd NPs with notable catalytic activity can facilitate the reaction. The paper shows that control samples evaluated in this reaction exhibited about 1.0% 4-NP reduction to 4-AP indicating negligible catalytic activity.

The best catalytic performance was achieved by the *E. coli*-Pd/Fe_1 sample of equal molar ratios of Pd and Fe. Generally, samples containing both Pd and Fe displayed superior catalytic performance compared to Pd-only samples. An obvious increase in the catalytic activity proportional to the molar concentration of Fe in the samples was observed; however, saturation was reached at the highest Fe concentration. In **Paper I**, we propose that the observed plateau in the reaction rate might be attributed either to a limitation in the incorporation of Fe into the nanoparticle or to the increase in particle size, which reduces the surface available for interaction with the solution.

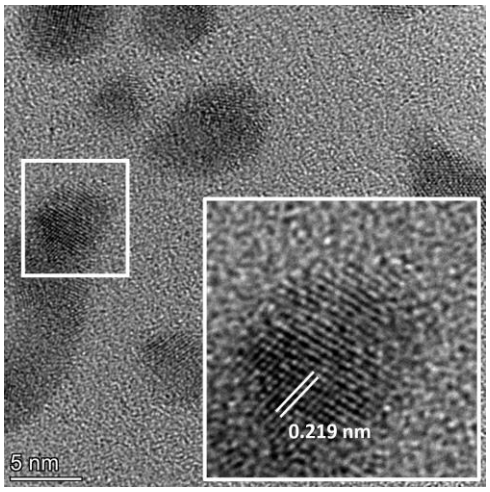

Figure 16. High-resolution TEM bright field images showing lattice spacing of Pd-Fe NPs in E.coli-Pd/Fe_1 sample.

VSM results showed Pd NPs hysteresis loops with a saturation magnetization (M_s) of 0.05 emu/g. According to Nouh *et al*. [322], ferromagnetism in Pd NPs can be induced by the interaction between biological capping agents and the NP surface. The maximal magnetic moments for Pd-Fe NPs with Pd/Fe ratios of 1:0.5, 1:1, and 1:2 were 0.27 emu/g, 0.29 emu/g, and 0.34 emu/g, respectively. In samples with Pd and Fe, the magnetization increased continuously with the applied magnetic field, showing low coercivity values indicative of paramagnetic or superparamagnetic behavior. However, the observed weak magnetism was insufficient for recovering nanoparticles using normal magnets. Standard magnetometry methods assess the overall material effect in bulk and cannot distinguish magnetic fields produced by intracellular and extracellular nanoparticles. Nanoparticles synthesized at different locations in the cell structures have distinct size distributions and elemental compositions, and it is appropriate to expect that they also own particular magnetic moments. To clarify this, innovative techniques are needed. Hence, we aimed (**Aim (c)**) to develop a novel methodology to characterize the magnetic moments of nanoparticles within cellular structures (**Paper II, Paper III, and Paper IV**).

3. Scanning probe microscopy advanced applications for characterization of nanoparticles within cellular structures

MFM has previously been used to investigate the magnetic properties of single nanoparticles, also for biosynthetic NPs. (Chapter 3 Section 2.2.3). Hence, we considered that the use of scanning probe methods would be optimal for the morphological and magnetic characterization of the NP-loaded bacteria. It is, however, necessary to develop a different sample preparation from the typical methods to study our samples in AFM and MFM (Chapter 3 Section 2.1.2). In typical sample preparation for AFM and MFM studies, purified nanoparticles or nanoparticles loaded onto bacteria are placed on smooth surfaces. While these methods enable the examination of extracellular nanoparticles or the overall particle population, they do not allow for the correlation of the location where NPs form with their morphology and magnetic properties. The standard TEM sample preparation using ultrathin sections of resin-embedded samples seems to fit all the requirements for the study of nanoparticles within cellular structures in AFM and MFM. Similar to the approach reported by Matsko *et. al* [327], in **Paper II** we embedded in resin the cells with Pd and Pd-Fe NPs and sliced them into thin smooth cross-sections of 90-100 nm of thickness using an ultra-sharp diamond knife. The transverse cut of the cells provides direct access for the tip to the intracellular matrix. Therefore, the adopted methodology for embedding bacteria with biosynthetic nanoparticles presents the possibility to observe by AFM their localization in the cellular structures in the places where they were originally formed.

The impregnation of biological structures with resin varies in efficiency depending on the permeability of the structures and the viscosity of the polymer. Thus, the specimen would also have local variations in hardness. Then, the contrast in AFM images would mainly be influenced by local differences in the stiffness of the specimen, elemental composition, and strength of van der Waals forces. Small features like periplasmic and intracellular NPs, due to their small size, can remain concealed in AFM images amid topographic details. Nanoparticles measuring around 2 nm are significantly smaller than the resin slices, which have a thickness of about 90 nm. Only nanoparticles situated close to or exactly on the sample surface are visible in AFM and MFM amplitude and height images. The measured dimensions of NPs by this technique showed notable differences between lateral diameter and height evident in both AFM and MFM studies. The distortion in AFM images is the result of tip convolution and sample geometries [328–330]. A simple tip deconvolution method [329] that assumes a spherical apex of tip and NPs was used to estimate the actual Pd NPs diameters. The diameters found were 9.9 ± 5.3 nm (AFM) and 6.6 ± 1.8 nm (MFM) for Pd NPs, which are comparable to our TEM measurements. Conversely, Pd-Fe NP calculated diameters are significantly larger than TEM values, with AFM and MFM diameters of 19.8 ± 5.1 nm and 13.5 ± 5.0 nm, respectively. Thus, at this point, it is not possible to confirm or disprove that the particles observed with AFM or MFM are clusters or indeed individual NPs using this sample preparation. It is still necessary to evaluate better deconvolution methodologies.

As mentioned earlier in Chapter 3 Section 2.2.3, the image contrast in AFM is expressed as a sum of long-distance and short-distance, attractive and repulsive forces acting between the tip and the surface [298]. Using a magnetic tip (MFM) on top of a non-magnetic sample showed that the contrast was not visible after scanning the sample at 50 nm of height. When scanning bacteria loaded with Pd NPs, dark regions inside the bacteria and in a few extracellular locations are still visible up to 80 nm of lift height. The phase shift caused by non-magnetic forces is often smaller than that of magnetic forces. As a result, magnetic forces tend to

dominate over other intermolecular forces at long distances from the surface [331]. This enables us to employ the two-pass scanning technique to distinguish magnetic interactions from other forces originating from the sample surface. Hence, the dark contrast observed in this sample between 50 nm and 80 nm of tip lift height is likely due to magnetic forces from the magnetic nanoparticles in the specimen.

To isolate information about the magnetic field from the sample topography, the specimen must be studied at heights above the non-magnetic force detection levels (50 nm for this sample, **Paper II**). Studying the magnetic response of individual MNPs at this lift height is challenging due to weak magnetic properties and small distances between nanoparticles, which cause the magnetic field lines to merge. This complicates the determination of individual NP contributions and their location. The addition of Fe to the nanoparticles increases the magnetic moment of the NPs, hence the MFM phase signal from the sample is visible far above the maximum detection lift height of the pure Pd NPs (up to 80 nm).

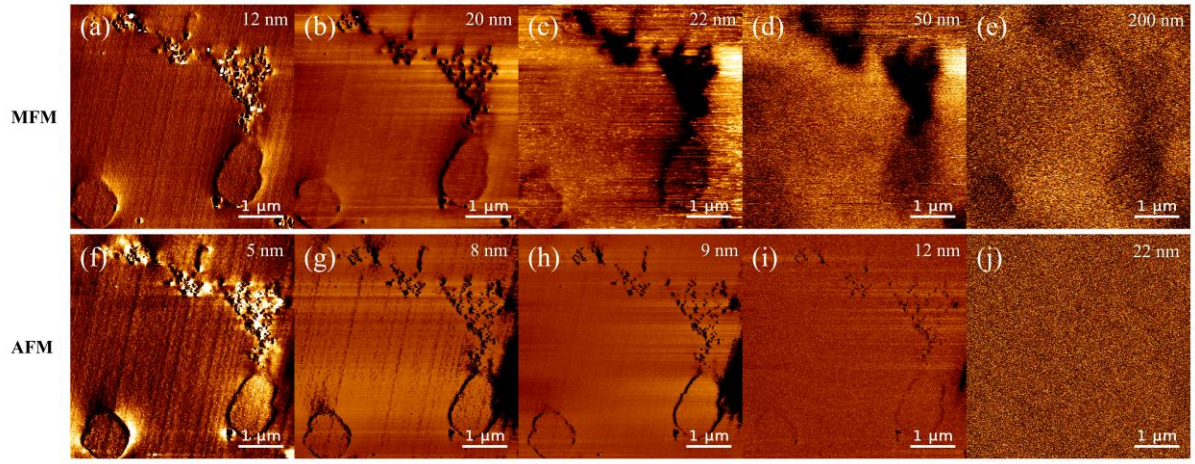

Figure 17. Example of phase shift images of Pd-Fe NPs synthetized by E. coli embedded in resin recorded with a magnetic tip at lift heights of a) 12, b) 20, c) 22, d) 50, and e) 200 nm and with a non-magnetic tip at lift heights of f) 5, g) 8, h) 9, i) 12, and j) 22 nm.

At that point, an additional method was tried to separate the magnetic contributions from the non-magnetic ones at distances closer to the surface. The paper describes the study of specimens with both a non-magnetic and the same tip with magnetic coating (Figure 17). We subtracted the AFM data from the MFM data coming from single nanoparticles and obtained a "pure magnetic" signal. The data was compared to the predicted phase shift curves at different heights for the nanoparticles using a two-dipole model of interaction between the magnetic tip and the nanoparticles. The discrepancy between the measured data and the model can probably be attributed to the variability of the magnetic moment of each nanoparticle. The heterogeneous composition and uneven distribution of Fe in the NPs make predicting their exact magnetic behavior difficult. In addition, the nanoparticles in our samples are embedded in resin at varying distances from the surface, often clustered together. The measured magnetic response could reflect the collective signal from agglomerated NPs at different positions on and different depths in the specimen.

In **Paper III**, further optimization of the method was attempted. A simulation of the tip interaction with a nanoparticle was performed by finite element analysis. The estimated phase shift curve was compared with the experimental AFM and MFM phase shift signals coming from single Pd-Fe NPs. It was easy to distinguish from the plot the height at which the van der Waals forces become irrelevant compared to other forces (magnetic force). Measurements at this height would have a strong magnetic component, low topography contribution, and minimal merging of the magnetic fields coming from different points in the sample. Therefore, MFM studies of magnetic nanoparticles would give better results at this optimal height.
Finally, an additional optimization of the nanoparticle magnetic field characterization by MFM using our sample preparation was done. The magnetic phase shift in Pd-Fe NPs coming from intracellular Pd-Fe is much weaker than that in the extracellular ones (**Paper IV)**. This might be related to the different size distributions and compositions of the nanoparticle populations. **Paper IV** describes the doping of the sample surface with 10 nm commercial Fe_2O_3 NPs under a strong external perpendicular magnetic field. These NPs, due to their magnetic nature, accumulate in an ordered pattern in extracellular regions without a magnetic signal and are evenly distributed on top of weak magnetic nanoparticles. The decoration methodology is similar to Bitter's method [332] used to visualize vortices of magnetic flux in superconducting materials. After doping, bacterial cells exhibited a more pronounced black appearance and a well-defined line profile around them, but the advancements were not yet sufficient for the individual resolution of intracellular Pd-Fe NPs.
AFM and MFM characterization offer valuable insights into the properties of biosynthetic nanoparticles, although at lower resolution compared to TEM studies. Both methods should be employed as complementary techniques for characterizing nanoparticles in biological structures providing important information, such as particle size, localization, magnetic behavior, and general morphology.

4. Future work

As a result of joint work on the BEDPAN project, bimetallic Pd-Fe nanoparticles were biosynthesized using a novel approach. In this thesis, a detailed characterization of the nanoparticles using multiple advanced techniques was done to reveal their most important features. The addition of Fe in this work was used as a pathway for the tailoring of microbial nanoparticle properties. In the past, it has been shown that by tuning the metal concentration and cell density, it is possible to obtain well-defined nanoparticles with a narrow size distribution and homogeneous morphology using bacteria [136,333]. Doping of Pd nanoparticles with Fe in general had the effect of increasing the average particle size and contracting the crystal lattice. Nanoparticles synthesized intracellularly were smaller and made mainly of pure Pd, while extracellular nanoparticles had traces of Fe, increased mean size and different size distribution. The synergy between Pd and Fe results in improved catalytic activity for 4-NP reduction, related to Fe concentration in the particles. The magnetic properties of the nanoparticles were examined by the novel methodology developed in this work using scanning probe microscopy and slices of embedded samples. This technique allowed the identification of the different magnetic features generated in intracellular and extracellular NPs.

Future work in nanoparticle synthesis will now be focus on the development of better bacterial strains that can synthesize nanoparticles with the desired features. In the BEDPAN project and parallel to this thesis, the findings of this work are now used for the development of efficient mechanisms to supervise and adjust these parameters, in combination with choosing the ideal bacterial strains. A variety of experiments have been conducted to understand how heavy metal ions influence bacterial physiological processes. The results of Joudeh *et al.* [334] study gave insights into candidate genes that might be responsible for the uptake of Pd^{2+} ions in *E. coli*. To determine how these transporter complexes directly contribute to Pd transport, and ultimately to NP formation, more research is needed. Currently, some of the relevant mutants are being studied for their interaction with Pd and ability to reduce it into nanoparticles in comparison with wild-type strains. Some desirable results based on the results of the present thesis are the development of mutant bacteria strains that, for instance, synthesize only intracellular nanoparticles. Such particles, according to this work, are smaller, have narrower size distributions, and should possess enhanced catalytic activity and possibly, beneficial magnetic properties.

There seems to be enormous potential for a cost-effective and environmentally friendly synthesis of metal nanoparticles by bacteria. Yet, some special considerations must be assessed before the implementation of these approaches on a large scale and for commercial applications. The most common disadvantages of nanoparticle synthesis using microorganisms are the dispersity of the particles, low yield, and agglomeration [52]. Optimized conditions for bacterial growth and nanoparticle formation must be determined in detail before any large-scale synthesis is considered, and it is crucial to evaluate how controllable these parameters are on larger scales.

Biosynthetic nanoparticles also present biocappings. Certain capping agents play a role in producing small and uniform nanoparticles by preventing agglomeration and reducing toxicity [335]. Even so, there is often a need for a purification process of these biocoatings depending on the intended application. Excess proteins, ligands, and impurities can impede the catalytic performance of nanoparticles. Hence, purification methods such as dialysis, filtration, and sucrose density centrifugation could be introduced to address this issue. However, many of these purification methods are found to be time-consuming, labor-intensive, or not cost-effective, potentially hindering the profitable utilization of the nanoparticles for their intended purposes [29]. The development of better purification methods for biosynthetic nanoparticles is, therefore, desirable.

References

1. Jimenez-Sandoval, R.; Pedireddy, S.; Katuri, K.P.; Saikaly, P.E. Facile Biological-Based Synthesis of Size-Controlled Palladium Nanoclusters Anchored on the Surface of Geobacter Sulfurreducens and Their Application in Electrocatalysis. *ACS Sustain. Chem. Eng.* 2023, *11*, 1100–1109, doi:10.1021/acssuschemeng.2c06143.
2. Gao, C.; Lyu, F.; Yin, Y. Encapsulated Metal Nanoparticles for Catalysis. *Chem. Rev.* 2021, *121*, 834–881, doi:10.1021/acs.chemrev.0c00237.
3. Yaqoob, A.A.; Ahmad, H.; Parveen, T.; Ahmad, A.; Oves, M.; Ismail, I.M.I.; Qari, H.A.; Umar, K.; Mohamad Ibrahim, M.N. Recent Advances in Metal Decorated Nanomaterials and Their Various Biological Applications: A Review. *Front. Chem.* 2020, *8*, 341, doi:10.3389/fchem.2020.00341.
4. Makela, A. V.; Schott, M.A.; Madsen, C.S.; Greeson, E.M.; Contag, C.H. Magnetic Particle Imaging of Magnetotactic Bacteria as Living Contrast Agents Is Improved by Altering Magnetosome Arrangement. *Nano Lett.* 2022, *22*, 4630–4639, doi:10.1021/acs.nanolett.1c05042.
5. Javed, Y.; Akhtar, K.; Anwar, H.; Jamil, Y. MRI Based on Iron Oxide Nanoparticles Contrast Agents: Effect of Oxidation State and Architecture. *J. Nanoparticle Res. 2017 1911* 2017, *19*, 1–25, doi:10.1007/S11051-017-4045-X.
6. Nanda, A.; Saravanan, M. Biosynthesis of Silver Nanoparticles from Staphylococcus Aureus and Its Antimicrobial Activity against MRSA and MRSE. *Nanomedicine Nanotechnology, Biol. Med.* 2009, *5*, 452–456, doi:10.1016/j.nano.2009.01.012.
7. Jaidev, L.R.; Narasimha, G. Fungal Mediated Biosynthesis of Silver Nanoparticles, Characterization and Antimicrobial Activity. *Colloids Surfaces B Biointerfaces* 2010, *81*, 430–433, doi:10.1016/j.colsurfb.2010.07.033.
8. Das, C.G.A.; Kumar, V.G.; Dhas, T.S.; Karthick, V.; Govindaraju, K.; Joselin, J.M.; Baalamurugan, J. Antibacterial Activity of Silver Nanoparticles (Biosynthesis): A Short Review on Recent Advances. *Biocatal. Agric. Biotechnol.* 2020, *27*, 101593, doi:10.1016/j.bcab.2020.101593.
9. Oves, M.; Rauf, M.A.; Hussain, A.; Qari, H.A.; Khan, A.A.P.; Muhammad, P.; Rehman, M.T.; Alajmi, M.F.; Ismail, I.I.M. Antibacterial Silver Nanomaterial Synthesis From Mesoflavibacter zeaxanthinifaciens and Targeting Biofilm Formation. *Front. Pharmacol.* 2019, *10*, doi:10.3389/fphar.2019.00801.
10. Bogireddy, N.K.R.; Kiran Kumar, H.A.; Mandal, B.K. Biofabricated Silver Nanoparticles as Green Catalyst in the Degradation of Different Textile Dyes. *J. Environ. Chem. Eng.* 2016, *4*, 56–64, doi:10.1016/j.jece.2015.11.004.
11. Krebsz, M.; Kótai, L.; Sajó, I.E.; Váczi, T.; Pasinszki, T. Carbon Microsphere-Supported Metallic Nickel Nanoparticles as Novel Heterogeneous Catalysts and Their Application for the Reduction of Nitrophenol. *Molecules* 2021, *26*, 5680, doi:10.3390/molecules26185680.
12. Weng, X.; Guo, M.; Luo, F.; Chen, Z. One-Step Green Synthesis of Bimetallic Fe/Ni Nanoparticles by Eucalyptus Leaf Extract: Biomolecules Identification, Characterization and Catalytic Activity. *Chem. Eng. J.* 2017, *308*, 904–911, doi:10.1016/j.cej.2016.09.134.
13. Stephen, A.J.; Rees, N. V.; Mikheenko, I.; Macaskie, L.E. Platinum and Palladium Bio-Synthesized Nanoparticles as Sustainable Fuel Cell Catalysts. *Front. Energy Res.* 2019, *7*, 66, doi:10.3389/fenrg.2019.00066.
14. Søbjerg, L.S.; Gauthier, D.; Lindhardt, A.T.; Bunge, M.; Finster, K.; Meyer, R.L.; Skrydstrup, T. Bio-Supported Palladium Nanoparticles as a Catalyst for Suzuki–Miyaura and Mizoroki–Heck Reactions. *Green Chem.* 2009, *11*, 2041, doi:10.1039/b918351p.
15. Narasaiah, B.P.; Mandal, B.K. Remediation of Azo-Dyes Based Toxicity by Agro-Waste Cotton Boll Peels Mediated Palladium Nanoparticles. *J. Saudi Chem. Soc.* 2020, *24*, 267–281,

doi:10.1016/j.jscs.2019.11.003.
16. Patil, S.; Sastry, M.; Bharde, A. Size and Shape Directed Novel Green Synthesis of Plasmonic Nanoparticles Using Bacterial Metabolites and Their Anticancer Effects. *Front. Microbiol.* 2022, *13*, 963, doi:10.3389/fmicb.2022.866849.
17. Jamkhande, P.G.; Ghule, N.W.; Bamer, A.H.; Kalaskar, M.G. Metal Nanoparticles Synthesis: An Overview on Methods of Preparation, Advantages and Disadvantages, and Applications. *J. Drug Deliv. Sci. Technol.* 2019, *53*, 101174, doi:10.1016/j.jddst.2019.101174.
18. Vijayakumar, M.; Priya, K.; Nancy, F.T.; Noorlidah, A.; Ahmed, A.B.A. Biosynthesis, Characterisation and Anti-Bacterial Effect of Plant-Mediated Silver Nanoparticles Using *Artemisia nilagirica*. *Ind. Crops Prod.* 2013, *41*, 235–240, doi:10.1016/j.indcrop.2012.04.017.
19. de Jesus, R.A.; de Assis, G.C.; de Oliveira, R.J.; Costa, J.A.S.; da Silva, C.M.P.; Bilal, M.; Iqbal, H.M.N.; Ferreira, L.F.R.; Figueiredo, R.T. Environmental Remediation Potentialities of Metal and Metal Oxide Nanoparticles: Mechanistic Biosynthesis, Influencing Factors, and Application Standpoint. *Environ. Technol. Innov.* 2021, *24*, 101851, doi:10.1016/j.eti.2021.101851.
20. Shojaei, M.; Shokuhfar, A.; Zolriasatein, A. Synthesis and Characterization of $CuAlS_2$ Nanoparticles by Mechanical Milling. *Mater. Today Commun.* 2021, *27*, 102243, doi:10.1016/j.mtcomm.2021.102243.
21. Orozco-Montes, V.; Caillard, A.; Brault, P.; Chamorro-Coral, W.; Bigarre, J.; Sauldubois, A.; Andreazza, P.; Cuynet, S.; Baranton, S.; Coutanceau, C. Synthesis of Platinum Nanoparticles by Plasma Sputtering onto Glycerol: Effect of Argon Pressure on Their Physicochemical Properties. *J. Phys. Chem. C* 2021, *125*, 3169–3179, doi:10.1021/acs.jpcc.0c09746.
22. Butterfield, A.G.; Steimle, B.C.; Schaak, R.E. Retrosynthetic Design of Morphologically Complex Metal Sulfide Nanoparticles Using Sequential Partial Cation Exchange and Chemical Etching. *ACS Mater. Lett.* 2020, *2*, 1106–1114, doi:10.1021/acsmaterialslett.0c00287.
23. Menazea, A.A. Femtosecond Laser Ablation-Assisted Synthesis of Silver Nanoparticles in Organic and Inorganic Liquids Medium and Their Antibacterial Efficiency. *Radiat. Phys. Chem.* 2020, *168*, 108616, doi:10.1016/j.radphyschem.2019.108616.
24. Lozhkomoev, A.S.; Pervikov, A. V.; Kazantsev, S.O.; Sharipova, A.F.; Rodkevich, N.G.; Toropkov, N.E.; Suliz, K. V.; Svarovskaya, N. V.; Kondranova, A.M.; Lerner, M.I. Synthesis of Fe/Fe3O4 Core-Shell Nanoparticles by Electrical Explosion of the Iron Wire in an Oxygen-Containing Atmosphere. *J. Nanoparticle Res.* 2021, *23*, 73, doi:10.1007/s11051-021-05180-x.
25. Fu, X.; Cai, J.; Zhang, X.; Li, W.-D. Di; Ge, H.; Hu, Y. Top-down Fabrication of Shape-Controlled, Monodisperse Nanoparticles for Biomedical Applications. *Adv. Drug Deliv. Rev.* 2018, *132*, 169–187, doi:10.1016/j.addr.2018.07.006.
26. Tang, S.; Qiao, R.; Lin, Y.; Li, Y.; Zhao, Q.; Yuan, D.; Yun, G.; Guo, J.; Dickey, M.D.; Huang, T.J.; et al. Functional Liquid Metal Nanoparticles Produced by Liquid-Based Nebulization. *Adv. Mater. Technol.* 2019, *4*, 1800420, doi:10.1002/admt.201800420.
27. Henglein, A. Radiolytic Preparation of Ultrafine Colloidal Gold Particles in Aqueous Solution: Optical Spectrum, Controlled Growth, and Some Chemical Reactions. *Langmuir* 1999, *15*, 6738–6744, doi:10.1021/la9901579.
28. Nomoev, A. V.; Bardakhanov, S.P. Synthesis and Structure of Ag-Si Nanoparticles Obtained by the Electron-Beam Evaporation/Condensation Method. *Tech. Phys. Lett.* 2012, *38*, 375–378, doi:10.1134/S1063785012040268.
29. Campaña, A.L.; Saragliadis, A.; Mikheenko, P.; Linke, D. Insights into the Bacterial Synthesis of Metal Nanoparticles. *Front. Nanotechnol.* 2023, *5*, doi:10.3389/fnano.2023.1216921.
30. Chan, H.-K.; Kwok, P.C.L. Production Methods for Nanodrug Particles Using the Bottom-up Approach. *Adv. Drug Deliv. Rev.* 2011, *63*, 406–416, doi:10.1016/j.addr.2011.03.011.
31. Zheng, K.; Branicio, P.S. Synthesis of Metallic Glass Nanoparticles by Inert Gas Condensation. *Phys. Rev. Mater.* 2020, *4*, 076001, doi:10.1103/PhysRevMaterials.4.076001.
32. Stoller, M.; Ochando-Pulido, J.M. ZnO Nano-Particles Production Intensification by Means of a Spinning Disk Reactor. *Nanomaterials* 2020, *10*, 1321, doi:10.3390/nano10071321.

33. Parashar, M.; Shukla, V.K.; Singh, R. Metal Oxides Nanoparticles via Sol–Gel Method: A Review on Synthesis, Characterization and Applications. *J. Mater. Sci. Mater. Electron.* 2020, *31*, 3729–3749, doi:10.1007/s10854-020-02994-8.
34. Andrade Neto, N.F.; Nascimento, L.E.; Correa, M.; Bohn, F.; Bomio, M.R.D.; Motta, F.V. Characterization and Photocatalytic Application of Ce^{4+}, Co^{2+}, Mn^{2+} and Ni^{2+} Doped Fe_3O_4 Magnetic Nanoparticles Obtained by the Co-Precipitation Method. *Mater. Chem. Phys.* 2020, *242*, 122489, doi:10.1016/j.matchemphys.2019.122489.
35. Mangaiyarkarasi, R.; Priyanga, M.; Santhiya, N.; Umadevi, S. In Situ Preparation of Palladium Nanoparticles in Ionic Liquid Crystal Microemulsion and Their Application in Heck Reaction. *J. Mol. Liq.* 2020, *310*, 113241, doi:10.1016/j.molliq.2020.113241.
36. Vinay, S.P.; Udayabhanu; Nagaraju, G.; Chandrappa, C.P.; Chandrasekhar, N. Hydrothermal Synthesis of Gold Nanoparticles Using Spider Cobweb as Novel Biomaterial: Application to Photocatalytic. *Chem. Phys. Lett.* 2020, *748*, 137402, doi:10.1016/j.cplett.2020.137402.
37. Yang, Y.; Song, B.; Ke, X.; Xu, F.; Bozhilov, K.N.; Hu, L.; Shahbazian-Yassar, R.; Zachariah, M.R. Aerosol Synthesis of High Entropy Alloy Nanoparticles. *Langmuir* 2020, *36*, 1985–1992, doi:10.1021/acs.langmuir.9b03392.
38. Quintanilla, A.; Valvo, M.; Lafont, U.; Kelder, E.M.; Kreutzer, M.T.; Kapteijn, F. Synthesis of Anisotropic Gold Nanoparticles by Electrospraying into a Reductive-Surfactant Solution. *Chem. Mater.* 2010, *22*, 1656–1663, doi:10.1021/cm903712y.
39. Gautam, M.; Kim, J.O.; Yong, C.S. Fabrication of Aerosol-Based Nanoparticles and Their Applications in Biomedical Fields. *J. Pharm. Investig.* 2021, *51*, 361–375, doi:10.1007/s40005-021-00523-1.
40. Tavares, J.; Swanson, E.J.; Coulombe, S. Plasma Synthesis of Coated Metal Nanoparticles with Surface Properties Tailored for Dispersion. *Plasma Process. Polym.* 2008, *5*, 759–769, doi:10.1002/ppap.200800074.
41. Katsui, H.; Goto, T. Chemical Vapor Deposition. In *Multi-dimensional Additive Manufacturing*; Springer Singapore: Singapore, 2021; pp. 75–95.
42. Restrepo, C.V.; Villa, C.C. Synthesis of Silver Nanoparticles, Influence of Capping Agents, and Dependence on Size and Shape: A Review. *Environ. Nanotechnology, Monit. Manag.* 2021, *15*, 100428, doi:10.1016/j.enmm.2021.100428.
43. Iravani, S. Bacteria in Nanoparticle Synthesis: Current Status and Future Prospects. *Int. Sch. Res. Not.* 2014, *2014*, 1–18, doi:10.1155/2014/359316.
44. Ahmad, F.; Ashraf, N.; Ashraf, T.; Zhou, R.-B.; Yin, D.-C. Biological Synthesis of Metallic Nanoparticles (MNPs) by Plants and Microbes: Their Cellular Uptake, Biocompatibility, and Biomedical Applications. *Appl. Microbiol. Biotechnol.* 2019, *103*, 2913–2935, doi:10.1007/s00253-019-09675-5.
45. Li, S.-N.; Wang, R.; Ho, S.-H. Algae-Mediated Biosystems for Metallic Nanoparticle Production: From Synthetic Mechanisms to Aquatic Environmental Applications. *J. Hazard. Mater.* 2021, *420*, 126625, doi:10.1016/j.jhazmat.2021.126625.
46. Li, Q.; Liu, F.; Li, M.; Chen, C.; Gadd, G.M. Nanoparticle and Nanomineral Production by Fungi. *Fungal Biol. Rev.* 2022, *41*, 31–44, doi:10.1016/j.fbr.2021.07.003.
47. Soni, V.; Raizada, P.; Singh, P.; Cuong, H.N.; S, R.; Saini, A.; Saini, R. V.; Le, Q. Van; Nadda, A.K.; Le, T.-T.; et al. Sustainable and Green Trends in Using Plant Extracts for the Synthesis of Biogenic Metal Nanoparticles toward Environmental and Pharmaceutical Advances: A Review. *Environ. Res.* 2021, *202*, 111622, doi:10.1016/j.envres.2021.111622.
48. Prasad, S.R.; Teli, S.B.; Ghosh, J.; Prasad, N.R.; Shaikh, V.S.; Nazeruddin, G.M.; Al-Sehemi, A.G.; Patel, I.; Shaikh, Y.I. A Review on Bio-Inspired Synthesis of Silver Nanoparticles: Their Antimicrobial Efficacy and Toxicity. *Eng. Sci.* 2021, doi:10.30919/es8d479.
49. Khalil, A.T.; Ovais, M.; Iqbal, J.; Ali, A.; Ayaz, M.; Abbas, M.; Ahmad, I.; Devkota, H.P. Microbes-Mediated Synthesis Strategies of Metal Nanoparticles and Their Potential Role in Cancer Therapeutics. *Semin. Cancer Biol.* 2022, *86*, 693–705, doi:10.1016/j.semcancer.2021.06.006.

50. Zhan, G.; Li, D.; Zhang, L. Aerobic Bioreduction of Nickel(II) to Elemental Nickel with Concomitant Biomineralization. *Appl. Microbiol. Biotechnol.* 2012, *96*, 273–281, doi:10.1007/s00253-011-3827-9.
51. Kianpour, S.; Ebrahiminezhad, A.; Deyhimi, M.; Negahdaripour, M.; Raee, M.J.; Mohkam, M.; Rezaee, H.; Irajie, C.; Berenjian, A.; Ghasemi, Y. Structural Characterization of Polysaccharide-Coated Iron Oxide Nanoparticles Produced by *Staphylococcus warneri* , Isolated from a Thermal Spring. *J. Basic Microbiol.* 2019, *59*, 569–578, doi:10.1002/jobm.201800684.
52. Narayanan, K.B.; Sakthivel, N. Biological Synthesis of Metal Nanoparticles by Microbes. *Adv. Colloid Interface Sci.* 2010, *156*, 1–13, doi:10.1016/j.cis.2010.02.001.
53. Igiri, B.E.; Okoduwa, S.I.R.; Idoko, G.O.; Akabuogu, E.P.; Adeyi, A.O.; Ejiogu, I.K. Toxicity and Bioremediation of Heavy Metals Contaminated Ecosystem from Tannery Wastewater: A Review. *J. Toxicol.* 2018, *2018*, 1–16, doi:10.1155/2018/2568038.
54. Palmer, L.D.; Skaar, E.P. Transition Metals and Virulence in Bacteria. *Annu. Rev. Genet.* 2016, *50*, 67–91, doi:10.1146/annurev-genet-120215-035146.
55. Saravanan, A.; Kumar, P.S.; Karishma, S.; Vo, D.-V.N.; Jeevanantham, S.; Yaashikaa, P.R.; George, C.S. A Review on Biosynthesis of Metal Nanoparticles and Its Environmental Applications. *Chemosphere* 2021, *264*, 128580, doi:10.1016/j.chemosphere.2020.128580.
56. Pham, V.H.T.; Kim, J.; Chang, S.; Chung, W. Bacterial Biosorbents, an Efficient Heavy Metals Green Clean-Up Strategy: Prospects, Challenges, and Opportunities. *Microorganisms* 2022, *10*, 610, doi:10.3390/microorganisms10030610.
57. Bruins, M.R.; Kapil, S.; Oehme, F.W. Microbial Resistance to Metals in the Environment. *Ecotoxicol. Environ. Saf.* 2000, *45*, 198–207, doi:10.1006/eesa.1999.1860.
58. Tsuruta, T. Biosorption and Recycling of Gold Using Various Microorganisms. *J. Gen. Appl. Microbiol.* 2004, *50*, 221–228, doi:10.2323/jgam.50.221.
59. Deplanche, K.; Caldelari, I.; Mikheenko, I.P.; Sargent, F.; Macaskie, L.E. Involvement of Hydrogenases in the Formation of Highly Catalytic Pd(0) Nanoparticles by Bioreduction of Pd(II) Using *Escherichia coli* Mutant Strains. *Microbiology* 2010, *156*, 2630–2640, doi:10.1099/mic.0.036681-0.
60. Khan, M.; Ijaz, M.; Chotana, G.A.; Murtaza, G.; Malik, A.; Shamim, S. *Bacillus altitudinis* MT422188: A Potential Agent for Zinc Bioremediation. *Bioremediat. J.* 2022, *26*, 228–248, doi:10.1080/10889868.2021.1927973.
61. Johnstone, T.C.; Nolan, E.M. Beyond Iron: Non-Classical Biological Functions of Bacterial Siderophores. *Dalt. Trans.* 2015, *44*, 6320–6339, doi:10.1039/c4dt03559c.
62. Nies, D.H. Resistance to Cadmium, Cobalt, Zinc, and Nickel in Microbes. *Plasmid* 1992, *27*, 17–28, doi:10.1016/0147-619X(92)90003-S.
63. Komeda, H.; Kobayashi, M.; Shimizu, S. A Novel Transporter Involved in Cobalt Uptake. *Proc. Natl. Acad. Sci.* 1997, *94*, 36–41, doi:10.1073/pnas.94.1.36.
64. Bhamidimarri, S.P.; Young, T.R.; Shanmugam, M.; Soderholm, S.; Baslé, A.; Bumann, D.; van den Berg, B. Acquisition of Ionic Copper by the Bacterial Outer Membrane Protein OprC through a Novel Binding Site. *PLOS Biol.* 2021, *19*, e3001446, doi:10.1371/journal.pbio.3001446.
65. Krewulak, K.D.; Vogel, H.J. Structural Biology of Bacterial Iron Uptake. *Biochim. Biophys. Acta - Biomembr.* 2008, *1778*, 1781–1804, doi:10.1016/j.bbamem.2007.07.026.
66. Ma, Z.; Jacobsen, F.E.; Giedroc, D.P. Coordination Chemistry of Bacterial Metal Transport and Sensing. *Chem. Rev.* 2009, *109*, 4644–4681, doi:10.1021/cr900077w.
67. Lau, C.K.Y.; Krewulak, K.D.; Vogel, H.J. Bacterial Ferrous Iron Transport: The Feo System. *FEMS Microbiol. Rev.* 2016, *40*, 273–298, doi:10.1093/femsre/fuv049.
68. Crespo, K.A.; Baronetti, J.L.; Quinteros, M.A.; Páez, P.L.; Paraje, M.G. Intra- and Extracellular Biosynthesis and Characterization of Iron Nanoparticles from Prokaryotic Microorganisms with Anticoagulant Activity. *Pharm. Res.* 2017, *34*, 591–598, doi:10.1007/s11095-016-2084-0.
69. Lusa, M.; Lehto, J.; Bomberg, M. The Uptake of Ni^{2+} and Ag^{+} by Bacterial Strains Isolated from a

Boreal Nutrient-Poor Bog. *AIMS Microbiol.* 2016, *2*, 120–137, doi:10.3934/microbiol.2016.2.120.
70. Omajali, J.B.; Mikheenko, I.P.; Merroun, M.L.; Wood, J.; Macaskie, L.E. Characterization of Intracellular Palladium Nanoparticles Synthesized by *Desulfovibrio desulfuricans* and *Bacillus benzeovorans*. *J. Nanoparticle Res.* 2015, *17*, 264, doi:10.1007/s11051-015-3067-5.
71. Waldron, K.J.; Robinson, N.J. How Do Bacterial Cells Ensure That Metalloproteins Get the Correct Metal? *Nat. Rev. Microbiol.* 2009, *7*, 25–35, doi:10.1038/nrmicro2057.
72. Wiesemann, N.; Mohr, J.; Grosse, C.; Herzberg, M.; Hause, G.; Reith, F.; Nies, D.H. Influence of Copper Resistance Determinants on Gold Transformation by Cupriavidus Metallidurans Strain CH34. *J. Bacteriol.* 2013, *195*, 2298–2308, doi:10.1128/JB.01951-12.
73. Zammit, C.M.; Reith, F. Gold Biomineralization in Bacterium Cupriavidus Metallidurans. In *Encyclopedia of Metalloproteins*; Springer New York: New York, NY, 2013; pp. 862–867.
74. Andrei, A.; Öztürk, Y.; Khalfaoui-Hassani, B.; Rauch, J.; Marckmann, D.; Trasnea, P.-I.; Daldal, F.; Koch, H.-G. Cu Homeostasis in Bacteria: The Ins and Outs. *Membranes (Basel).* 2020, *10*, 242, doi:10.3390/membranes10090242.
75. Rouch, D.A.; Lee, B.T.O.; Morby, A.P. Understanding Cellular Responses to Toxic Agents: A Model for Mechanism-Choice in Bacterial Metal Resistance. *J. Ind. Microbiol.* 1995, *14*, 132–141, doi:10.1007/BF01569895.
76. Li, X.Z.; Nikaido, H.; Williams, K.E. Silver-Resistant Mutants of Escherichia Coli Display Active Efflux of Ag^+ and Are Deficient in Porins. *J. Bacteriol.* 1997, *179*, 6127–6132, doi:10.1128/jb.179.19.6127-6132.1997.
77. Lutkenhaus, J.F. Role of a Major Outer Membrane Protein in *Escherichia coli*. *J. Bacteriol.* 1977, *131*, 631–637, doi:10.1128/jb.131.2.631-637.1977.
78. Nies, D.H.; Silver, S. Ion Efflux Systems Involved in Bacterial Metal Resistances. *J. Ind. Microbiol.* 1995, *14*, 186–199, doi:10.1007/BF01569902.
79. Delmar, J.A.; Su, C.-C.; Yu, E.W. Bacterial Multidrug Efflux Transporters. *Annu. Rev. Biophys.* 2014, *43*, 93–117, doi:10.1146/annurev-biophys-051013-022855.
80. Hynninen, A. Zinc, Cadmium and Lead Resistance Mechanisms in Bacteria and Their Contribution to Biosensing, University of Helsinki, 2010.
81. Rensing, C.; Fan, B.; Sharma, R.; Mitra, B.; Rosen, B.P. CopA: An *Escherichia coli* Cu(I)-Translocating P-Type ATPase. *Proc. Natl. Acad. Sci.* 2000, *97*, 652–656, doi:10.1073/pnas.97.2.652.
82. Kim, E.-H.; Nies, D.H.; McEvoy, M.M.; Rensing, C. Switch or Funnel: How RND-Type Transport Systems Control Periplasmic Metal Homeostasis. *J. Bacteriol.* 2011, *193*, 2381–2387, doi:10.1128/JB.01323-10.
83. Lin, I.W.-S.; Lok, C.-N.; Che, C.-M. Biosynthesis of Silver Nanoparticles from Silver(i) Reduction by the Periplasmic Nitrate Reductase c-Type Cytochrome Subunit NapC in a Silver-Resistant E. Coli. *Chem. Sci.* 2014, *5*, 3144–3150, doi:10.1039/C4SC00138A.
84. Blindauer, C.A. Bacterial Metallothioneins: Past, Present, and Questions for the Future. *JBIC J. Biol. Inorg. Chem.* 2011, *16*, 1011–1024, doi:10.1007/s00775-011-0790-y.
85. Boedicker, J.Q.; Gangan, M.; Naughton, K.; Zhao, F.; Gralnick, J.A.; El-Naggar, M.Y. Engineering Biological Electron Transfer and Redox Pathways for Nanoparticle Synthesis. *Bioelectricity* 2021, *3*, 126–135, doi:10.1089/bioe.2021.0010.
86. Hood, M.I.; Skaar, E.P. Nutritional Immunity: Transition Metals at the Pathogen–Host Interface. *Nat. Rev. Microbiol.* 2012, *10*, 525–537, doi:10.1038/nrmicro2836.
87. Silver, S. Bacterial Resistances to Toxic Metal Ions - a Review. *Gene* 1996, *179*, 9–19, doi:10.1016/S0378-1119(96)00323-X.
88. Kosolapov, D.B.; Kuschk, P.; Vainshtein, M.B.; Vatsourina, A.V.; Wießner, A.; Kästner, M.; Müller, R.A. Microbial Processes of Heavy Metal Removal from Carbon-Deficient Effluents in Constructed Wetlands. *Eng. Life Sci.* 2004, *4*, 403–411, doi:10.1002/elsc.200420048.
89. Fatoki, O.S. Biomethylation in the Natural Environment: A Review. *S. Afr. J. Sci.* 1997, *93*, 366–

370.
90. Ridley, W.P.; Dizikes, L.J.; Wood, J.M. Biomethylation of Toxic Elements in the Environment. *Science (80-.).* 1977, *197*, 329–332, doi:10.1126/science.877556.
91. Ridley, W.P.; Dizikes, L.; Cheh, A.; Wood, J.M. Recent Studies on Biomethylation and Demethylation of Toxic Elements. *Environ. Health Perspect.* 1977, *19*, 43–46, doi:10.1289/ehp.771943.
92. *CRC Handbook of Chemistry and Physics*; Haynes, W.M., Ed.; CRC Press, 2014; ISBN 9780429170195.
93. Schuchmann, K.; Müller, V. A Bacterial Electron-Bifurcating Hydrogenase. *J. Biol. Chem.* 2012, *287*, 31165–31171, doi:10.1074/jbc.M112.395038.
94. Müller, V. Energy Conservation in Acetogenic Bacteria. *Appl. Environ. Microbiol.* 2003, *69*, 6345–6353, doi:10.1128/AEM.69.11.6345-6353.2003.
95. Herrmann, G.; Jayamani, E.; Mai, G.; Buckel, W. Energy Conservation via Electron-Transferring Flavoprotein in Anaerobic Bacteria. *J. Bacteriol.* 2008, *190*, 784–791, doi:10.1128/JB.01422-07.
96. Reichart, O.; Szakmár, K.; Jozwiak, Á.; Felföldi, J.; Baranyai, L. Redox Potential Measurement as a Rapid Method for Microbiological Testing and Its Validation for Coliform Determination. *Int. J. Food Microbiol.* 2007, *114*, 143–148, doi:10.1016/j.ijfoodmicro.2006.08.016.
97. Kröger, A.; Geisler, V.; Lemma, E.; Theis, F.; Lenger, R. Bacterial Fumarate Respiration. *Arch. Microbiol.* 1992, *158*, 311–314, doi:10.1007/BF00245358.
98. Vincent, S.G.T.; Jennerjahn, T.; Ramasamy, K. Environmental Variables and Factors Regulating Microbial Structure and Functions. In *Microbial Communities in Coastal Sediments*; Elsevier, 2021; pp. 79–117 ISBN 978-0-12-815165-5.
99. Bloch, K.; Pardesi, K.; Satriano, C.; Ghosh, S. Bacteriogenic Platinum Nanoparticles for Application in Nanomedicine. *Front. Chem.* 2021, *9*, 32, doi:10.3389/fchem.2021.624344.
100. Lloyd, J.R. Microbial Reduction of Metals and Radionuclides. *FEMS Microbiol. Rev.* 2003, *27*, 411–425, doi:10.1016/S0168-6445(03)00044-5.
101. Barton, L.L.; Fauque, G.D. Chapter 2 Biochemistry, Physiology and Biotechnology of Sulfate-Reducing Bacteria. In *Advances in Applied Microbiology*; Academic Press, 2009; Vol. 68, pp. 41–98 ISBN 9780123748034.
102. Chen, Y.; Hu, K.; Chen, Y. The Effect of Biotic and Abiotic Environmental Factors on Pd(II) Adsorption and Reduction by *Bacillus megaterium* Y-4. *Chemosphere* 2019, *220*, 1058–1066, doi:10.1016/j.chemosphere.2019.01.011.
103. Rajora, N.; Kaushik, S.; Jyoti, A.; Kothari, S.L. Rapid Synthesis of Silver Nanoparticles by *Pseudomonas stutzeri* Isolated from Textile Soil under Optimised Conditions and Evaluation of Their Antimicrobial and Cytotoxicity Properties. *IET Nanobiotechnology* 2016, *10*, 367–373, doi:10.1049/iet-nbt.2015.0107.
104. Kalimuthu, K.; Suresh Babu, R.; Venkataraman, D.; Bilal, M.; Gurunathan, S. Biosynthesis of Silver Nanocrystals by *Bacillus licheniformis*. *Colloids Surfaces B Biointerfaces* 2008, *65*, 150–153, doi:10.1016/j.colsurfb.2008.02.018.
105. Yang, J.; Ju, P.; Dong, X.; Duan, J.; Xiao, H.; Tang, X.; Zhai, X.; Hou, B. Green Synthesis of Functional Metallic Nanoparticles by Dissimilatory Metal-Reducing Bacteria "*Shewanella*": A Comprehensive Review. *J. Mater. Sci. Technol.* 2023, *158*, 63–76, doi:10.1016/j.jmst.2023.01.041.
106. Bulgarini, A.; Lampis, S.; Turner, R.J.; Vallini, G. Biomolecular Composition of Capping Layer and Stability of Biogenic Selenium Nanoparticles Synthesized by Five Bacterial Species. *Microb. Biotechnol.* 2021, *14*, 198–212, doi:10.1111/1751-7915.13666.
107. Griffin, S.; Masood, M.; Nasim, M.; Sarfraz, M.; Ebokaiwe, A.; Schäfer, K.-H.; Keck, C.; Jacob, C. Natural Nanoparticles: A Particular Matter Inspired by Nature. *Antioxidants* 2017, *7*, 3, doi:10.3390/antiox7010003.
108. Yan, L.; Zhang, S.; Chen, P.; Liu, H.; Yin, H.; Li, H. Magnetotactic Bacteria, Magnetosomes and Their Application. *Microbiol. Res.* 2012, *167*, 507–519, doi:10.1016/j.micres.2012.04.002.

109. Monteil, C.L.; Lefevre, C.T. Magnetoreception in Microorganisms. *Trends Microbiol.* 2020, *28*, 266–275, doi:10.1016/j.tim.2019.10.012.
110. Le Nagard, L.; Morillo-López, V.; Fradin, C.; Bazylinski, D.A. Growing Magnetotactic Bacteria of the Genus *Magnetospirillum*: Strains MSR-1, AMB-1 and MS-1. *J. Vis. Exp.* 2018, 58536, doi:10.3791/58536.
111. Goswami, P.; He, K.; Li, J.; Pan, Y.; Roberts, A.P.; Lin, W. Magnetotactic Bacteria and Magnetofossils: Ecology, Evolution and Environmental Implications. *npj Biofilms Microbiomes* 2022, *8*, 43, doi:10.1038/s41522-022-00304-0.
112. Gareev, K.G.; Grouzdev, D.S.; Kharitonskii, P. V.; Kosterov, A.; Koziaeva, V. V.; Sergienko, E.S.; Shevtsov, M.A. Magnetotactic Bacteria and Magnetosomes: Basic Properties and Applications. *Magnetochemistry* 2021, *7*, 86, doi:10.3390/magnetochemistry7060086.
113. Schleifer, K.H.; Schüler, D.; Spring, S.; Weizenegger, M.; Amann, R.; Ludwig, W.; Köhler, M. The Genus *Magnetospirillum* Gen. Nov. Description of *Magnetospirillum gryphiswaldense* Sp. Nov. and Transfer of *Aquaspirillum magnetotacticum* to *Magnetospirillum magnetotacticum* Comb. Nov. *Syst. Appl. Microbiol.* 1991, *14*, 379–385, doi:10.1016/S0723-2020(11)80313-9.
114. Nudelman, H.; Zarivach, R. Structure Prediction of Magnetosome-Associated Proteins. *Front. Microbiol.* 2014, *5*, 9, doi:10.3389/fmicb.2014.00009.
115. Dziuba, M.; Riese, C.N.; Borgert, L.; Wittchen, M.; Busche, T.; Kalinowski, J.; Uebe, R.; Schüler, D. The Complex Transcriptional Landscape of Magnetosome Gene Clusters in *Magnetospirillum gryphiswaldense*. *mSystems* 2021, *6*, 893–914, doi:10.1128/mSystems.00893-21.
116. Uzun, M.; Alekseeva, L.; Krutkina, M.; Koziaeva, V.; Grouzdev, D. Unravelling the Diversity of Magnetotactic Bacteria through Analysis of Open Genomic Databases. *Sci. Data* 2020, *7*, 252, doi:10.1038/s41597-020-00593-0.
117. D., S. The Biomineralization of Magnetosomes in *Magnetospirillum gryphiswaldense*. *Int. Microbiol.* 2002, *5*, 209–214, doi:10.1007/s10123-002-0086-8.
118. Matsunaga, T.; Sakaguchi, T.; Tadakoro, F. Magnetite Formation by a Magnetic Bacterium Capable of Growing Aerobically. *Appl. Microbiol. Biotechnol.* 1991, *35*, 651–655, doi:10.1007/BF00169632.
119. Cypriano, J.; Castro, J.; Taveira, I.; Correa, T.; Acosta-Avalos, D.; Abreu, F.; Farina, M.; Keim, C.N. Magnetosome Biomineralization by Magnetotactic Bacteria. In; Springer, Cham, 2022; pp. 243–281.
120. AlphandÃ©ry, E. Applications of Magnetosomes Synthesized by Magnetotactic Bacteria in Medicine. *Front. Bioeng. Biotechnol.* 2014, *2*, 5, doi:10.3389/fbioe.2014.00005.
121. Singh, N.; Jenkins, G.J.S.; Asadi, R.; Doak, S.H. Potential Toxicity of Superparamagnetic Iron Oxide Nanoparticles (SPION). *Nano Rev.* 2010, *1*, 5358, doi:10.3402/nano.v1i0.5358.
122. Toropova, Y.; Golovkin, A.; Malashicheva, A.; Korolev, D.; Gorshkov, A.; Gareev, K.; Afonin, M.; Galagudza, M. In Vitro Toxicity of FemOn, FemOn-SiO2 Composite, and SiO2-FemOn Core-Shell Magnetic Nanoparticles. *Int. J. Nanomedicine* 2017, *Volume 12*, 593–603, doi:10.2147/IJN.S122580.
123. Alphandéry, E.; Faure, S.; Seksek, O.; Guyot, F.; Chebbi, I. Chains of Magnetosomes Extracted from AMB-1 Magnetotactic Bacteria for Application in Alternative Magnetic Field Cancer Therapy. *ACS Nano* 2011, *5*, 6279–6296, doi:10.1021/nn201290k.
124. Gwisai, T.; Mirkhani, N.; Christiansen, M.G.; Nguyen, T.T.; Ling, V.; Schuerle, S. Magnetic Torque–Driven Living Microrobots for Increased Tumor Infiltration. *Sci. Robot.* 2022, *7*, doi:10.1126/scirobotics.abo0665.
125. Xing, J.; Yin, T.; Li, S.; Xu, T.; Ma, A.; Chen, Z.; Luo, Y.; Lai, Z.; Lv, Y.; Pan, H.; et al. Sequential Magneto-Actuated and Optics-Triggered Biomicrorobots for Targeted Cancer Therapy. *Adv. Funct. Mater.* 2021, *31*, 2008262, doi:10.1002/adfm.202008262.
126. Nan, X.; Lai, W.; Li, D.; Tian, J.; Hu, Z.; Fang, Q. Biocompatibility of Bacterial Magnetosomes as MRI Contrast Agent: A Long-Term In Vivo Follow-Up Study. *Nanomaterials* 2021, *11*, 1235,

doi:10.3390/nano11051235.
127. Shi, L.; Dong, H.; Reguera, G.; Beyenal, H.; Lu, A.; Liu, J.; Yu, H.-Q.; Fredrickson, J.K. Extracellular Electron Transfer Mechanisms between Microorganisms and Minerals. *Nat. Rev. Microbiol.* 2016, *14*, 651–662, doi:10.1038/nrmicro.2016.93.
128. Lovley, D.R. Dissimilatory Metal Reduction. *Annu. Rev. Microbiol.* 1993, *47*, 263–290, doi:10.1146/annurev.mi.47.100193.001403.
129. Mehta, T.; Coppi, M. V.; Childers, S.E.; Lovley, D.R. Outer Membrane c -Type Cytochromes Required for Fe(III) and Mn(IV) Oxide Reduction in Geobacter Sulfurreducens. *Appl. Environ. Microbiol.* 2005, *71*, 8634–8641, doi:10.1128/AEM.71.12.8634-8641.2005.
130. Lovley, D.R.; Giovannoni, S.J.; White, D.C.; Champine, J.E.; Phillips, E.J.P.; Gorby, Y.A.; Goodwin, S. *Geobacter metallireducen*s Gen. Nov. Sp. Nov., a Microorganism Capable of Coupling the Complete Oxidation of Organic Compounds to the Reduction of Iron and Other Metals. *Arch. Microbiol.* 1993, *159*, 336–344, doi:10.1007/BF00290916.
131. Shi, L.; Rosso, K.M.; Clarke, T.A.; Richardson, D.J.; Zachara, J.M.; Fredrickson, J.K. Molecular Underpinnings of Fe(III) Oxide Reduction by *Shewanella oneidensis* MR-1. *Front. Microbiol.* 2012, *3*, 50, doi:10.3389/fmicb.2012.00050.
132. Iravani, S.; Varma, R.S. Bacteria in Heavy Metal Remediation and Nanoparticle Biosynthesis. *ACS Sustain. Chem. Eng.* 2020, *8*, 5395–5409, doi:10.1021/acssuschemeng.0c00292.
133. Chen, C.-Y.; Chang, Y.-C.; Tsai, T.-H.; Liu, M.-H.; Chung, Y.-C. Multifunctional Activities of Gold Nanoparticles Biosynthesized Using Bacteria Isolated from Mining Areas. *Appl. Sci.* 2021, *11*, 3670, doi:10.3390/app11083670.
134. Pourali, P.; Badiee, S.H.; Manafi, S.; Noorani, T.; Rezaei, A.; Yahyaei, B. Biosynthesis of Gold Nanoparticles by Two Bacterial and Fungal Strains, *Bacillus cereus* and *Fusarium oxysporum*, and Assessment and Comparison of Their Nanotoxicity in Vitro by Direct and Indirect Assays. *Electron. J. Biotechnol.* 2017, *29*, 86–93, doi:10.1016/j.ejbt.2017.07.005.
135. Tikariha, S.; Banerjee, S.; Dev, A.; Singh, S. Growth Phase-Dependent Synthesis of Gold Nanoparticles Using *Bacillus licheniformis*. In *Applications of Biotechnology for Sustainable Development*; Springer Singapore: Singapore, 2017; pp. 121–128 ISBN 9789811055386.
136. Bing, W.; Sun, H.; Wang, F.; Song, Y.; Ren, J. Hydrogen-Producing Hyperthermophilic Bacteria Synthesized Size-Controllable Fine Gold Nanoparticles with Excellence for Eradicating Biofilm and Antibacterial Applications. *J. Mater. Chem. B* 2018, *6*, 4602–4609, doi:10.1039/C8TB00549D.
137. Kikuchi, F.; Kato, Y.; Furihata, K.; Kogure, T.; Imura, Y.; Yoshimura, E.; Suzuki, M. Formation of Gold Nanoparticles by Glycolipids of *Lactobacillus casei*. *Sci. Rep.* 2016, *6*, 34626, doi:10.1038/srep34626.
138. Sharma, N.; Pinnaka, A.K.; Raje, M.; FNU, A.; Bhattacharyya, M.S.; Choudhury, A.R. Exploitation of Marine Bacteria for Production of Gold Nanoparticles. *Microb. Cell Fact.* 2012, *11*, 86, doi:10.1186/1475-2859-11-86.
139. Patil, M.P.; Kang, M.; Niyonizigiye, I.; Singh, A.; Kim, J.-O.; Seo, Y.B.; Kim, G.-D. Extracellular Synthesis of Gold Nanoparticles Using the Marine Bacterium *Paracoccus haeundaensis* BC74171T and Evaluation of Their Antioxidant Activity and Antiproliferative Effect on Normal and Cancer Cell Lines. *Colloids Surfaces B Biointerfaces* 2019, *183*, 110455, doi:10.1016/j.colsurfb.2019.110455.
140. Desai, M.P.; Patil, R. V.; Harke, S.S.; Pawar, K.D. Bacterium Mediated Facile and Green Method for Optimized Biosynthesis of Gold Nanoparticles for Simple and Visual Detection of Two Metal Ions. *J. Clust. Sci.* 2021, *32*, 341–350, doi:10.1007/s10876-020-01793-9.
141. Singh, P.; Singh, H.; Kim, Y.J.; Mathiyalagan, R.; Wang, C.; Yang, D.C. Extracellular Synthesis of Silver and Gold Nanoparticles by Sporosarcina koreensis DC4 and Their Biological Applications. *Enzyme Microb. Technol.* 2016, *86*, 75–83, doi:10.1016/j.enzmictec.2016.02.005.
142. Shunmugam, R.; Renukadevi Balusamy, S.; Kumar, V.; Menon, S.; Lakshmi, T.; Perumalsamy, H. Biosynthesis of Gold Nanoparticles Using Marine Microbe (*Vibrio alginolyticus*) and Its

Anticancer and Antioxidant Analysis. *J. King Saud Univ. - Sci.* 2021, *33*, 101260, doi:10.1016/j.jksus.2020.101260.
143. Singh, H.; Du, J.; Yi, T.-H. Biosynthesis of Silver Nanoparticles Using Aeromonas Sp. THG-FG1.2 and Its Antibacterial Activity against Pathogenic Microbes. *Artif. Cells, Nanomedicine, Biotechnol.* 2017, *45*, 584–590, doi:10.3109/21691401.2016.1163715.
144. Saravanan, M.; Barik, S.K.; MubarakAli, D.; Prakash, P.; Pugazhendhi, A. Synthesis of Silver Nanoparticles from *Bacillus brevis* (NCIM 2533) and Their Antibacterial Activity against Pathogenic Bacteria. *Microb. Pathog.* 2018, *116*, 221–226, doi:10.1016/j.micpath.2018.01.038.
145. Ibrahim, S.; Ahmad, Z.; Manzoor, M.Z.; Mujahid, M.; Faheem, Z.; Adnan, A. Optimization for Biogenic Microbial Synthesis of Silver Nanoparticles through Response Surface Methodology, Characterization, Their Antimicrobial, Antioxidant, and Catalytic Potential. *Sci. Rep.* 2021, *11*, 770, doi:10.1038/s41598-020-80805-0.
146. Mukherjee, K.; Gupta, R.; Kumar, G.; Kumari, S.; Biswas, S.; Padmanabhan, P. Synthesis of Silver Nanoparticles by *Bacillus clausii* and Computational Profiling of Nitrate Reductase Enzyme Involved in Production. *J. Genet. Eng. Biotechnol.* 2018, *16*, 527–536, doi:10.1016/j.jgeb.2018.04.004.
147. Esmail, R.; Afshar, A.; Morteza, M.; Abolfazl, A.; Akhondi, E. Synthesis of Silver Nanoparticles with High Efficiency and Stability by Culture Supernatant of *Bacillus* ROM6 Isolated from Zarshouran Gold Mine and Evaluating Its Antibacterial Effects. *BMC Microbiol.* 2022, *22*, 97, doi:10.1186/s12866-022-02490-5.
148. Baltazar-Encarnación, E.; Escárcega-González, C.E.; Vasto-Anzaldo, X.G.; Cantú-Cárdenas, M.E.; Morones-Ramírez, J.R. Silver Nanoparticles Synthesized through Green Methods Using *Escherichia coli* Top 10 (Ec-Ts) Growth Culture Medium Exhibit Antimicrobial Properties against Nongrowing Bacterial Strains. *J. Nanomater.* 2019, *2019*, 1–8, doi:10.1155/2019/4637325.
149. Abishad, P.; Vergis, J.; Unni, V.; Ram, V.P.; Niveditha, P.; Yasur, J.; Juliet, S.; John, L.; Byrappa, K.; Nambiar, P.; et al. Green Synthesized Silver Nanoparticles Using *Lactobacillus acidophilus* as an Antioxidant, Antimicrobial, and Antibiofilm Agent Against Multi-Drug Resistant Enteroaggregative Escherichia Coli. *Probiotics Antimicrob. Proteins* 2022, *14*, 904–914, doi:10.1007/s12602-022-09961-1.
150. Riaz Rajoka, M.S.; Mehwish, H.M.; Zhang, H.; Ashraf, M.; Fang, H.; Zeng, X.; Wu, Y.; Khurshid, M.; Zhao, L.; He, Z. Antibacterial and Antioxidant Activity of Exopolysaccharide Mediated Silver Nanoparticle Synthesized by *Lactobacillus brevis* Isolated from Chinese Koumiss. *Colloids Surfaces B Biointerfaces* 2020, *186*, 110734, doi:10.1016/j.colsurfb.2019.110734.
151. Huq, M.A.; Akter, S. Bacterial Mediated Rapid and Facile Synthesis of Silver Nanoparticles and Their Antimicrobial Efficacy against Pathogenic Microorganisms. *Materials (Basel).* 2021, *14*, 2615, doi:10.3390/ma14102615.
152. Quinteros, M.A.; Bonilla, J.O.; Alborés, S. V.; Villegas, L.B.; Páez, P.L. Biogenic Nanoparticles: Synthesis, Stability and Biocompatibility Mediated by Proteins of *Pseudomonas aeruginosa*. *Colloids Surfaces B Biointerfaces* 2019, *184*, 110517, doi:10.1016/j.colsurfb.2019.110517.
153. Gopinath, V.; Priyadarshini, S.; Loke, M.F.; Arunkumar, J.; Marsili, E.; MubarakAli, D.; Velusamy, P.; Vadivelu, J. Biogenic Synthesis, Characterization of Antibacterial Silver Nanoparticles and Its Cell Cytotoxicity. *Arab. J. Chem.* 2017, *10*, 1107–1117, doi:10.1016/j.arabjc.2015.11.011.
154. Bachii, S.A.; Sahib, W.H.A.-A.; Salah, A.A.R. Preparation and Characterization of Silver Nanoparticles Biosynthesis by *Pseudomonas stutzeri* Environmental Bacteria Isolated from Oil Fields and Their Antimicrobial Activity. *Sci. J. Med. Res.* 2021, *5*.
155. Desai, M.P.; Patil, R. V.; Pawar, K.D. Selective and Sensitive Colorimetric Detection of Platinum Using *Pseudomonas stutzeri* Mediated Optimally Synthesized Antibacterial Silver Nanoparticles. *Biotechnol. Reports* 2020, *25*, e00404, doi:10.1016/j.btre.2019.e00404.
156. Oves, M.; Khan, M.S.; Zaidi, A.; Ahmed, A.S.; Ahmed, F.; Ahmad, E.; Sherwani, A.; Owais, M.; Azam, A. Antibacterial and Cytotoxic Efficacy of Extracellular Silver Nanoparticles Biofabricated from Chromium Reducing Novel OS4 Strain of *Stenotrophomonas maltophilia*. *PLoS One* 2013,

8, e59140, doi:10.1371/journal.pone.0059140.
157. Attard, G.; Casadesús, M.; Macaskie, L.E.; Deplanche, K. Biosynthesis of Platinum Nanoparticles by *Escherichia coli* MC4100: Can Such Nanoparticles Exhibit Intrinsic Surface Enantioselectivity? *Langmuir* 2012, *28*, 5267–5274, doi:10.1021/la204495z.
158. Eramabadi, P.; Masoudi, M.; Makhdoumi, A.; Mashreghi, M. Microbial Cell Lysate Supernatant (CLS) Alteration Impact on Platinum Nanoparticles Fabrication, Characterization, Antioxidant and Antibacterial Activity. *Mater. Sci. Eng. C* 2020, *117*, 111292, doi:10.1016/j.msec.2020.111292.
159. Gaidhani, S. V.; Yeshvekar, R.K.; Shedbalkar, U.U.; Bellare, J.H.; Chopade, B.A. Bio-Reduction of Hexachloroplatinic Acid to Platinum Nanoparticles Employing *Acinetobacter calcoaceticus*. *Process Biochem.* 2014, *49*, 2313–2319, doi:10.1016/j.procbio.2014.10.002.
160. Chen, Y.; Chen, Y.; Wu, J.; Zhang, J. The Effect of Biotic and Abiotic Environmental Factors on Pd(II) Adsorption and Reduction by *Bacillus wiedmannii* MSM. *Ecotoxicol. Environ. Saf.* 2018, *162*, 546–553, doi:10.1016/j.ecoenv.2018.07.043.
161. Matsena, M.T.; Tichapondwa, S.M.; Chirwa, E.M.N. Synthesis of Biogenic Palladium Nanoparticles Using *Citrobacter* Sp. for Application as Anode Electrocatalyst in a Microbial Fuel Cell. *Catalysts* 2020, *10*, 838, doi:10.3390/catal10080838.
162. Matsena, M.T.; Chirwa, E.M.N. Comparative Analysis of Biological versus Chemical Synthesis of Palladium Nanoparticles for Catalysis of Chromium (VI) Reduction. *Sci. Rep.* 2021, *11*, 16674, doi:10.1038/s41598-021-96024-0.
163. Tan, L.; Ray Jones, T.; Poitras, J.; Xie, J.; Liu, X.; Southam, G. Biochemical Synthesis of Palladium Nanoparticles: The Influence of Chemical Fixatives Used in Electron Microscopy on Nanoparticle Formation and Catalytic Performance. *J. Hazard. Mater.* 2020, *398*, 122945, doi:10.1016/j.jhazmat.2020.122945.
164. Mikheenko, I.P.; Bennett, J.A.; Omajali, J.B.; Walker, M.; Johnson, D.B.; Grail, B.M.; Wong-Pascua, D.; Moseley, J.D.; Macaskie, L.E. Selective Hydrogenation Catalyst Made via Heat-Processing of Biogenic Pd Nanoparticles and Novel 'Green' Catalyst for Heck Coupling Using Waste Sulfidogenic Bacteria. *Appl. Catal. B Environ.* 2022, *306*, 121059, doi:10.1016/j.apcatb.2021.121059.
165. Bachar, O.; Meirovich, M.M.; Kurzion, R.; Yehezkeli, O. In Vivo and in Vitro Protein Mediated Synthesis of Palladium Nanoparticles for Hydrogenation Reactions. *Chem. Commun.* 2020, *56*, 11211–11214, doi:10.1039/D0CC04812G.
166. Gomez-Bolivar, J.; Mikheenko, I.P.; Macaskie, L.E.; Merroun, M.L. Characterization of Palladium Nanoparticles Produced by Healthy and Microwave-Injured Cells of *Desulfovibrio desulfuricans* and *Escherichia coli*. *Nanomaterials* 2019, *9*, 857, doi:10.3390/nano9060857.
167. Wang, W.; Zhang, B.; Liu, Q.; Du, P.; Liu, W.; He, Z. Biosynthesis of Palladium Nanoparticles Using *Shewanella loihica* PV-4 for Excellent Catalytic Reduction of Chromium(Vi). *Environ. Sci. Nano* 2018, *5*, 730–739, doi:10.1039/C7EN01167A.
168. Zhang, Y.; Zhao, Q.; Chen, B. Reduction and Removal of Cr(VI) in Water Using Biosynthesized Palladium Nanoparticles Loaded *Shewanella oneidensis* MR-1. *Sci. Total Environ.* 2022, *805*, 150336, doi:10.1016/j.scitotenv.2021.150336.
169. Zhang, S.; Zhou, H.; Liao, H.; Tan, P.; Tian, W.; Pan, J. Microbial Synthesis of Efficient Palladium Electrocatalyst with High Loadings for Oxygen Reduction Reaction in Acidic Medium. *J. Colloid Interface Sci.* 2022, *611*, 161–171, doi:10.1016/j.jcis.2021.12.080.
170. Fatemi, M.; Mollania, N.; Momeni-Moghaddam, M.; Sadeghifar, F. Extracellular Biosynthesis of Magnetic Iron Oxide Nanoparticles by *Bacillus cereus* Strain HMH1: Characterization and in Vitro Cytotoxicity Analysis on MCF-7 and 3T3 Cell Lines. *J. Biotechnol.* 2018, *270*, 1–11, doi:10.1016/j.jbiotec.2018.01.021.
171. Khan, S.; Akhtar, N.; Rehman, S.U.; Shujah, S.; Rha, E.S.; Jamil, M. Biosynthesized Iron Oxide Nanoparticles (Fe_3O_4 NPs) Mitigate Arsenic Toxicity in Rice Seedlings. *Toxics* 2020, *9*, 2, doi:10.3390/toxics9010002.

172. Majeed, S.; Danish, M.; Mohamad Ibrahim, M.N.; Sekeri, S.H.; Ansari, M.T.; Nanda, A.; Ahmad, G. Bacteria Mediated Synthesis of Iron Oxide Nanoparticles and Their Antibacterial, Antioxidant, Cytocompatibility Properties. *J. Clust. Sci.* 2021, *32*, 1083–1094, doi:10.1007/s10876-020-01876-7.
173. Zaki, S.A.E.-F.; Kamal, A.; Ashmawy, N.A.; Shoeib, A.A. Nano-Metals Forming Bacteria in Egypt. I. Synthesis, Characterization and Effect on Some Phytopathogenic Bacteria in Vitro. *Sci. Rep.* 2021, *11*, 12876, doi:10.1038/s41598-021-92171-6.
174. Hsu, C.-M.; Huang, Y.-H.; Chen, H.-J.; Lee, W.-C.; Chiu, H.-W.; Maity, J.P.; Chen, C.-C.; Kuo, Y.-H.; Chen, C.-Y. Green Synthesis of Nano-Co3O4 by Microbial Induced Precipitation (MIP) Process Using *Bacillus pasteurii* and Its Application as Supercapacitor. *Mater. Today Commun.* 2018, *14*, 302–311, doi:10.1016/j.mtcomm.2018.02.005.
175. Mubraiz, N.; Bano, A.; Mahmood, T.; Khan, N. Microbial and Plant Assisted Synthesis of Cobalt Oxide Nanoparticles and Their Antimicrobial Activities. *Agronomy* 2021, *11*, 1607, doi:10.3390/agronomy11081607.
176. Shim, H.-W.; Jin, Y.-H.; Seo, S.-D.; Lee, S.-H.; Kim, D.-W. Highly Reversible Lithium Storage in *Bacillus subtilis*-Directed Porous Co 3 O 4 Nanostructures. *ACS Nano* 2011, *5*, 443–449, doi:10.1021/nn1021605.
177. Marimuthu, S.; Rahuman, A.A.; Kirthi, A.V.; Santhoshkumar, T.; Jayaseelan, C.; Rajakumar, G. Eco-Friendly Microbial Route to Synthesize Cobalt Nanoparticles Using *Bacillus thuringiensis* against Malaria and Dengue Vectors. *Parasitol. Res.* 2013, *112*, 4105–4112, doi:10.1007/s00436-013-3601-2.
178. Sundararaju, S.; Arumugam, M.; Bhuyar, P. *Microbacterium Sp*. MRS-1, a Potential Bacterium for Cobalt Reduction and Synthesis of Less/Non-Toxic Cobalt Oxide Nanoparticles (Co_3O_4). *Beni-Suef Univ. J. Basic Appl. Sci.* 2020, *9*, 44, doi:10.1186/s43088-020-00070-y.
179. Shim, H.-W.; Lim, A.-H.; Kim, J.-C.; Jang, E.; Seo, S.-D.; Lee, G.-H.; Kim, T.D.; Kim, D.-W. Scalable One-Pot Bacteria-Templating Synthesis Route toward Hierarchical, Porous-Co_3O_4 Superstructures for Supercapacitor Electrodes. *Sci. Rep.* 2013, *3*, 2325, doi:10.1038/srep02325.
180. Eltarahony, M.; Zaki, S.; ElKady, M.; Abd-El-Haleem, D. Biosynthesis, Characterization of Some Combined Nanoparticles, and Its Biocide Potency against a Broad Spectrum of Pathogens. *J. Nanomater.* 2018, *2018*, 1–16, doi:10.1155/2018/5263814.
181. Yu, X.; Jiang, J. Phosphate Microbial Mineralization Removes Nickel Ions from Electroplating Wastewater. *J. Environ. Manage.* 2019, *245*, 447–453, doi:10.1016/j.jenvman.2019.05.091.
182. Sathyavathi, S.; Manjula, A.; Rajendhran, J.; Gunasekaran, P. Extracellular Synthesis and Characterization of Nickel Oxide Nanoparticles from *Microbacterium Sp*. MRS-1 towards Bioremediation of Nickel Electroplating Industrial Effluent. *Bioresour. Technol.* 2014, *165*, 270–273, doi:10.1016/j.biortech.2014.03.031.
183. Al-Kordy, H.M.H.; Sabry, S.A.; Mabrouk, M.E.M. Statistical Optimization of Experimental Parameters for Extracellular Synthesis of Zinc Oxide Nanoparticles by a Novel Haloalaliphilic *Alkalibacillus Sp*.W7. *Sci. Rep.* 2021, *11*, 10924, doi:10.1038/s41598-021-90408-y.
184. Ebadi, M.; Zolfaghari, M.R.; Aghaei, S.S.; Zargar, M.; Shafiei, M.; Zahiri, H.S.; Noghabi, K.A. A Bio-Inspired Strategy for the Synthesis of Zinc Oxide Nanoparticles (ZnO NPs) Using the Cell Extract of C*yanobacterium Nostoc Sp*. EA03: From Biological Function to Toxicity Evaluation. *RSC Adv.* 2019, *9*, 23508–23525, doi:10.1039/C9RA03962G.
185. Mahdi, Z.S.; Talebnia Roshan, F.; Nikzad, M.; Ezoji, H. Biosynthesis of Zinc Oxide Nanoparticles Using Bacteria: A Study on the Characterization and Application for Electrochemical Determination of Bisphenol A. *Inorg. Nano-Metal Chem.* 2020, *51*, 1–9, doi:10.1080/24701556.2020.1835962.
186. Taran, M.; Rad, M.; Alavi, M. Biosynthesis of TiO_2 and ZnO Nanoparticles by *Halomonas elongata* IBRC-M 10214 in Different Conditions of Medium. *BioImpacts* 2017, *8*, 81–89, doi:10.15171/bi.2018.10.

187. Xiao, X.; Ma, X.-B.; Yuan, H.; Liu, P.-C.; Lei, Y.-B.; Xu, H.; Du, D.-L.; Sun, J.-F.; Feng, Y.-J. Photocatalytic Properties of Zinc Sulfide Nanocrystals Biofabricated by Metal-Reducing Bacterium *Shewanella oneidensis* MR-1. *J. Hazard. Mater.* 2015, *288*, 134–139, doi:10.1016/j.jhazmat.2015.02.009.
188. Noman, M.; Shahid, M.; Ahmed, T.; Niazi, M.B.K.; Hussain, S.; Song, F.; Manzoor, I. Use of Biogenic Copper Nanoparticles Synthesized from a Native *Escherichia Sp*. as Photocatalysts for Azo Dye Degradation and Treatment of Textile Effluents. *Environ. Pollut.* 2020, *257*, 113514, doi:10.1016/j.envpol.2019.113514.
189. El-Saadony, M.T.; Abd El-Hack, M.E.; Taha, A.E.; Fouda, M.M.G.; Ajarem, J.S.; N. Maodaa, S.; Allam, A.A.; Elshaer, N. Ecofriendly Synthesis and Insecticidal Application of Copper Nanoparticles against the Storage Pest *Tribolium castaneum*. *Nanomaterials* 2020, *10*, 587, doi:10.3390/nano10030587.
190. Xia, X.; Wu, S.; Li, N.; Wang, D.; Zheng, S.; Wang, G. Novel Bacterial Selenite Reductase CsrF Responsible for Se(IV) and Cr(VI) Reduction That Produces Nanoparticles in *Alishewanella Sp.* WH16-1. *J. Hazard. Mater.* 2018, *342*, 499–509, doi:10.1016/j.jhazmat.2017.08.051.
191. Dong, G.; Wang, Y.; Gong, L.; Wang, M.; Wang, H.; He, N.; Zheng, Y.; Li, Q. Formation of Soluble Cr(III) End-Products and Nanoparticles during Cr(VI) Reduction by *Bacillus cereus* Strain XMCr-6. *Biochem. Eng. J.* 2013, *70*, 166–172, doi:10.1016/j.bej.2012.11.002.
192. Kanakalakshmi, A.; Janaki, V.; Shanthi, K.; Kamala-Kannan, S. Biosynthesis of Cr(III) Nanoparticles from Electroplating Wastewater Using Chromium-Resistant *Bacillus subtilis* and Its Cytotoxicity and Antibacterial Activity. *Artif. Cells, Nanomedicine, Biotechnol.* 2017, *45*, 1304–1309, doi:10.1080/21691401.2016.1228660.
193. Sharma, A.; Chaturvedi, R.; Islam, A.; Singh, P.K. Eco-Friendly Synthesis F Cadmium Sulfide Nanoparticles Using Supernatant of *Bacillus badius* and Its Characterization. *Mater. Today Proc.* 2021, *45*, 3419–3421, doi:10.1016/j.matpr.2020.12.926.
194. Carrasco, V.; Amarelle, V.; Lagos-Moraga, S.; Quezada, C.P.; Espinoza-González, R.; Faccio, R.; Fabiano, E.; Pérez-Donoso, J.M. Production of Cadmium Sulfide Quantum Dots by the Lithobiontic Antarctic Strain *Pedobacter Sp*. UYP1 and Their Application as Photosensitizer in Solar Cells. *Microb. Cell Fact.* 2021, *20*, 41, doi:10.1186/s12934-021-01531-4.
195. Xu, S.; Luo, X.; Huang, Q.; Chen, W. Calcium-Crosslinked Alginate-Encapsulated Bacteria for Remediating of Cadmium-Polluted Water and Production of CdS Nanoparticles. *Appl. Microbiol. Biotechnol.* 2021, *105*, 2171–2179, doi:10.1007/s00253-021-11155-8.
196. Jain, A.S.; Pawar, P.S.; Sarkar, A.; Junnuthula, V.; Dyawanapelly, S. Bionanofactories for Green Synthesis of Silver Nanoparticles: Toward Antimicrobial Applications. *Int. J. Mol. Sci.* 2021, *22*, 11993, doi:10.3390/ijms222111993.
197. Beveridge, T.J.; Murray, R.G.E. Sites of Metal Deposition in the Cell Wall of *Bacillus subtilis*. *J. Bacteriol.* 1980, *141*, 876–887, doi:10.1128/jb.141.2.876-887.1980.
198. Klaus, T.; Joerger, R.; Olsson, E.; Granqvist, C.-G. Silver-Based Crystalline Nanoparticles, Microbially Fabricated. *Proc. Natl. Acad. Sci.* 1999, *96*, 13611–13614, doi:10.1073/pnas.96.24.13611.
199. Navarro, C.; Wu, L.-F.; Mandrand-Berthelot, M.-A. The Nik Operon of *Escherichia coli* Encodes a Periplasmic Binding-Protein-Dependent Transport System for Nickel. *Mol. Microbiol.* 1993, *9*, 1181–1191, doi:10.1111/j.1365-2958.1993.tb01247.x.
200. Dulay, H.; Tabares, M.; Kashefi, K.; Reguera, G. Cobalt Resistance via Detoxification and Mineralization in the Iron-Reducing Bacterium *Geobacter sulfurreducens*. *Front. Microbiol.* 2020, *11*, 2992, doi:10.3389/fmicb.2020.600463.
201. Dash, S.R.; Bag, S.S.; Golder, A.K. Bio-Inspired PtNPs/Graphene Nanocomposite Based Electrocatalytic Sensing of Metabolites of Dipyrone. *Anal. Chim. Acta* 2021, *1167*, 338562, doi:10.1016/j.aca.2021.338562.
202. Baskaran, B.; Muthukumarasamy, A.; Chidambaram, S.; Sugumaran, A.; Ramachandran, K.; Rasu Manimuthu, T. Cytotoxic Potentials of Biologically Fabricated Platinum Nanoparticles

from *Streptomyces Sp*. on MCF-7 Breast Cancer Cells. *IET Nanobiotechnology* 2017, *11*, 241–246, doi:10.1049/iet-nbt.2016.0040.
203. Hosny, M.; Fawzy, M.; El-Fakharany, E.M.; Omer, A.M.; El-Monaem, E.M.A.; Khalifa, R.E.; Eltaweil, A.S. Biogenic Synthesis, Characterization, Antimicrobial, Antioxidant, Antidiabetic, and Catalytic Applications of Platinum Nanoparticles Synthesized from *Polygonum salicifolium* Leaves. *J. Environ. Chem. Eng.* 2022, *10*, 106806, doi:10.1016/j.jece.2021.106806.
204. Wang, Y.; Sevinc, P.C.; Belchik, S.M.; Fredrickson, J.; Shi, L.; Lu, H.P. Single-Cell Imaging and Spectroscopic Analyses of Cr(VI) Reduction on the Surface of Bacterial Cells. *Langmuir* 2013, *29*, 950–956, doi:10.1021/la303779y.
205. Burgos, W.D.; McDonough, J.T.; Senko, J.M.; Zhang, G.; Dohnalkova, A.C.; Kelly, S.D.; Gorby, Y.; Kemner, K.M. Characterization of Uraninite Nanoparticles Produced by *Shewanella oneidensis* MR-1. *Geochim. Cosmochim. Acta* 2008, *72*, 4901–4915, doi:10.1016/j.gca.2008.07.016.
206. Ramos-Ruiz, A.; Sesma-Martin, J.; Sierra-Alvarez, R.; Field, J.A. Continuous Reduction of Tellurite to Recoverable Tellurium Nanoparticles Using an Upflow Anaerobic Sludge Bed (UASB) Reactor. *Water Res.* 2017, *108*, 189–196, doi:10.1016/j.watres.2016.10.074.
207. Omajali, J.B.; Gomez-Bolivar, J.; Mikheenko, I.P.; Sharma, S.; Kayode, B.; Al-Duri, B.; Banerjee, D.; Walker, M.; Merroun, M.L.; Macaskie, L.E. Novel Catalytically Active Pd/Ru Bimetallic Nanoparticles Synthesized by *Bacillus benzeovorans*. *Sci. Rep.* 2019, *9*, 4715, doi:10.1038/s41598-019-40312-3.
208. Hosseinkhani, B.; Søbjerg, L.S.; Rotaru, A.-E.; Emtiazi, G.; Skrydstrup, T.; Meyer, R.L. Microbially Supported Synthesis of Catalytically Active Bimetallic Pd-Au Nanoparticles. *Biotechnol. Bioeng.* 2012, *109*, 45–52, doi:10.1002/bit.23293.
209. Weng, Y.; Li, J.; Ding, X.; Wang, B.; Dai, S.; Zhou, Y.; Pang, R.; Zhao, Y.; Xu, H.; Tian, B.; et al. Functionalized Gold and Silver Bimetallic Nanoparticles Using *Deinococcus radiodurans* Protein Extract Mediate Degradation of Toxic Dye Malachite Green. *Int. J. Nanomedicine* 2020, *Volume 15*, 1823–1835, doi:10.2147/IJN.S236683.
210. Li, J.; Tian, B.; Li, T.; Dai, S.; Weng, Y.; Lu, J.; Xu, X.; Jin, Y.; Pang, R.; Hua, Y. Biosynthesis of Au, Ag and Au–Ag Bimetallic Nanoparticles Using Protein Extracts of *Deinococcus radiodurans* and Evaluation of Their Cytotoxicity. *Int. J. Nanomedicine* 2018, *Volume 13*, 1411–1424, doi:10.2147/IJN.S149079.
211. Deplanche, K.; Merroun, M.L.; Casadesus, M.; Tran, D.T.; Mikheenko, I.P.; Bennett, J.A.; Zhu, J.; Jones, I.P.; Attard, G.A.; Wood, J.; et al. Microbial Synthesis of Core/Shell Gold/Palladium Nanoparticles for Applications in Green Chemistry. *J. R. Soc. Interface* 2012, *9*, 1705–1712, doi:10.1098/rsif.2012.0003.
212. Gomez-Bolivar, J.; Mikheenko, I.P.; Orozco, R.L.; Sharma, S.; Banerjee, D.; Walker, M.; Hand, R.A.; Merroun, M.L.; Macaskie, L.E. Synthesis of Pd/Ru Bimetallic Nanoparticles by *Escherichia coli* and Potential as a Catalyst for Upgrading 5-Hydroxymethyl Furfural Into Liquid Fuel Precursors. *Front. Microbiol.* 2019, *10*, 1–17, doi:10.3389/fmicb.2019.01276.
213. Nair, B.; Pradeep, T. Coalescence of Nanoclusters and Formation of Submicron Crystallites Assisted by *Lactobacillu*s Strains. *Cryst. Growth Des.* 2002, *2*, 293–298, doi:10.1021/cg0255164.
214. de França Bettencourt, G.M.; Degenhardt, J.; Zevallos Torres, L.A.; de Andrade Tanobe, V.O.; Soccol, C.R. Green Biosynthesis of Single and Bimetallic Nanoparticles of Iron and Manganese Using Bacterial Auxin Complex to Act as Plant Bio-Fertilizer. *Biocatal. Agric. Biotechnol.* 2020, *30*, 101822, doi:10.1016/j.bcab.2020.101822.
215. Tuo, Y.; Liu, G.; Dong, B.; Zhou, J.; Wang, A.; Wang, J.; Jin, R.; Lv, H.; Dou, Z.; Huang, W. Microbial Synthesis of Pd/Fe_3O_4, Au/Fe_3O_4 and PdAu/Fe_3O_4 Nanocomposites for Catalytic Reduction of Nitroaromatic Compounds. *Sci. Rep.* 2015, *5*, 13515, doi:10.1038/srep13515.
216. Xu, H.; Xiao, Y.; Xu, M.; Cui, H.; Tan, L.; Feng, N.; Liu, X.; Qiu, G.; Dong, H.; Xie, J. Microbial Synthesis of Pd–Pt Alloy Nanoparticles Using *Shewanella oneidensis* MR-1 with Enhanced Catalytic Activity for Nitrophenol and Azo Dyes Reduction. *Nanotechnology* 2019, *30*, 065607,

doi:10.1088/1361-6528/aaf2a6.
217. De Corte, S.; Hennebel, T.; Fitts, J.P.; Sabbe, T.; Bliznuk, V.; Verschuere, S.; van der Lelie, D.; Verstraete, W.; Boon, N. Biosupported Bimetallic Pd–Au Nanocatalysts for Dechlorination of Environmental Contaminants. *Environ. Sci. Technol.* 2011, *45*, 8506–8513, doi:10.1021/es2019324.
218. Kimber, R.L.; Parmeggiani, F.; Neill, T.S.; Merroun, M.L.; Goodlet, G.; Powell, N.A.; Turner, N.J.; Lloyd, J.R. Biotechnological Synthesis of Pd/Ag and Pd/Au Nanoparticles for Enhanced Suzuki–Miyaura Cross-coupling Activity. *Microb. Biotechnol.* 2021, *14*, 2435–2447, doi:10.1111/1751-7915.13762.
219. Tuo, Y.; Liu, G.; Dong, B.; Yu, H.; Zhou, J.; Wang, J.; Jin, R. Microbial Synthesis of Bimetallic PdPt Nanoparticles for Catalytic Reduction of 4-Nitrophenol. *Environ. Sci. Pollut. Res.* 2017, *24*, 5249–5258, doi:10.1007/s11356-016-8276-7.
220. Govindaraju, K.; Basha, S.K.; Kumar, V.G.; Singaravelu, G. Silver, Gold and Bimetallic Nanoparticles Production Using Single-Cell Protein (*Spirulina platensis*) Geitler. *J. Mater. Sci.* 2008, *43*, 5115–5122, doi:10.1007/s10853-008-2745-4.
221. Sasireka, K.S.; Lalitha, P. Biogenic Synthesis of Bimetallic Nanoparticles and Their Applications. *Rev. Inorg. Chem.* 2021, *41*, 223–244, doi:10.1515/revic-2020-0024.
222. Chernyshev, V.M.; Ananikov, V.P. Nickel and Palladium Catalysis: Stronger Demand than Ever. *ACS Catal.* 2022, *12*, 1180–1200, doi:10.1021/acscatal.1c04705.
223. Nornickel Palladium (Pd) - Nornickel Annual Report 2021. 2021, 4.
224. Saldan, I.; Semenyuk, Y.; Marchuk, I.; Reshetnyak, O. Chemical Synthesis and Application of Palladium Nanoparticles. *J. Mater. Sci.* 2015, *50*, 2337–2354, doi:10.1007/s10853-014-8802-2.
225. Litrán, R.; Sampedro, B.; Rojas, T.C.; Multigner, M.; Sánchez-López, J.C.; Crespo, P.; López-Cartes, C.; García, M.A.; Hernando, A.; Fernández, A. Magnetic and Microstructural Analysis of Palladium Nanoparticles with Different Capping Systems. *Phys. Rev. B* 2006, *73*, 054404, doi:10.1103/PhysRevB.73.054404.
226. Hong, S.C.; Lee, J. Il Magnetism and the Stoner Exchange Parameter of Fcc Palladium. *J. Korean Phys. Soc.* 2008, *52*, 1099–1102, doi:10.3938/JKPS.52.1099.
227. Abdullah, N.; Bahruji, H.; Rogers, S.M.; Wells, P.P.; Catlow, C.R.A.; Bowker, M. Pd Local Structure and Size Correlations to the Activity of Pd/TiO_2 for Photocatalytic Reforming of Methanol. *Phys. Chem. Chem. Phys.* 2019, *21*, 16154–16160, doi:10.1039/C9CP00826H.
228. Taniyama, T.; Ohta, E.; Sato, T. Observation of 4d Ferromagnetism in Free-Standing Pd Fine Particles. *Europhys. Lett.* 1997, *38*, 195–200, doi:10.1209/epl/i1997-00225-3.
229. Creamer, N.J.; Mikheenko, I.P.; Johnson, C.; Cottrell, S.P.; Macaskie, L.E. Local Magnetism in Palladium Bionanomaterials Probed by Muon Spectroscopy. *Biotechnol. Lett.* 2011, *33*, 969–976, doi:10.1007/s10529-011-0532-9.
230. Zhao, X.; Chang, Y.; Chen, W.-J.; Wu, Q.; Pan, X.; Chen, K.; Weng, B. Recent Progress in Pd-Based Nanocatalysts for Selective Hydrogenation. *ACS Omega* 2022, *7*, 17–31, doi:10.1021/acsomega.1c06244.
231. Green Synthesis, A.; Vrestal, J.; Kustov, L.M.; Salman, S.H.; Khashan, K.S.; Hadi, A.A. Green Synthesis and Characterization of Palladium Nanoparticles by Pulsed Laser Ablation and Their Antibacterial Activity. *Met. 2023, Vol. 13, Page 273* 2023, *13*, 273, doi:10.3390/MET13020273.
232. Fu, G.; Jiang, X.; Ding, L.; Tao, L.; Chen, Y.; Tang, Y.; Zhou, Y.; Wei, S.; Lin, J.; Lu, T. Green Synthesis and Catalytic Properties of Polyallylamine Functionalized Tetrahedral Palladium Nanocrystals. *Appl. Catal. B Environ.* 2013, *138–139*, 167–174, doi:10.1016/j.apcatb.2013.02.052.
233. MubarakAli, D.; Kim, H.; Venkatesh, P.S.; Kim, J.-W.; Lee, S.-Y. A Systemic Review on the Synthesis, Characterization, and Applications of Palladium Nanoparticles in Biomedicine. *Appl. Biochem. Biotechnol.* 2023, *195*, 3699–3718, doi:10.1007/s12010-022-03840-9.
234. Rivera-González, H.; Torres-Pacheco, L.; Álvarez-Contreras, L.; Olivas, A.; Guerra-Balcázar, M.; Valdez, R.; Arjona, N. Synthesis of Pd Fe_3O_4 Nanoparticles Varying the Stabilizing Agent and

Additive and Their Effect on the Ethanol Electro-Oxidation in Alkaline Media. *J. Electroanal. Chem.* 2019, *835*, 301–312, doi:10.1016/j.jelechem.2019.01.044.
235. Kaya, D.; Isik, H.H.; Isik, I.B.; Sigircik, G.; Tuken, T.; Karadag, F.; Ekicibil, A. Electrocatalytic Hydrogen Evolution on Metallic and Bimetallic Pd–Co Alloy Nanoparticles. *Int. J. Hydrogen Energy* 2023, *48*, 14633–14641, doi:10.1016/j.ijhydene.2023.01.049.
236. Khan, M.; Ashraf, M.; Shaik, M.R.; Adil, S.F.; Islam, M.S.; Kuniyil, M.; Khan, M.; Hatshan, M.R.; Alshammari, R.H.; Siddiqui, M.R.H.; et al. Pyrene Functionalized Highly Reduced Graphene Oxide-Palladium Nanocomposite: A Novel Catalyst for the Mizoroki-Heck Reaction in Water. *Front. Chem.* 2022, *10*, 872366, doi:10.3389/fchem.2022.872366.
237. Joudeh, N.; Saragliadis, A.; Koster, G.; Mikheenko, P.; Linke, D. Synthesis Methods and Applications of Palladium Nanoparticles: A Review. *Front. Nanotechnol.* 2022, *4*, doi:10.3389/fnano.2022.1062608.
238. Zeng, C.; Liu, P.; Xiao, Z.; Li, Y.; Song, L.; Cao, Z.; Wu, D.; Zhang, Y.-F. Highly Selective Adsorption and Recovery of Palladium from Spent Catalyst Wastewater by 1,4,7,10-Tetraazacyclododecane-Modified Mesoporous Silica. *ACS Sustain. Chem. Eng.* 2022, *10*, 1103–1114, doi:10.1021/acssuschemeng.1c05915.
239. Assunção, A.; Matos, A.; Da Costa, A.M.R.; Candeias, A.; Costa, M.C. A Bridge between Liquid–Liquid Extraction and the Use of Bacterial Communities for Palladium and Platinum Recovery as Nanosized Metal Sulphides. *Hydrometallurgy* 2016, *163*, 40–48, doi:10.1016/J.HYDROMET.2016.03.012.
240. Wang, J.; Zhu, X.; Fan, J.; Xue, K.; Ma, S.; Zhao, R.; Wu, H.; Gao, Q. Improved Palladium Extraction from Spent Catalyst Using Ultrasound-Assisted Leaching and Sulfuric Acid–Sodium Chloride System. *Sep. 2023, Vol. 10, Page 355* 2023, *10*, 355, doi:10.3390/SEPARATIONS10060355.
241. Peng, Z.; Li, Z.; Lin, X.; Tang, H.; Ye, L.; Ma, Y.; Rao, M.; Zhang, Y.; Li, G.; Jiang, T. Pyrometallurgical Recovery of Platinum Group Metals from Spent Catalysts. *JOM* 2017, *69*, 1553–1562, doi:10.1007/s11837-017-2450-3.
242. Nasrollahzadeh, M.; Sajjadi, M.; Dadashi, J.; Ghafuri, H. Pd-Based Nanoparticles: Plant-Assisted Biosynthesis, Characterization, Mechanism, Stability, Catalytic and Antimicrobial Activities. *Adv. Colloid Interface Sci.* 2020, *276*, 102103, doi:10.1016/j.cis.2020.102103.
243. Meva, F.E.A.; Ntoumba, A.A.; Kedi, P.B.E.; Tchoumbi, E.; Schmitz, A.; Schmolke, L.; Klopotowski, M.; Moll, B.; Kökcam-Demir, Ü.; Mpondo Mpondo, E.A.; et al. Silver and Palladium Nanoparticles Produced Using a Plant Extract as Reducing Agent, Stabilized with an Ionic Liquid: Sizing by X-Ray Powder Diffraction and Dynamic Light Scattering. *J. Mater. Res. Technol.* 2019, *8*, 1991–2000, doi:10.1016/J.JMRT.2018.12.017.
244. Sonbol, H.; Ameen, F.; AlYahya, S.; Almansob, A.; Alwakeel, S. Padina Boryana Mediated Green Synthesis of Crystalline Palladium Nanoparticles as Potential Nanodrug against Multidrug Resistant Bacteria and Cancer Cells. *Sci. Reports 2021 111* 2021, *11*, 1–19, doi:10.1038/s41598-021-84794-6.
245. Arya, A.; Gupta, K.; Chundawat, T.S. In Vitro Antimicrobial and Antioxidant Activity of Biogenically Synthesized Palladium and Platinum Nanoparticles Using *Botryococcus braunii*. *Turkish J. Pharm. Sci.* 2020, *17*, 299, doi:10.4274/TJPS.GALENOS.2019.94103.
246. Mohana, S.; Sumathi, S. Multi-Functional Biological Effects of Palladium Nanoparticles Synthesized Using *Agaricus bisporus*. *J. Clust. Sci.* 2020, *31*, 391–400, doi:10.1007/S10876-019-01652-2/FIGURES/11.
247. Mikheenko, I.P.; Rousset, M.; Dementin, S.; Macaskie, L.E. Bioaccumulation of Palladium by *Desulfovibrio fructosivorans* Wild-Type and Hydrogenase-Deficient Strains. *Appl. Environ. Microbiol.* 2008, *74*, 6144–6146, doi:10.1128/AEM.02538-07.
248. Mishra, K.; Basavegowda, N.; Lee, Y.R. Biosynthesis of Fe, Pd, and Fe-Pd Bimetallic Nanoparticles and Their Application as Recyclable Catalysts for [3 + 2] Cycloaddition Reaction: A Comparative Approach. *Catal. Sci. Technol.* 2015, *5*, 2612–2621, doi:10.1039/c5cy00099h.

249. Nasrollahzadeh, M.; Sajadi, S.M.; Rostami-Vartooni, A.; Khalaj, M. Green Synthesis of Pd/Fe_3O_4 Nanoparticles Using *Euphorbia condylocarpa* M. Bieb Root Extract and Their Catalytic Applications as Magnetically Recoverable and Stable Recyclable Catalysts for the Phosphine-Free Sonogashira and Suzuki Coupling Reactions. *J. Mol. Catal. A Chem.* 2015, *396*, 31–39.
250. Luo, F.; Yang, D.; Chen, Z.; Megharaj, M.; Naidu, R. Characterization of Bimetallic Fe/Pd Nanoparticles by Grape Leaf Aqueous Extract and Identification of Active Biomolecules Involved in the Synthesis. *Sci. Total Environ.* 2016, *562*, 526–532.
251. Era, Y.; Dennis, J.A.; Wallace, S.; Horsfall, L.E. Micellar Catalysis of the Suzuki Miyaura Reaction Using Biogenic Pd Nanoparticles from *Desulfovibrio alaskensis*. *Green Chem.* 2021, *23*, 8886–8890, doi:10.1039/D1GC02392F.
252. Chen, Y.; Chen, Z.; Yang, D.; Zhu, L.; Liang, Z.; Pang, Y.; Zhou, L. Novel Microbial Palladium Nanoparticles with a High Photothermal Effect for Antibacterial Applications. *ACS Omega* 2022, *20*, 39, doi:10.1021/acsomega.2c07037.
253. Pontrelli, S.; Chiu, T.Y.; Lan, E.I.; Chen, F.Y.H.; Chang, P.; Liao, J.C. *Escherichia coli* as a Host for Metabolic Engineering. *Metab. Eng.* 2018, *50*, 16–46, doi:10.1016/J.YMBEN.2018.04.008.
254. JoVE Science Education database *Microbiology. Growth Curves: Generating Growth Curves Using Colony Forming Units and Optical Density Measurements*; Cambridge, MA, 2024;
255. Dasages, G.C. Absorptiometriques Des Elements Mineraux 1978.
256. Brackenbury, K.F.G.; Jones, L.; Nel, I.; Koch, K.R.; Wyrley-Birch, J.M. Tin(II) Chloride in the Analytical Chemistry of the Platinum Metals: From the "Purple of Cassius" to Polyurethane Foams. *Polyhedron* 1987, *6*, 71–78, doi:10.1016/S0277-5387(00)81240-1.
257. Bonthula, S.; Bonthula, S.R.; Pothu, R.; Srivastava, R.K.; Boddula, R.; Radwan, A.B.; Al-Qahtani, N. Recent Advances in Copper-Based Materials for Sustainable Environmental Applications. *Sustain. Chem.* 2023, *4*, 246–271, doi:10.3390/suschem4030019.
258. Kisielowski, C.; Freitag, B.; Bischoff, M.; van Lin, H.; Lazar, S.; Knippels, G.; Tiemeijer, P.; van der Stam, M.; von Harrach, S.; Stekelenburg, M.; et al. Detection of Single Atoms and Buried Defects in Three Dimensions by Aberration-Corrected Electron Microscope with 0.5-Å Information Limit. *Microsc. Microanal.* 2008, *14*, 469–477, doi:10.1017/S1431927608080902.
259. Radamson, H.H. Electron Microscopy. In *Analytical Methods and Instruments for Micro- and Nanomaterials*; Springer, Cham, 2023; pp. 115–146 ISBN 978-3-031-26434-4.
260. Mast, J.; Verleysen, E.; Hodoroaba, V.-D.; Kaegi, R. Characterization of Nanomaterials by Transmission Electron Microscopy: Measurement Procedures. In *Characterization of Nanoparticles*; Elsevier, 2020; pp. 29–48 ISBN 9780128141830.
261. Fultz, B.; Howe, J. The TEM and Its Optics. In *Physics*; Springer, Berlin, Heidelberg, 2013; pp. 59–115 ISBN 978-3-642-29761-8.
262. Ayache, J.; Beaunier, L.; Boumendil, J.; Ehret, G.; Laub, D. The Different Observation Modes in Electron Microscopy (SEM, TEM, STEM). In *Sample Preparation Handbook for Transmission Electron Microscopy*; Springer New York: New York, NY, 2010; pp. 33–55 ISBN 978-0-387-98182-6.
263. Kaliva, M.; Vamvakaki, M. Nanomaterials Characterization. In *Polymer Science and Nanotechnology*; Elsevier, 2020; pp. 401–433 ISBN 9780128168066.
264. Heinrich, H. High-Resolution Transmission Electron Microscopy for Nanocharacterization. In; Springer, New York, NY, 2008; pp. 414–503 ISBN 978-0-387-48805-9.
265. Mohd Yusof, H.; Abdul Rahman, N.; Mohamad, R.; Zaidan, U.H.; Samsudin, A.A. Biosynthesis of Zinc Oxide Nanoparticles by Cell-Biomass and Supernatant of *Lactobacillus plantarum* TA4 and Its Antibacterial and Biocompatibility Properties. *Sci. Rep.* 2020, *10*, 19996, doi:10.1038/s41598-020-76402-w.
266. Hassan Afandy, H.; Sabir, D.K.; Aziz, S.B. Antibacterial Activity of the Green Synthesized Plasmonic Silver Nanoparticles with Crystalline Structure against Gram-Positive and Gram-Negative Bacteria. *Nanomaterials* 2023, *13*, 1327, doi:10.3390/nano13081327.
267. Franken, L.E.; Grünewald, K.; Boekema, E.J.; Stuart, M.C.A. A Technical Introduction to

Transmission Electron Microscopy for Soft-Matter: Imaging, Possibilities, Choices, and Technical Developments. *Small* 2020, *16*, 1906198, doi:10.1002/smll.201906198.
268. Meyer, E.; Bennewitz, R.; Hug, H.J. Introduction to Scanning Probe Microscopy. In; Springer, Cham, 2021; pp. 1–12 ISBN 978-3-030-37089-3.
269. Winkler, R.; Ciria, M.; Ahmad, M.; Plank, H.; Marcuello, C. A Review of the Current State of Magnetic Force Microscopy to Unravel the Magnetic Properties of Nanomaterials Applied in Biological Systems and Future Directions for Quantum Technologies. *Nanomater. 2023, Vol. 13, Page 2585* 2023, *13*, 2585, doi:10.3390/NANO13182585.
270. Yaseen, M.; Cowsill, B.J.; Lu, J.R. Characterisation of Biomedical Coatings. In *Coatings for Biomedical Applications*; Elsevier, 2012; pp. 176–220.
271. García, R.; Paulo, A.S. Attractive and Repulsive Tip-Sample Interaction Regimes in Tapping-Mode Atomic Force Microscopy. *Phys. Rev. B - Condens. Matter Mater. Phys.* 1999, *60*, 4961–4967, doi:10.1103/PhysRevB.60.4961.
272. Dufrêne, Y.F.; Ando, T.; Garcia, R.; Alsteens, D.; Martinez-Martin, D.; Engel, A.; Gerber, C.; Müller, D.J. Imaging Modes of Atomic Force Microscopy for Application in Molecular and Cell Biology. *Nat. Nanotechnol. 2017 124* 2017, *12*, 295–307, doi:10.1038/nnano.2017.45.
273. Munz, M.; Cuenya, B.R.; Kley, C.S. In Situ Investigation of Catalytic Interfaces by Scanning Probe Microscopy under Electrochemical Conditions. In *Encyclopedia of Solid-Liquid Interfaces*; Elsevier, 2024; pp. 656–680.
274. El Kirat, K.; Burton, I.; Dupres, V.; Dufrene, Y.F. Sample Preparation Procedures for Biological Atomic Force Microscopy. *J. Microsc.* 2005, *218*, 199–207, doi:10.1111/j.1365-2818.2005.01480.x.
275. Modigunta, J.K.R.; Vadivel, S.; Murali, G.; In, I.; Sawangphruk, M. Atomic Force Microscopy: An Advanced Imaging Technique—From Molecules to Morphologies. In *Microscopic Techniques for the Non-Expert*; Springer International Publishing: Cham, 2022; pp. 115–136 ISBN 9783030995423.
276. Sans-Serramitjana, E.; Gallardo-Benavente, C.; Melo, F.; Pérez-Donoso, J.M.; Rumpel, C.; Barra, P.J.; Durán, P.; Mora, M. de L.L. A Comparative Study of the Synthesis and Characterization of Biogenic Selenium Nanoparticles by Two Contrasting Endophytic Selenobacteria. *Microorganisms* 2023, *11*, 1600, doi:10.3390/microorganisms11061600.
277. Jayaseelan, C.; Rahuman, A.A.; Kirthi, A.V.; Marimuthu, S.; Santhoshkumar, T.; Bagavan, A.; Gaurav, K.; Karthik, L.; Rao, K.V.B. Novel Microbial Route to Synthesize ZnO Nanoparticles Using *Aeromonas hydrophila* and Their Activity against Pathogenic Bacteria and Fungi. *Spectrochim. Acta Part A Mol. Biomol. Spectrosc.* 2012, *90*, 78–84, doi:10.1016/j.saa.2012.01.006.
278. Sayyid, N.H.; Zghair, Z.R. Biosynthesis of Silver Nanoparticles Produced by *Klebsiella pneumoniae*. *Mater. Today Proc.* 2021, *42*, 2045–2049, doi:10.1016/j.matpr.2020.12.257.
279. Saravanan, M.; Vemu, A.K.; Barik, S.K. Rapid Biosynthesis of Silver Nanoparticles from *Bacillus megaterium* (NCIM 2326) and Their Antibacterial Activity on Multi Drug Resistant Clinical Pathogens. *Colloids Surfaces B Biointerfaces* 2011, *88*, 325–331, doi:10.1016/j.colsurfb.2011.07.009.
280. Carvalho, P.M.; Felício, M.R.; Santos, N.C.; Gonçalves, S.; Domingues, M.M. Application of Light Scattering Techniques to Nanoparticle Characterization and Development. *Front. Chem.* 2018, *6*, 386753, doi:10.3389/fchem.2018.00237.
281. Nasrollahzadeh, M.; Atarod, M.; Sajjadi, M.; Sajadi, S.M.; Issaabadi, Z. Plant-Mediated Green Synthesis of Nanostructures: Mechanisms, Characterization, and Applications. *Interface Sci. Technol.* 2019, *28*, 199–322, doi:10.1016/B978-0-12-813586-0.00006-7.
282. Amendola, V.; Meneghetti, M. Size Evaluation of Gold Nanoparticles by UV–vis Spectroscopy. *J. Phys. Chem. C* 2009, *113*, 4277–4285, doi:10.1021/jp8082425.
283. Haiss, W.; Thanh, N.T.K.; Aveyard, J.; Fernig, D.G. Determination of Size and Concentration of Gold Nanoparticles from UV-Vis Spectra. *Anal. Chem.* 2007, *79*, 4215–4221,

doi:10.1021/AC0702084/SUPPL_FILE/AC0702084SI20070321_014144.PDF.
284. Holder, C.F.; Schaak, R.E. Tutorial on Powder X-Ray Diffraction for Characterizing Nanoscale Materials. *ACS Nano* 2019, *13*, 7359–7365, doi:10.1021/acsnano.9b05157.
285. Zhao, P.; Tang, D.; Xie, J.; Zhang, C. Magnetism and Magnetic Materials. In *Magnetic Levitation*; Springer Nature Singapore: Singapore, 2024; pp. 1–15 ISBN 978-981-99-8314-8.
286. Langørgen, A. Magnetic Force Microscopy and Micromagnetic Simulations of Nanoscale Magnetic Structures and Modified Artificial Spin Ices, NTNU, 2020.
287. Zhao, P.; Tang, D.; Xie, J.; Zhang, C. Magnetism and Magnetic Materials. *Magn. Levitation* 2024, 1–15, doi:10.1007/978-981-99-8314-8_1.
288. Devi, E.C.; Singh, S.D. Tracing the Magnetization Curves: A Review on Their Importance, Strategy, and Outcomes. *J. Supercond. Nov. Magn.* 2021, *34*, 15–25, doi:10.1007/s10948-020-05733-6.
289. Dodrill, B.; Lindemuth, J.R. Vibrating Sample Magnetometry. In *Magnetic Measurement Techniques for Materials Characterization*; Springer International Publishing: Cham, 2021; pp. 15–37 ISBN 9783030704438.
290. Sandler, S.E.; Fellows, B.; Mefford, O.T. Best Practices for Characterization of Magnetic Nanoparticles for Biomedical Applications. *Anal. Chem.* 2019, *91*, 14159–14169, doi:10.1021/acs.analchem.9b03518.
291. Hurley, K.R.; Ring, H.L.; Kang, H.; Klein, N.D.; Haynes, C.L. Characterization of Magnetic Nanoparticles in Biological Matrices. *Anal. Chem.* 2015, *87*, 11611–11619, doi:10.1021/acs.analchem.5b02229.
292. Dumas, R.K.; Hogan, T. Recent Advances in SQUID Magnetometry. In *Magnetic Measurement Techniques for Materials Characterization*; Springer International Publishing: Cham, 2021; Vol. 1, pp. 39–62 ISBN 9783030704438.
293. Schreiber, S.; Savia, M.; Pelekhov, D. V.; Iscru, D.F.; Selcu, C.; Hammel, P.C.; Agarwal, G. Magnetic Force Microscopy of Superparamagnetic Nanoparticles. *Small* 2008, *4*, 270–278, doi:10.1002/smll.200700116.
294. Wei, J.D.; Knittel, I.; Lang, C.; Schüler, D.; Hartmann, U. Magnetic Properties of Single Biogenic Magnetite Nanoparticles. *J. Nanoparticle Res.* 2011, *13*, 3345–3352, doi:10.1007/s11051-011-0357-4.
295. Angeloni, L.; Passeri, D.; Scaramuzzo, F.A.; Schiavi, P.G.; Pagnanelli, F.; Rossi, M. Magnetic Force Microscopy Characterization of Core–Shell Cobalt-Oxide/Hydroxide Nanoparticles. *J. Magn. Magn. Mater.* 2020, *516*, 167299, doi:10.1016/j.jmmm.2020.167299.
296. Giessibl, F.J. Advances in Atomic Force Microscopy. *Rev. Mod. Phys.* 2003, *75*, 949–983, doi:10.1103/RevModPhys.75.949.
297. Slade, A.L.; Yip, C.M. Scanning Probe Microscopy – Applications for the Study of Soft Materials. In *Molecular Interfacial Phenomena of Polymers and Biopolymers*; Elsevier, 2005; pp. 161–213 ISBN 9781855739284.
298. Cordova, G.; Lee, B.Y.; Leonenko, Z. Magnetic Force Microscopy for Nanoparticle Characterization. *NanoWorld J.* 2016, *2*, 10–14, doi:10.17756/nwj.2016-022.
299. Passeri, D.; Angeloni, L.; Reggente, M.; Rossi, M. Magnetic Force Microscopy. *Magn. Charact. Tech. Nanomater.* 2017, 209–259, doi:10.1007/978-3-662-52780-1_7/FIGURES/16.
300. Passeri, D.; Dong, C.; Reggente, M.; Angeloni, L.; Barteri, M.; Scaramuzzo, F.A.; de Angelis, F.; Marinelli, F.; Antonelli, F.; Rinaldi, F.; et al. Magnetic Force Microscopy: Quantitative Issues in Biomaterials. *Biomatter* 2014, *4*, 1–16, doi:10.4161/biom.29507.
301. Schmool, D.S.; Kachkachi, H. Single-Particle Phenomena in Magnetic Nanostructures. In *Solid State Physics - Advances in Research and Applications*; Academic Press, 2015; Vol. 66, pp. 301–423 ISBN 9780128034132.
302. High-Resolution STEM Imaging. In *Transmission Electron Microscopy and Diffractometry of Materials*; Springer Berlin Heidelberg: Berlin, Heidelberg, 2008; pp. 583–609 ISBN 978-3-540-73886-2.

303. Leng, Y. X-Ray Spectroscopy for Elemental Analysis. In *Materials Characterization: Introduction to Microscopic and Spectroscopic Methods*; Wiley, 2013; pp. 191–219.
304. Javad, R.; Mosaddegh, N. Application of Atomic Absorption for Determination of Metal Nanoparticles in Organic-Inorganic Nanocomposites. In *Atomic Absorption Spectroscopy*; InTech, 2012 ISBN 978-953-307-817-5.
305. Ivanova, E.H. Atomic Absorption Spectrometry: Principles and Instrumentation. In *Encyclopedia of Analytical Science*; Elsevier, 2005; pp. 149–156 ISBN 9780123693976.
306. Wilschefski, S.; Baxter, M. Inductively Coupled Plasma Mass Spectrometry: Introduction to Analytical Aspects. *Clin. Biochem. Rev.* 2019, *40*, 115–133, doi:10.33176/AACB-19-00024.
307. Peak, D. Fourier Transform Infrared Spectroscopy. In *Encyclopedia of Soils in the Environment*; Elsevier, 2005; Vol. 4, pp. 80–85 ISBN 9780080547954.
308. Greczynski, G.; Hultman, L. A Step-by-Step Guide to Perform x-Ray Photoelectron Spectroscopy. *J. Appl. Phys.* 2022, *132*, 11101, doi:10.1063/5.0086359.
309. Mudalige, T.; Qu, H.; Van Haute, D.; Ansar, S.M.; Paredes, A.; Ingle, T. Characterization of Nanomaterials. In *Nanomaterials for Food Applications*; Elsevier, 2019; pp. 313–353 ISBN 9780128141311.
310. Ross, J.R.H. How Does a Catalyst Work? In *Contemporary Catalysis*; Elsevier, 2019; pp. 69–89 ISBN 978-0-444-63474-0.
311. Narayan, N.; Meiyazhagan, A.; Vajtai, R. Metal Nanoparticles as Green Catalysts. *Materials (Basel).* 2019, *12*, 3602, doi:10.3390/ma12213602.
312. Hervés, P.; Pérez-Lorenzo, M.; Liz-Marzán, L.M.; Dzubiella, J.; Lu, Y.; Ballauff, M. Catalysis by Metallic Nanoparticles in Aqueous Solution: Model Reactions. *Chem. Soc. Rev.* 2012, *41*, 5577, doi:10.1039/c2cs35029g.
313. Fang, X.; Wang, Y.; Wang, Z.; Jiang, Z.; Dong, M. Microorganism Assisted Synthesized Nanoparticles for Catalytic Applications. *Energies* 2019, *12*, 190, doi:10.3390/en12010190.
314. Krajczewski, J.; Kołątaj, K.; Kudelski, A. Plasmonic Nanoparticles in Chemical Analysis. *RSC Adv.* 2017, *7*, 17559–17576, doi:10.1039/C7RA01034F.
315. Adewuyi, A.; Lau, W.J. Nanomaterial Development and Its Applications for Emerging Pollutant Removal in Water. In *Handbook of Nanotechnology Applications*; Elsevier, 2021; pp. 67–97 ISBN 9780128215067.
316. Wong-Pinto, L.; Menzies, A.; Ordóñez, J.I. Bionanomining: Biotechnological Synthesis of Metal Nanoparticles from Mining Waste—Opportunity for Sustainable Management of Mining Environmental Liabilities. *Appl. Microbiol. Biotechnol.* 2020, *104*, 1859–1869, doi:10.1007/s00253-020-10353-0.
317. Angappane, S.; Park, J.; Jang, Y.; Hyeon, T.; Park, J.G. Magnetic Pd Nanoparticles: Effects of Surface Atoms. In Proceedings of the Journal of Physics Condensed Matter; IOP Publishing, July 23 2008; Vol. 20, p. 295209.
318. Kumar, V.; Kawazoe, Y. Icosahedral Growth, Magnetic Behavior, and Adsorbate-Induced Metal-Nonmetal Transition in Palladium Clusters. *Phys. Rev. B - Condens. Matter Mater. Phys.* 2002, *66*, 1–11, doi:10.1103/PhysRevB.66.144413.
319. Venäläinen, A.; Jalkanen, P.; Tuboltsev, V.; Savin, A.; Räisänen, J. Growth Mode-Dependent Ferromagnetic Properties of Palladium Nanoclusters. *J. Appl. Phys.* 2018, *124*, doi:10.1063/1.5022364.
320. Kondo, Y.; Swieca, K.; Pobell, F. Magnetic Properties of Pd Doped with Fe: Intermediate between Ferromagnetism and Spinglass Behavior. *J. Low Temp. Phys.* 1995, *100*, 195–218, doi:10.1007/BF00751506.
321. Bunge, M.; Søbjerg, L.S.; Rotaru, A.; Gauthier, D.; Lindhardt, A.T.; Hause, G.; Finster, K.; Kingshott, P.; Skrydstrup, T.; Meyer, R.L. Formation of Palladium(0) Nanoparticles at Microbial Surfaces. *Biotechnol. Bioeng.* 2010, *107*, 206–215, doi:10.1002/bit.22801.
322. Zhou, L.; Wu, C.; Xie, Y.; Xia, S. Biogenic Palladium Prepared by Activated Sludge Microbes for the Hexavalent Chromium Catalytic Reduction: Impact of Relative Biomass. *Front. Environ. Sci.*

Eng. 2020, *14*, 27, doi:10.1007/s11783-019-1206-4.
323. Sidhu, A.K.; Verma, N.; Kaushal, P. Role of Biogenic Capping Agents in the Synthesis of Metallic Nanoparticles and Evaluation of Their Therapeutic Potential. *Front. Nanotechnol.* 2022, *3*, 801620, doi:10.3389/fnano.2021.801620.
324. Taleshi, F.; Hosseini, A.A. Synthesis of Uniform MgO/CNT Nanorods by Precipitation Method. *J. Nanostructure Chem.* 2012, *3*, 4, doi:10.1186/2193-8865-3-4.
325. Tan, L.; Dong, H.; Liu, X.; He, J.; Xu, H.; Xie, J. Mechanism of Palladium(Ii) Biosorption by *Providencia vermicola*. *RSC Adv.* 2017, *7*, 7060–7072, doi:10.1039/C6RA27589C.
326. Patel, S.; Kundu, S.; Halder, P.; Rickards, L.; Paz-Ferreiro, J.; Surapaneni, A.; Madapusi, S.; Shah, K. Thermogravimetric Analysis of Biosolids Pyrolysis in the Presence of Mineral Oxides. *Renew. Energy* 2019, *141*, 707–716, doi:10.1016/j.renene.2019.04.047.
327. Matsko, N.; Mueller, M. AFM of Biological Material Embedded in Epoxy Resin. *J. Struct. Biol.* 2004, *146*, 334–343, doi:10.1016/j.jsb.2004.01.010.
328. Tabet, M.F. Deconvolution of Tip Affected Atomic Force Microscope Images and Comparison to Rutherford Backscattering Spectrometry. *J. Vac. Sci. Technol. B Microelectron. Nanom. Struct.* 1997, *15*, 800, doi:10.1116/1.589412.
329. Raşa, M.; Kuipers, B.W.M.; Philipse, A.P. Atomic Force Microscopy and Magnetic Force Microscopy Study of Model Colloids. *J. Colloid Interface Sci.* 2002, *250*, 303–315, doi:10.1006/jcis.2002.8345.
330. Vesenka, J.; Manne, S.; Giberson, R.; Marsh, T.; Henderson, E. Colloidal Gold Particles as an Incompressible Atomic Force Microscope Imaging Standard for Assessing the Compressibility of Biomolecules. *Biophys. J.* 1993, *65*, 992–997, doi:10.1016/S0006-3495(93)81171-8.
331. Zhang, Y.; Yang, M.; Ozkan, M.; Ozkan, C.S. Magnetic Force Microscopy of Iron Oxide Nanoparticles and Their Cellular Uptake. *Biotechnol. Prog.* 2009, *25*, 923–928, doi:10.1002/BTPR.215.
332. Bitter, F. On Inhomogeneities in the Magnetization of Ferromagnetic Materials. *Phys. Rev.* 1931, *38*, 1903–1905, doi:10.1103/PhysRev.38.1903.
333. Yu, Y.-Y.; Cheng, Q.-W.; Sha, C.; Chen, Y.-X.; Naraginti, S.; Yong, Y.-C. Size-Controlled Biosynthesis of FeS Nanoparticles for Efficient Removal of Aqueous Cr(VI). *Chem. Eng. J.* 2020, *379*, 122404, doi:10.1016/j.cej.2019.122404.
334. Joudeh, N.; Saragliadis, A.; Schulz, C.; Voigt, A.; Almaas, E.; Linke, D. Transcriptomic Response Analysis of *Escherichia coli* to Palladium Stress. *Front. Microbiol.* 2021, *12*, 2840, doi:10.3389/fmicb.2021.741836.
335. Yahyaei, B.; Peyvandi, N.; Akbari, H.; Arabzadeh, S.; Afsharnezhad, S.; Ajoudanifar, H.; Pourali, P. Production, Assessment, and Impregnation of Hyaluronic Acid with Silver Nanoparticles That Were Produced by Streptococcus Pyogenes for Tissue Engineering Applications. *Appl. Biol. Chem.* 2016, *59*, 227–237, doi:10.1007/s13765-016-0147-x.

Paper I

Microbial synthesis and characterization of bimetallic Pd-Fe nanoparticles produced by *Escherichia coli*

Ana Lucia Campaña, Jaime Gomez-Bolivar, Mohamed L. Merrun, Nadeem Joudeh, Athanasios Saragliadis, Dirk Linke, and Pavlo Mikheenko

Manuscript

Paper II

Detection of microbial nanoparticles within biological structures by AFM and MFM

Ana Lucía Campaña, Nadeem Joudeh, Mohamed L. Merrun, Dirk Linke, and Pavlo Mikheenko

Manuscript

Paper III

Probing Van der Waals and magnetic forces in bacteria with magnetic nanoparticles

Ana Lucia Campaña, Nadeem Joudeh, Henrik Høyer, Anja Røyne, Dirk Linke, and Pavlo Mikheenko

DOI: 10.1109/nap51477.2020.9309722

Paper IV

Magnetic decoration of *Escherichia coli* loaded with Palladium nanoparticles

Ana Lucia Campaña, Nadeem Joudeh,
Dirk Linke, and Pavlo Mikheenko

DOI: 10.1109/nap51885.2021.9568523